AN INVESTIGATION OF SHEAR RESPONSE OF COMPOSITE MATERIAL SYSTEMS

by

Yanhong Zhang

Dissertation submitted to the Faculty of the
Virginia Polytechnic Institute and State University
in partial fulfillment of the requirements for the degree of

DOCTOR OF PHILOSOPHY
in
Engineering Mechanics

APPROVED:

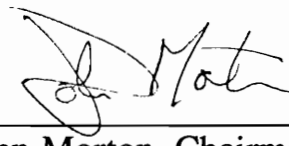

John Morton, Chairman

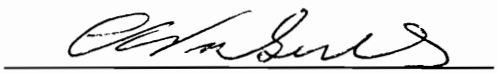

Charles W. Smith

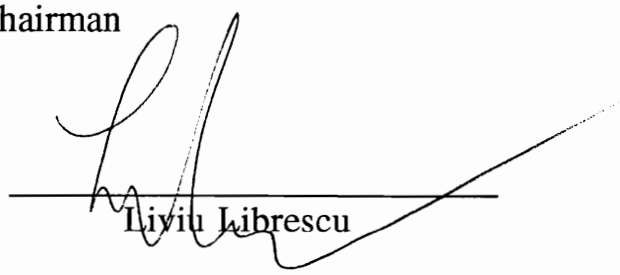

Liviu Librescu

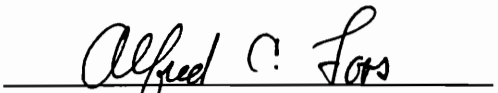

Alfred C. Loos

Yuriko Renardy

March, 1994
Blacksburg, Virginia

AN INVESTIGATION OF SHEAR RESPONSE OF COMPOSITE MATERIAL SYSTEMS

by
Yanhong Zhang
John Morton, Chairman
Engineering Science and Mechanics

(Abstract)

An investigation of shear response for various composite material systems is presented. The uniformity of the strain fields is studied experimentally and numerically for different specimen configurations. Conventional strain gage measurements and the moiré interferometry technique are employed to obtain information of actual deformation of the specimen. Based on the contour maps of displacement obtained from moiré tests, the localized hybrid method is used to quantify the magnitude and scale of the nonuniform deformation in the real strain fields. The finite element analysis is also performed for predicting the global nonuniformity of the strain fields. It is shown that the significant nonuniformity in shear deformation observed in experimental results can not be predicted by the existing analytical and numerical models. It is considered that the nonuniformity is primarily at a local level, which is associated with the material inhomogeneity. The implication of the local nonuniform deformation fields on the material property evaluation and failure prediction are discussed. The nonlinearity of shear response is investigated experimentally by performing strain gage and moiré tests. Curve fitting techniques proved to be a convenient and effective tool for characterizing the nonlinear shear response of composites. It is suggested that not only the initial shear modulus but also other coefficients of the fitting function be used for the evaluation of nonlinear shear behavior of a composite. The experimental results show that the nonlinearity has no significant effect on the shear strain distribution, verifying the validity of correction factors in the nonlinear range. Shear stress at a selected shear strain level is suggested as an engineering definition for shear strength of composites. The shear response of some novel composites is also investigated, the test results of which are presented.

ACKNOWLEDGMENTS

I wish to express my thanks to the many people who have been supportive throughout the Ph.D. program.

- A special thanks to Prof. John Morton, the chairman of the committee, for his guidance and encouragement during my doctoral studies and research. His rigorous attitude towards research is believed to be influential to my future professional career.

- To other members in my doctoral committee, Prof. C. W. Smith, Prof. L. Librescu, Dr. A. C. Loos and Dr. Y. Renardy, for their participation and valuable advices on the dissertation.

- To Dr. Shih-Yung Lin and Dr. Jau-Je Wu for their assistance with the moiré experiments. Without their help, this part of the research work would have never been finished.

- To my former and present fellow group members, Dr. Henjen Ho, Dr. Kuen Tat Teh, Dr. Ming-Yi Tsai, Dr. Todd Wieland, David Johnson, Hary Budiman, Robert Bennett, Andre Lavoie and Diane Peters, for their help, corporation and friendship.

- To all my family, especially my mother, for their love and understanding.

- To all my friends for being there during the good and the hard times.

The funding for this research project provided by National Science Foundation Science and Technology Center for High Performance Polymeric Adhesives and Composites at Virginia Tech under contract DMR#912004 is greatly acknowledged.

TABLE OF CONTENTS

LIST OF TABLES

LIST OF FIGURES

CHAPTER 1. INTRODUCTION

1.1 Introduction

In order to characterize any new composite material system, knowledge of its mechanical behavior is required. Of the basic mechanical properties, shear properties play a critical role. Shear properties are needed not only for the characterization of shear response but also for the analysis of related mechanical behavior such as compression performance. Moreover, shear properties are also useful parameters for evaluating the effects of processing variables on the performance of new material system. Therefore, shear response has been a subject of considerable interest since advanced composite materials were first developed.

Usually, investigation of the mechanical properties of a composite material system is based on two engineering assumptions: material homogeneity and linear elastic behavior. Based on these assumptions, classical laminate theory (CLT) as well as several failure criteria have been established, in which each ply of the laminate is assumed to be homogeneous, orthotropic and linear elastic. Five elastic constants, E_{11}, E_{22}, υ_{12}, G_{12}, G_{23}, rather than just E and υ for isotropic materials, are used to characterize the elastic behavior of the transversely isotropic composite materials. These elastic constants must be measured experimentally. In addition, traditional experimental measurements of the mechanical properties of metals, which satisfy the two assumptions, have been either applied directly to, or developed for, composite materials with modifications made only to the isotropic characteristics. In other words, the isotropic properties of metals are replaced by orthotropic properties for a composite material, while the assumption of material homogeneity is maintained and rationalized by smearing the material properties of each component and then defining equivalent or average mechanical properties for the composite material system. However, composite materials, especially fibrous composites, are in-homogeneous. Furthermore, the distribution of the fiber bundles, which are used for the manufacture of preimpregnated sheets, is not perfectly uniform so that regions of varying effective fiber volume fraction (occasionally as resin rich regions) exist in the composite. Consequently, different local responses due to differences between the mechanical properties of the fiber and matrix are to be expected. Moreover, most commonly used polymer matrix materials display non-linear stress-strain behavior,

which may be non-linear elastic, non-linear plastic, or non-linear viscoelastic. When load is applied transverse to the fiber, the matrix effects become important. Therefore, nonlinearity has been observed in the in-plane shear response for most composite materials. For some composites, no linear range can be clearly identified in the shear stress-strain curve. Since the nonlinearity usually appears gradually, its effect cannot be neglected when evaluating the shear response of a structure and/or its components under the designed working load.

In previous studies of the in-plane shear response of composite material systems, most researchers focused their attention on the shear behavior within what was thought to be the linear range. Although some nonlinear and micromechanics models have been proposed to simulate analytically the nonlinearity of the shear response and inhomogeneity of the material systems, the experimental validation is still not trivial.

1.2 Objectives

The objectives of this study are (a) examination of the local responses caused by the inhomogeneity of the material system and its impact on the measured and assumed global in-plane shear response, (b) characterization of the in-plane shear response, particularly the nonlinear response and the influence of the nonlinearity on the modeled elastic solutions, (c) to address the issue of defining shear strength from an engineering point of view. A wide range of composite material systems is evaluated in this study, including traditional advanced fibrous composites, AS4/3501-6, AS4/3502, APC-2 (AS4/PEEK), and new composite material systems such as aerospace grade composites, AS4/LaRC-TPI, commodity resin based in-situ composites, PEKK/HX1000, developed by Professor Donald Baird of the Virginia Tech NSF S&TC and a new commercially available industrial grade composite material, hybrid glass/PETP, developed by DSM (Dutch State Mines).

1.3 Approach

In the present study, the shear response is investigated experimentally and numerically. In the experimental study, traditional strain gage techniques as well as the optical method of moiré interferometry are used. Various test methods are employed, including the

Iosipescu test, off-axis tensile test and ±45° tensile test. By applying the strain gage measuring technique, the shear stress-strain curves are obtained. Moiré interferometry is employed to obtain full-field in-plane displacement information. Based on the contour maps of displacement (fringe patterns) provided by moiré experiments, the localized hybrid method is applied to obtain the strain contours in the areas of interest. In addition, finite element analysis is performed for the prediction of global response. The observations will be studied and interpreted from the mechanics of composite point of view.

CHAPTER 2. REVIEW OF SHEAR TEST METHODS

2.1 Introduction

Because of the importance of shear behavior to the characterization of a composite material system, shear property measurement of composites is a frequently performed task. However, such measurement has proved to be more difficult than other tests such as tension and flexure.

An ideal shear test method should provide a state of pure shear in the specimen test section. In addition, the shear stress/strain field within the test section should be uniform. Moreover, in order to determine the shear strength accurately, the maximum shear stress should be achieved within the test section, and the failure of the specimen should be attributed to the critical shear stress rather than any other stress component. These requirements are difficult to achieve even for an isotropic material. The highly orthotropic nature of advanced laminated composite materials poses additional testing problems. Various coupling effects, for instance, may introduce undesirable stresses and strains in the test section. Large differences in the mechanical strengths for stress in various directions may lead to failure in unexpected modes at unexpected locations. For most of the shear test methods for composites, it is a common problem that a pure shear and uniform stress state within the test section is not attainable. The nonuniformity of the shear stress field has a direct effect on the determination of shear stiffness. In shear property measurement, shear modulus is usually calculated by dividing the *average* shear stress over the cross-section by measured shear strain. When the shear stress field is not uniform, the average shear stress may not be the same as, sometimes even differs radically from, the shear stress beneath the strain gage. Significant errors may, hence, be induced in the determination of shear modulus. Since the nonuniformity of shear stress field varies with the specimen geometry and loading condition, inconsistency is often observed in the shear modulus measured by different test methods if the nonuniformity is not taken into account. Further, the presence of normal strains and stresses in the test section, in addition to the desired shear strain and stress, not only makes the measurement of shear properties more complex, but also results in a controversy in the measured shear strength. Because specimens of same material but tested by different test methods with different configurations may fail in different failure modes, lack of consistency in

ultimate shear stresses, usually used as the material shear strength, obtained from different test methods is a common occurrence.

More than ten different shear test methods have been proposed and employed during the past twenty years. However, from the point of view of result accuracy as well as practical convenience, none of these methods is completely satisfactory. A brief review of some commonly used shear test methods for advanced composite materials is presented in this chapter. For each method, the advantages, disadvantages, as well as the limitation of its application are discussed.

In the following and later discussion, two coordinate systems are employed: x-y system is referred to as the global or body coordinates in which specimen geometry and loads are specified, and 1-2 system (parallel and transverse to the fiber direction, respectively) referred to as the local or material coordinates in which material properties are specified.

2.2 Off-Axis Tensile Test

When a transversely isotropic unidirectional laminate coupon is loaded in tension with the fibers oriented at an angle θ to the loading direction, the specimen will behave like an anisotropic material. The nature of extension-shear coupling of the specimen induces in-plane shear stress and strain, in addition to the normal stresses and strains. When the angle θ is small, the extension-shear coupling effect is large. In the material coordinate system, shear strains can reach values much higher than the normal strains. Therefore, 10° off-axis tensile specimen was first suggested for shear property measurement in the 1970's [1,2] and specimens with other angles have also been used in other studies [3-5]. The specimen used in the off-axis tensile test is a straight-sided one, most commonly 12.7 mm (0.5 in) wide and 254 mm (10 in) long, as shown in Fig. 2.1a. The specimen can be easily cut from the same unidirectional panel as used for test specimens for longitudinal and transverse characterization but at a designed angle θ. A three-gage rosette with gages oriented in x (0°), y (90°) and 45° directions is applied at the center of the specimen to measure strain in three directions. The shear strain γ_{12} is found from

$$\gamma_{12} = 2 \sin\theta \cos\theta (-\varepsilon_x + \varepsilon_y) + (\sin^2\theta - \cos^2\theta) \gamma_{xy} \qquad (2.1)$$

The average shear stress is obtained from the equilibrium of the specimen, as shown in Fig. 2.1a, that is

$$(\tau_{12})_{avg} = \frac{P}{A}\sin\theta\cos\theta \tag{2.2}$$

The initial shear modulus is then determined by

$$G_{12} = \frac{(\tau_{12})_{avg}}{\gamma_{12}} \tag{2.3}$$

Note that γ_{12} is a local or "point" value of the shear strain and $(\tau_{12})_{avg}$ is an average value of the shear stress over a cross-section parallel to the fiber direction.

The off-axis tensile test method has been popularly employed since it was first proposed because of the ease of specimen preparation, test performance and data reduction. However, while the extension-shear coupling effect makes this method available for shear property measurement, it also brings an undesirable problem to this method, that is, the end constraint effect. Because of the extension-shear coupling effect, the ends of the specimen tend to rotate when loaded in tension, as shown in Fig. 2.1b. As the specimen is gripped in clamp, rotation of the end is not allowed. The constrained deformation of the specimen, as shown in Fig. 2.1b, is then quite different from the unconstrained one. It has been shown that the prevention of end rotation by the gripping system induces additional shear force and moment to the specimen and the assumed uniform stress state within the test section is disturbed [6]. Consequently, errors may be induced in the determination of shear properties if the influence of end constraint is not taken into account. Several approaches, either analytical or numerical, have been proposed to asses the end constraint effect and quantify the nonuniformity of the disturbed stress/strain fields [4-9]. It is suggested that to minimize the end constraint effect on the test section the test specimen should be designed with a high aspect ratio [2,4,5]. In addition, equation (2.2) should be modified to calculate the shear stress corresponding to the combined loads of applied tension force and induced shear force and moment [4]. A correction factor is then required in equation (2.3) to obtain an accurate value of initial shear modulus, which will be discussed in detail in Chapter 3.

It was also suggested that the off-axis tensile specimen with small angle can be used for the determination of shear strength [2]. However, later studies have shown that the 10°

off-axis specimens always failed at low shear strain levels, compared with results from other shear test methods, due to the combination of transverse tension and shear stresses [10-11]. The shear stress-strain curves obtained from off-axis tensile test also exhibit less nonlinear than those from other test methods because of the early failure. It appears then that the off-axis tensile test is not a good test method for determination of shear strength for unidirectional composites.

2.3 ± 45° Tensile Test

The ± 45° tensile test is another simple shear test method similar to the off-axis tensile test. This test was first proposed in 1969 [12]. In this method, a straight-sided laminated coupon of symmetric angle-ply lay-up with fiber angles of +45° and -45° is tested in uniaxial tension, as shown in Fig. 2.2a. Using an angle-ply laminate specimen, rather than a unidirectional one, the extension-shear coupling effect is eliminated on the laminate level. The recommended width of specimen is 25.4 mm (1 in) [12]. A two-element strain gage rosette with gages oriented in 0° and 90° directions is employed to measure the axial and transverse strains. A simple procedure for determination of shear modulus was proposed in [13]. It has been shown that when there is no shear coupling, the average shear stress τ_{12} is given by

$$(\tau_{12})_{avg} = \frac{P}{A} \sin 45° \cos 45° = \frac{P}{2A} \tag{2.4}$$

where P is the applied axial load and A is the area of cross-section [13,14]. The *ply* shear strain γ_{12} is found from

$$\gamma_{12} = 2 \sin 45° \cos 45° (-\varepsilon_x + \varepsilon_y) + (\cos^2 45° - \sin^2 45°) \gamma_{xy} = (-\varepsilon_x + \varepsilon_y) \tag{2.5}$$

The initial shear modulus G_{12} is obtained from

$$G_{12} = \frac{(\tau_{12})_{avg}}{\gamma_{12}} = \frac{P/A}{2(-\varepsilon_x + \varepsilon_y)} \tag{2.6}$$

Because the specimen used in the ± 45° tensile test has a simple geometry and good reproducibility is attainable, it has been recommended as a simple, reliable and cost-effective test method for the determination of shear properties of continuous fiber

composites [10-12,15]. It has been widely used in the industry and was adopted by ASTM as a standard test method in 1976 [16].

There are some special problems associated with the laminated specimen. One of them is the free edge effect [12]. When a laminated coupon is loaded in uniaxial tension, each lamina, with fibers oriented at either +45° or -45° to the loading axis, tends to deform in shear, in addition to tension, due to the orthotropic nature, but the directions are opposite for the +45° ply and -45° ply. In order to satisfy the strain compatibility condition between lamina, additional in-plane shear stress τ_{xy} is induced, as shown in Fig. 2.2b. However, at the free edges of the coupon, the shear stress must fall to zero. Therefore, a complex stress state exists in an area near the free edges of the specimen. In order to minimize contribution of the free edge effect, it is recommended that a relatively large width of the test specimen be used [12]. It has been shown that the free edge effect does not significantly affect the whole shear stress-strain response [18]. Furthermore, the mechanism of damage of a laminate is more complicated than that of a lamina. Constraint between neighboring layers plays an important role in the damage initiation. It has been observed that early cracks always initiate in some "weak" plies such as surface ply and ply in the mid-plane (a block of two plies with the same fiber orientation), which has less constraint from neighboring plies than any other ply within the laminate [17-18]. It has also been documented that there is a strong dependency of the measured shear strength on the thickness and stacking sequence (sublaminate and ply-level scaling) of the laminate [15,17-18]. It is considered that there is a process of load redistribution after crack initiation. A thicker laminate which has plenty plies rather than weak plies can provide more opportunities for load redistribution than a thinner laminate. Therefore, the failure stress of a 32 ply laminate is much higher than that of a 8 ply laminate [17-18]. On the other hand, laminates of same thickness but different stacking sequence will have different numbers of weak ply, which also results in different capabilities of carrying load. It is suggested that the specification of the size and stacking sequence of the specimen tested in $\pm$ 45° tensile test should be presented more clearly in the standards so that more consistent results of shear strength can be achieved.

2.4 Iosipescu Shear Test

The Iosipescu shear test was first proposed in the 1960's, primarily for testing metals and other isotropic materials [19]. Subsequently, the test procedure was refined for the measurement of shear properties of composites, and the specimen and fixture improved and modified [20-24] to yield the configuration shown in Fig. 2.3. In this test, the fixture is loaded in compression, then the relative displacement between the movable and fixed portions of the fixture makes the middle section of the inserted specimen subjected to shear load. Two-element strain gage rosette, oriented at ±45° to the specimen longitudinal axis, is applied to the center of the specimen. The data reduction for the Iosipescu shear test is very simple. The shear strain γ_{xy} is found directly from the gage readings as

$$\gamma_{xy} = \varepsilon_{+45^\circ} - \varepsilon_{-45^\circ} \tag{2.7}$$

where ε_{+45° and ε_{-45° are normal strains measured at +45° and -45° directions to the specimen longitudinal axis. The average shear stress over the notch-axis is

$$(\tau_{xy})_{avg} = P / A \tag{2.8}$$

where P is the applied compressive load and A is the area of cross-section between two notches. The shear modulus G_{xy} is then calculated by

$$G_{xy} = \frac{(\tau_{xy})_{avg}}{\gamma_{xy}} = \frac{P / A}{\gamma_{xy}} \tag{2.9}$$

The Iosipescu shear test has some clear advantages. First of all, it can test a wide range of composites, not only continuous fiber composite, to which the off-axis and ±45° tensile tests can only applied, but also woven fabric continuous fiber reinforced composites as well as sheet molding compound material. In addition, the compact shape of the specimen leads to a great savings of test material. Since the specimen has dimensions of about 76.2 x 19.1 mm (3 x 0.75 in), a small panel of 76.2 x 76.2 mm (3 x 3 in), which is a commonly available size for new composites under development, is sufficient for performing some preliminary tests. Furthermore, both unidirectional and multi-directional laminates can be evaluated. The Iosipescu specimen can be used to measure shear stiffness and shear strength.

Numerous numerical and experimental studies have been conducted to assess the nonuniformity of the shear stress/strain field within the test section [5, 22-23, 25-30]. It has been shown that the shear stress/strain distributions between notches are always nonuniform. For the fiber reinforced unidirectional composites, the shear strain distributions are of different forms for different specimen configurations, 0° and 90°, which results in inconsistency in the values of shear moduli measured by 0° and 90° specimens if the nonuniformity is not taken into account. It is suggested that a correction factor, which has proved to be a function of the orthotropy ratio E_x/E_y [5,25-26,31], is required in the determination of the shear modulus. In addition, it is observed that for unidirectional 90° specimens, shear strains measured at front face and back face are different due to specimen twisting and the twisting effect on the determination of shear response can be eliminated by averaging the shear strain values obtained from front face and back face [25]. Using back-to-back strain gage rosettes is then recommended for testing 90° specimen.

2.5 Other Test Methods

Many other shear test methods have also been proposed and used [32-51]. However, for some of them, the specimen preparation is very complicated, such as cross beam [36], Arcan [34], torsion of solid circular bar [32-33] and picture frame [35]. Some of them can only be used for quality control due to the impossibility of strain measurement, such as slotted shear [37-38] and short beam [39]. They are not, therefore, popularly accepted in practice. Based on the acceptance of these methods, only two further test methods, torsion tube and rail shear, will be discussed briefly in this section.

2.5.1 Torsion Test of Thin-Walled Tube

Torsion tube test has been suggested and used by many researchers for determination of shear properties of fiber composites [40-46]. It can be applied to unidirectional materials or laminate made of plies with different fiber orientations. A hoop wound cylinder is usually employed as shown in Fig. 2.4 due to relative ease of specimen preparation, compared with tubes with fiber in other orientations, and good performance. The length of the specimen test section is about 101.6 mm (4 in). Two-gage rosettes, arranged at +45° and -45° to the specimen axial axis, are recommended to apply on the surface of the

tube. As the tube is loaded in pure torsion, only shear stress and strain are present in the wall of the tube. It has been shown that when the thickness-to-diameter ratio t / D is small (e.g. t / D < 0.02), the variation of shear stress through the thickness is negligible [40-42]. The data reduction is, therefore, very simple. The shear stress τ, shear strain γ and shear modulus G can be calculated from the following expressions:

$$\tau = \frac{T}{2\pi r^2 t} \tag{2.10}$$

$$\gamma = \varepsilon_{+45^\circ} - \varepsilon_{-45^\circ} \tag{2.11}$$

$$G = \frac{\tau}{\gamma} \tag{2.12}$$

where T is the applied torque, t is the thickness of the wall and r in the average of the inner and outer radii of the tube.

From a mechanics point of view, the torsion test is an ideal test method since it can provide the most pure and uniform shear stress state. It is often used as a reference for evaluating results obtained from other test methods. However, it is practical only for filament wound composites. For the normal sheet-based composites, the test is not only very expensive and leads to difficulties in fabricating a tube from a prepreg, but also it is possible that changes in the processing conditions result in changes in the properties of the material. Therefore, this test method is impractical for composites of flat form.

2.5.2 Rail Shear Test

There are two configurations for the rail shear test; these are two-rail and three-rail tests, as shown in Fig. 2.5. The two-rail shear test is favored in the aerospace industry for testing advanced fiber composite materials. Because of the wide usage of rail shear test, a standard guide is presented in the ASTM Standards [47].

In the two-rail test, a rectangular specimen, 76.2 x 152.4 mm (3 x 6 in), is clamped between two pairs of steel load rails. When tensile load is applied on the assembly, shear forces are introduced in the specimen. While in the three-rail test, the specimen, 136.5 x 152.4 mm ($5^3/_8$ x 6 in), is clamped on opposite edges and a load, either tension or compression, is applied to the third pair of steel rails in the center; shear loading is then produced in each specimen. A 45° strain gage is applied at the center of the specimen. It

was thought that the three-rail test would provide better results because the load is applied parallel to the clamped edges of the specimens. In practice, however, little difference has been seen in the results from these two methods.

The rail shear test method can be used to test unidirectional, cross-ply and angle-ply laminates as well as discontinuous fiber composites for shear modulus and strength. However, it is shown that significant normal stresses are always present in the test section [48-50], and for most composite materials the failure is caused by a combination of diagonal tension and compression forces in both of the rail tests. According to the results of the ASTM round-robin on the rail shear test for fiber composites [51], which shows a large variation in averages, the repeatability of this test is questionable. This test procedure is, therefore, issued only as a standard guide, not a standard method, in the ASTM standards.

2.6 Summary

Five shear test methods, all well-known to the composite testing community, have been introduced individually in the previous sections. In order to have a global view of these test methods, a comparison of different test procedures is worthwhile.

A thorough review and examination of most of the commonly used in-plane shear test methods has been conducted by Lee and Munro [52], in which eight test methods were evaluated based on combined criteria of accuracy and practical convenience, i.e. cost of fabrication, cost of testing, data reproducibility and accuracy of experimental results. According to these authors, the most promising shear test methods are Iosipescu shear test, $\pm 45°$ tensile test and 10° off-axis tensile test.

Besides Lee and Munro's work, there are other studies related to the comparison of different shear test methods [5,10-11,53]. These comparisons are concerned with three issues: shear modulus, shear strength and shear stress-strain response. For shear modulus, it is shown that after applying appropriate correction factors to the results of each test, the initial shear moduli obtained from 10° off-axis tensile test, $\pm 45°$ tensile test and Iosipescu shear test are in reasonable agreement with each other [5,53]. While shear strength is of concern, the values of the apparent failure shear stresses obtained from different test methods significantly differ from each other. The reason is that none of the

specimens failed in pure shear. The apparent failure shear stresses of 10° off-axis and 90° Iosipescu specimens are usually lower than those of other test specimens [5,10-11]. Inconsistency is also observed in shear stress-strain curves of different specimen configurations [5,10,25]. These curves may be close to each other in the initial stages of the response but then lie apart at high shear strain levels. The shear responses of ± 45° and 0° Iosipescu specimens tend to be more nonlinear in nature than those of 10° off-axis and 90° Iosipescu specimens.

It should be emphasized here that in the previous investigations, the shear properties of a composite material measured and studied by these shear test methods were essentially the initial shear modulus and ultimate shear stress. However, as mentioned in Chapter 1, the shear behavior of most composite materials exhibits nonlinear nature. Consequently, the initial shear modulus is not sufficient to characterize the nonlinear shear response of a composite material. Moreover, ultimate shear stress obtained from different test methods may correspond to different failure modes, which leads to an inconsistency in the measured shear strength. In the present investigation, the shear response of various composite material systems are studied experimentally by employing the most promising shear test methods, i. e. off-axis tensile test, ± 45° tensile test and Iosipescu shear test. Attentions are given not only on the measurement of initial shear stiffness but also on the characterization of the nonlinear shear behavior. The nonuniformity of shear deformation is investigated at both the global and local levels. Based on the experimental data of shear response of various composite materials, the definition of shear strength is further studied from an engineering point of view.

CHAPTER 3. NONUNIFORM DEFORMATION IN SHEAR SPECIMENS

3.1 Introduction

The investigation of nonuniform shear deformation has been conducted on composites with three different forms: (1) unidirectional fibrous composites, (2) laminated fibrous composites, (3) hybrid fabric composites. Three most popularly used test methods have been chosen to perform the shear test: off-axis tensile test for unidirectional composite, ±45° tensile test for laminated composite and Iosipescu shear test for hybrid fabric composite. The strain-gage measurement technique has been applied to obtain stress-strain curves. In addition to conventional strain-gage measurement, moiré interferometry has been employed to obtain full-field in-plane displacement information. In order to quantify the nonuniformity in the strain fields, the localized hybrid method, which has proved to be a powerful technique for moiré fringe data reduction, was applied. With the help of localized hybrid analysis, strain contours in both body and material coordinate systems were obtained. For 10° off-axis tensile specimen and Iosipescu shear specimens, finite element analysis was also conducted to examine the global nonuniformity.

3.2 Nonuniform Deformation in Unidirectional Fiber Composites

3.2.1 Material and Specimen Preparation

In order to investigate the effect of fiber angle on the nonuniformity in displacement and strain fields, five specimens of different fiber orientations, 0°, 90°, 10°, 15° and 45°, were studied. All the specimens, except the 10° specimen, were cut from a 20-ply unidirectional graphite/epoxy panel (AS4/3502). This panel was made from commercial prepreg manufactured by Hercules and cured according to the manufacturer's instructions. After fabrication, the panel was C-scanned for examination of defects. According to the C-scan photograph, this panel was found defect-free. The panel was a square plate, 30.5 x 30.5 cm (12" x 12"), with a nominal thickness of 2.5 mm. The specimens with fiber angle of 15° and 45° were 23.3 cm long and 1.27 cm wide. The 0° specimen was 24.1 cm long and 1.27 cm wide, which met the requirement of gage length for 0° tensile

specimens [54]. The dimensions of the 90° specimen were 21.6 cm x 2.54 cm (length x width), which followed the recommended dimensions [54]. The 10° specimen, which had been tested with moiré interferometry in [53], was cut from a 20-ply unidirectional graphite/epoxy panel (AS4/3501-6). The dimensions of the 10° specimen were 30.5 cm x 1.27 cm (length x width), as shown in [53].

On each tensile specimen, three strain-gage rosettes were mounted, as shown in Fig. 3.1, so that strains at different locations can be measured. The first strain-gage rosette was mounted at the center of the specimen. The second one was attached on the same side as the first one but about 2.54 cm away from the center of the specimen. The third one was fixed on the other side of the specimen, also 2.54 cm away from the center, being opposite to the second one. For 0° and 90° tensile specimens, two-element strain gage rosettes (Micro Measurements EA-13-125TV-350), with gage oriented in 0° (x) and 90° (y) directions, were applied. For 10°, 15° and 45° tensile specimens, stacked three-element strain gage rosettes (Micro Measurements WA-13-060WR-120), with gage oriented in 0°(x), 90° (y) and 45° directions, were employed. A 1200 line per mm crossed line moiré grating was also applied at the center of each tensile specimen, opposite to the first strain-gage rosette. The width of grating was the same as the specimen and the length was about 2.54 cm.

3.2.2 Test Programme

(a) Strain-gage Experiments

The instrumented tensile specimen was placed in the test machine and gripped in the wedge grips with sandpaper at each ends. The specimen was then loaded in tension to a predetermined value at a constant cross-head rate of 0.13 mm/min. The load and individual gage readings were recorded by a micro computer equipped with a data acquisition system.

In order to evaluate the effect of test machine and grip system on the deformation of the tensile specimens, two different test machines with different grip systems were used. First, all the five tensile specimens were tested in a conventional screw-driven test machine, Tinius Olsen. The grips used in this machine are installed in a manner that for the lower grip, neither movement nor rotation are allowed; while for the upper grip, small movements in x-y plane and y-z plane as well as small rotation are allowable. In other

words, the lower grip is almost rigidly fixed on the foundation of the test machine, while the upper grip is restrained just by a hinge. After being tested in the Tinius Olsen test machine, the 10° and 45° tensile specimens were tested again in a hydraulic test machine, Instron 4206. The grip system used in the Instron is slightly different from that in Tinius Olsen. The restraint to the lower grip in the former is the same as that in the latter. However, the upper grip used in the Instron is also rigidly fixed to the machine without freedom to either move or rotation. In each machine, each tensile specimen was tested several times with various positions relative to the machine. For instance, if at the first time the specimen was placed with the side with grating facing the front (in Tinius Olsen machine) or left (in Instron 4206 machine), it would be positioned with the grating facing the back or right at the second time; at the third time it was tested upside down, etc.

(b) Moiré Experiments

Moiré interferometry was employed to provide full-field in-plane displacement information in an area of interest. The moiré data are obtained in the form of contour maps of displacement components, known as moiré fringe patterns [55-56]. The interferometer used in the experiments in the present study gave a fringe pattern sensitivity of 0.417 μm per fringe. Furthermore, the strain distributions within the area covered by grating is determined by differentiating the data in the moiré fringe patterns.

In the moiré experiments, the instrumented specimen was placed in the conventional screw-driven test machine Tinius Olsen with the side of the specimen with grating facing the front. A three-mirror interferometer [56] was positioned in front of the specimen and the grating was illuminated with two mutually collimated beams from a helium neon laser. Before the load was applied to the specimen, the interferometer was adjusted to produce no-load (null-field) fringe patterns. The specimen was then loaded to a predetermined value at a constant cross-head rate of 0.13 mm/min. While under constant loading, the transverse (u) and longitudinal (v) displacement fringe patterns were recorded photographically. Several pairs of fringe patterns were obtained during each test. In the mean time, the load and individual strain gage readings were recorded using a micro-computer equipped with a data acquisition system.

The determination of in-plane strains from the moiré experiment is the differentiation of data from two fringe patterns, i. e. u and v fringe patterns

$$\varepsilon_x = \frac{\partial u}{\partial x} = \frac{1}{f}\frac{\partial N_x}{\partial x} \tag{3.1}$$

$$\varepsilon_y = \frac{\partial v}{\partial y} = \frac{1}{f}\frac{\partial N_y}{\partial y} \tag{3.2}$$

$$\gamma_{xy} = \frac{\partial u}{\partial y} + \frac{\partial v}{\partial x} = \frac{1}{f}\left(\frac{\partial N_x}{\partial y} + \frac{\partial N_y}{\partial x}\right) \tag{3.3}$$

where f, f=2400 lines/mm, is the frequency of the virtual reference grating, and N_x, N_y are the fringe orders.

3.2.3 Stress-Strain Curves

(a) 0° Tensile Specimen

The 0° tensile specimen has been tested in the Tinius Olsen test machine three times. The normal stress-strain curves obtained in the material coordinate system are shown in Fig. 3.2a through Fig. 3.2c. Since in each test the position of the specimen relative to the test machine was different, the strains measured by the same gage rosette may have different meanings for different tests. The notations used in the figures have the following meanings: "front-upper" means the strain was measured at a gage rosette positioned on the front face and above the center of the specimen; "back-lower" denotes the strain measured at a gage rosette which was on the back face and below the center of the specimen, etc. Since curves obtained from rosette 2 and rosette 3 stand for the normal stress-strain responses at points of same x and y coordinates but on opposite sides of the specimen, comparison of these two curves will give the sense of out-of-plane bending. On the other hand, comparison of curves obtained from rosette 1 and rosette 2, which represent the stress-strain responses on the same side of the specimen but at different positions, will give the sense of nonuniformity of deformation. These notations will be used continuously and consistently in the following figures for specimens with other angles so that similar arguments will be employed in the following discussion.

As seen in Fig. 3.2, the curves of rosette 2 and 3 always depart from each other, indicating an out-of-plane bending about x-axis is always present. The direction of the bending may change. For instance, in Fig. 3.2a, the normal strain ε_1 on the back face is larger than that on the front face, implying the bending moment is positive; while in Fig.

3.2c, ε_1 on the back face is smaller than that on the front face, corresponding to a negative bending moment.

The curves for rosettes 1 and 2 show three different relations: (i) being identical, as in Fig. 3.2c; (ii) being identical at the initial stage, then departing from each other, as in Fig. 3.2a; (iii) being radically different, as in Fig. 3.2b. It appears that sometimes the deformation of a 0° tensile specimen is nonuniform.

Because of the presence of out-of-plane bending, the normal strains measured on the front and back faces may be different. Consequently, a scatter in the calculated tensile stiffness E_1, the ratio of the applied normal stress σ_1 to the measured normal strain ε_1, is expected if only one strain gage rosette is applied. However, when the normal strains are measured on both sides and an average value is used in the stress-strain curve, the stress-strain curves obtained from different tests become almost identical, as shown in Fig. 3.2d. This observation indicates that the effect of out-of-plane bending on the determination of tensile stiffness E_1 can be eliminated by applying strain gage rosettes on both sides of the specimen.

(b) 90° Tensile Specimen

The 90° tensile specimen has been tested in the Tinius Olsen test machine four times. The stress-strain curves, ε_2 versus σ_2, obtained from the four tests are shown in Fig. 3.3a through Fig. 3.3d. The averaged normal stress-strain curves of the four tests are shown in Fig. 3.3e. From these figures, the following observations are obtained: (i) curves obtained from rosette 2 and 3 never come together, indicating the presence of out-of-plane bending; (ii) the direction of the bending may change, e.g. it may be positive as in Fig. 3.3a or negative as in Fig. 3.3c; (iii) the curves of rosette 1 and 2 always lie apart, and the curve obtained from rosette 1 is always above that from rosette 2, i.e. the strain measured at rosette 1 is always smaller than that measured at rosette 2 no matter how the relative positions of these two gage rosettes to the test machine were, implying the normal strain field within the specimen test section is not uniform; (iv) the averaged stress-strain curves are in very good agreement with each other, confirming the elimination of out-of-plane bending effect on determination of E_2 by measuring strain on both sides of the test specimen.

(c) 10° Off-Axis Tensile Specimen

The 10° off-axis tensile specimen has been tested in the Tinius Olsen test machine four times and then in the Instron 4206 for another four times. The longitudinal normal stress-strain curves, ε_y versus σ_y, are shown in Fig. 3.4 and Fig. 3.5. It is seen that the curves obtained from rosette 2 and rosette 3 always depart from each other no matter how the specimen was positioned in the test machine and what kind of grip system was used, showing the presence of out-of-plane bending is not a problem caused by a special test machine or a special grip system, but a common problem for the tensile test of composites.

The shear strain γ_{xy} is plotted against the applied normal stress σ_y in Fig. 3.6. It is seen the curves obtained from rosette 2 and rosette 3 lie apart to a certain extent. Because there is the bending-twisting coupling effect when the fiber is oriented at an angle to the loading axis, i.e. the D_{16} and D_{26} in the laminate bending stiffness matrix are not zero, the existence of out-of-plane bending, as seen in Fig. 3.4, will induce twisting in the specimen. Therefore, it is not surprising that the shear strains measured at the front and back faces of the specimen are not identical.

By applying the transformation law, the shear stress and strain in the material coordinate system, the 1-2 plane, are obtained. The shear stress-strain curves in 1-2 plane are shown in Fig. 3.7a through Fig. 3.7d. According to equation (2.1), the value of shear strain γ_{12} is a combination of values of ε_x, ε_y and γ_{xy}. Hence, the inconsistency in the values obtained at front and back faces for these three strain components will affect the values of γ_{12} on different sides of the specimen. The departure of curves obtained from rosette 2 and rosette 3 shows the difference between the shear stress-strain responses of the front face and the back face of the specimen, as seen in Fig. 3.7. This difference will lead to an inconsistency in the calculated shear stiffness if the strain gage rosette is applied only on one side of the tensile specimen. However, when strain gage rosettes are used on both sides of the specimen, an average stress-strain response can be obtained. From Fig. 3.7e, it is seen that the average stress-strain curves from different tests are very consistent, especially at the initial stage, implying the effect of out-of-plane bending and twisting on the determination of initial shear stiffness of an off-axis tensile specimen can be eliminated by applying strain gage rosettes on both sides of the specimen. It is also seen in Fig. 3.7, the shear stress-strain curves obtained at rosette 1 and rosette 2 are not

coincident. They are fairly close at the initial stage but lie apart at higher strain levels, and the strain obtained at rosette 2 is always larger than that of rosette 1. This observation indicates that the shear strain field within the specimen test section is not uniform.

(d) 15° Off-Axis Tensile Specimen

The 15° off-axis tensile specimen has been tested in the Tinius Olsen test machine four times. The normal stress-strain curves in x-y plane are shown in Fig. 3.8. The existence of out-of-plane bending to a certain degree is revealed again from the departure of curves obtained at rosette 2 and rosette 3. The shear strain versus normal stress curves in x-y plane and shear stress-strain curves in 1-2 plane are shown in Fig. 3.9 and Fig. 3.10, respectively. Only two curves, obtained from rosette 1 and rosette 3, are shown in figure (b), (c) and (d) in Fig. 3.9 and 3.10 since the shear strain at rosette 2 cannot be calculated after the first test due to the damage of the strain gage oriented at 45° to the loading axis, Similar observations are obtained as in the 10° off-axis specimen, that is, the shear responses at front and back faces of the specimen are not coincident, which may caused by the specimen twisting.

(e) 45° Off-Axis Tensile Specimen.

The 45° specimen has been tested in the Tinius Olsen test machine four times and in the Instron 4206 test machine once. The normal stress-strain curves obtained from tests performed in Tinius Olsen test machine are shown in Fig. 3.11. The out-of-plane bending effect can be seen in each figure from the departure of curves obtained at rosette 2 and rosette 3. Consequently, the twisting effect is seen in the curves of γ_{xy} versus σ_y, as shown in Fig. 3.13. The twisting effect can also be seen in Fig. 3.12b, the curves of γ_{xy} versus σ_y obtained from the test conducted in Instron 4206 machine. This indicates that specimen twisting is a general problem for off-axis tensile test. It is shown again, as seen in Fig. 3.14e, that the twisting effect on the determination of initial shear stiffness can be eliminated by applying strain gage rosettes on both sides of the test specimen. Another observation of 45° specimen is the nonuniformity in shear deformation. In Fig. 3.12c and Fig. 3.14, the shear strain in 1-2 plane γ_{12} is plotted against the shear stress τ_{12}. It can be seen in each figure that the curves obtained at rosette 1 and rosette 2 lie apart to a certain extent. In some cases, these two curves are very close at the initial stage, but then lie

apart at higher strain levels, as in Fig. 3.14b and Fig. 3.14d. This indicates that the shear strain field within the specimen test section is not uniform, especially at higher shear strain levels.

3.2.4 Moiré Fringe Patterns

From moiré experiments conducted in the present study, the moiré fringe patterns, i.e. the contour maps of u displacement and v displacement (called u-field and v-field, respectively), are obtained for all the tested tensile specimens, except the 10° off-axis specimen, which fringe patterns were obtained in [53]. The fringe patterns analyzed in this study are shown in Fig. 3.15 to Fig. 3.19. For some specimens, e.g. 10° and 45° off-axis specimens, clear evidence of nonuniformity can be seen in the in-plane displacement field as shown in Fig. 3.17 and Fig. 3.19, and the bands of nonuniformity, as marked in the fringe patterns, are apparently coincident with the fiber orientation angle.

3.2.5 Strain Fields

(a) Localized Hybrid Method of Strain Analysis

The localized hybrid method [57] provided a convenient and efficient technique for the reduction of moiré fringe data. This technique, which is a combination of moiré interferometry and the finite element method, can be applied to any region of interest within the area covered by the moiré grating. The localized hybrid analysis consists of four main steps: (i) create a finite element mesh over the region of interest; (ii) calculate the displacements at some nodes of the mesh by manual differentiating the moiré fringe patterns; (iii) impose the displacements obtained on the finite element analysis; (iv) calculate stress and strain fields corresponding to the specified displacement fields using finite element analysis. In the current investigation, the full-node hybrid method was employed. In this method, the experimentally determined displacements of all the nodes of the mesh, including both the boundary and internal nodes, are specified in the finite element analysis. Since the displacements are all known, the strains are determined directly from the differentiation of the displacement fields.

In the present study, a square region at the center of the specimen was selected as the region of interest for all the tested specimen, except the 10° specimen, as shown in Fig. 3.20a. The dimension of the selected region was about 12 x 12 mm. This region was

divided into 256 rectangular thin shell elements, which have the ability to model a layered composite material. For the 10° off-axis specimen, a rectangular region, about 21 x 12 mm, was chosen, as shown in Fig. 3.20b. The rectangular region was divided into 264 thin shell elements. The u and v displacements (relative to a reference point on the specimen) at all the nodes were determined manually from the moiré fringe patterns with a linear interpolation scheme applied between two consecutive fringes. The stresses and strains were then calculated using ABAQUS finite element code. For the 10° off-axis specimen (made of AS4/3501-6), the input elastic constants were E_{11} = 144.8 GPa, E_{22} = 9.7 GPa, υ_{12} = 0.3 and G_{12} = 5.86 GPa [Hercules Prepreg Materials Characterization Data Package]. For all the other tensile specimens (made of AS4/3502), E_{11} = 121.4 GPa, E_{22} = 9.3 GPa, υ_{12} = 0.29 and G_{12} = 6.6 GPa are used as input elastic constants, which were obtained from preliminary tensile and shear tests of this material.

(b) Strain Contours

Based on the u and v displacement fringe patterns, stress and strain fields within the area covered by the finite element mesh for each tested specimen were obtained using the full-node hybrid method. The strain contours in the body and material coordinate systems (x-y plane and 1-2 plane) of the five specimens are shown in Fig. 3.21 through Fig. 3.28.

The normal strain field in the fiber direction of the 0° tensile specimen is quite uniform, as shown in Fig. 3.21; while the normal strain field perpendicular to the fiber direction of the 90° tensile specimen shows a certain degree of nonuniformity. The regions of equal strain value are oriented almost horizontally so that the strain field exhibits a band nature, as seen in Fig. 3.22.

The strain fields of the three off-axis tensile specimens, 10°, 15° and 45°, have some common features, as seen in Fig. 3.23 to Fig. 3.28: (i) all the strain component fields in the x-y plane are nonuniform with some evidence of bands of deformation occurring in the field; (ii) the orientation of the bands is almost coincident with the fiber angle, which is indicated in figures by line A-A; (iii) when the strains are transformed to the material coordinate system (1-2 plane), the distribution of normal strains may become more uniform, but the shear strain fields remain nonuniform.

(c) Strain Distributions

The strain distributions along the horizontal center line of each specimen can be obtained from the data of full-node hybrid analysis. The distributions of strain in the material coordinate system (1-2 plane) for all the five tested specimens are shown in Fig. 3.29 through Fig. 3.33. Each strain component in the 1-2 plane is normalized with respect to its average (the average across the horizontal center line). For 0° and 90° specimen, the normal strain distributions are quite uniform; while for the off-axis tensile specimens, the strain distributions are essentially not uniform and in some cases the nonuniformity is significant. For instance, the values of $\gamma_{12}/(\gamma_{12})_{avg}$ of 10° off-axis specimen range from 0.9 to 1.09. It should be noted here that when the average value of a strain component is very small the fluctuation observed in its distribution may be meaningless due to the sensitivity limitation of the optical system. The ε_{2avg} of 10° off-axis specimen, for example, is about 200 $\mu\varepsilon$, a variation of $\Delta(\varepsilon_2/\varepsilon_{2avg})$ of 0.2, which is equivalent to $\Delta\varepsilon_2$ = 40 $\mu\varepsilon$, is near the limit of the measuring sensitivity. For the same consideration, the distribution of ε_1 of 45° specimen is not presented since it has an average value of only 35 $\mu\varepsilon$.

3.2.6 Analytical and Numerical Analysis of 10° Off-Axis Tensile Specimen

It has been recognized since the late 1960's that the stress/strain field in the test section of a 10° off-axis tensile specimen is not uniform due to the effect of the end constraint and shear-extension coupling. An analytical model has been proposed in [6] to assess the nonuniformity, in which closed-form solutions of stress and strain fields were obtained. Since a boundary value problem can be solved analytically only when the boundary conditions are not complicated, this analytical model is based on a simplified end condition. Instead of applying full constraint at each end, only the center point of the end is constrained, that is, the displacements in the x and y directions as well as the rotation of the specimen in x-y plane about this point are all constrained. Finite element analyses have been performed in [7,9] to model the effect of various boundary conditions and to simulate the effect of possible end constraints. In order to evaluate the global nonuniformity of the strain field in the specimen test section predicted by the existing analytical and numerical models and to compare it with the moiré results, a 2-D linear elastic finite element analysis was performed in the current investigation.

The 10° off-axis tensile coupon was modeled, as shown in Fig. 3.34, with 500 rectangular shell elements (S4R5, the element that admits laminated composite properties) in the ABAQUS finite element code. The input elastic constants are the same as those used in the localized hybrid analysis. Two boundary conditions were applied, as shown in Fig. 3.34. In model 1, zero displacements in both x and y directions were specified at one end of the specimen. On the other end, displacement in x direction was constrained and a constant displacement in the y direction was specified at each node. This symmetric and fully constrained end condition was employed to simulate a perfect clamping. While in model 2, an antisymmetric end condition was imposed, in which only half of the nodes at each end were constrained. This case may be considered as representative of specimen misalignment.

The shear strain distributions along the horizontal center line of the test specimen, obtained by two different finite element models, are shown in Fig. 3.35. An analytical result [6] is also presented in the same figure for comparison. The shear strain is normalized with respect to ε_0, the longitudinal normal strain at the center of the specimen in the body coordinate system (x-y plane). It is seen in Fig. 3.35 that the result of numerical model 1 is in very good agreement with that of the analytical model, while numerical model 2 gives higher values. All of the models predict a very small amount of global nonuniformity in the shear strain field. Indeed, the specimen dimensions were chosen to achieve a nearly uniform field. The shear strain distributions are all symmetric about the y axis with the minimum value at the center. The numerical models, model 1 and model 2, may be considered as two extreme cases of the end constraint: perfect clamping and significant misalignment, thus, they are thought to provide the possible shear strain distributions in two extreme cases, if the effect of the end constraint can be simulated by such numerical models. However, neither one nor the analytical model is able to reproduce the shear strain distribution in Fig. 3.25.

In Fig. 3.36, the shear strain distribution predicted by the analytical model is plotted together with that obtained by full-node hybrid analysis. Compared with the curve obtained from the full-node hybrid method, the distribution of γ_{12} predicted by the analytical model is almost uniform. It has been suggested in [6] that when the aspect ratio of the specimen, L/h (L = length of the specimen, h = half-width), is large enough, the strain fields obtained from this analytical model will approach the uniform state. In

the present case, the aspect ratio of the specimen is 39.5, it is not surprising then that the shear strain field predicted by the analytical model is essentially uniform.

3.2.7 Discussion

(a) Bending-Twisting Coupling

It has been observed from the stress-strain curves obtained by strain-gage experiments, as discussed in section 3.2.3, that out-of-plane bending is usually present for an unidirectional tensile specimen. According to the classical laminate theory, the relationship between moments and flexural deformations of the specimen is:

$$\begin{Bmatrix} M_x \\ M_y \\ M_{xy} \end{Bmatrix} = \begin{bmatrix} D_{11} & D_{12} & D_{16} \\ D_{12} & D_{22} & D_{26} \\ D_{16} & D_{26} & D_{66} \end{bmatrix} = \begin{Bmatrix} \kappa_x \\ \kappa_y \\ \kappa_{xy} \end{Bmatrix} \tag{3.4}$$

or

$$\begin{Bmatrix} \kappa_x \\ \kappa_y \\ \kappa_{xy} \end{Bmatrix} = \begin{bmatrix} d_{11} & d_{12} & d_{16} \\ d_{12} & d_{22} & d_{26} \\ d_{16} & d_{26} & d_{66} \end{bmatrix} = \begin{Bmatrix} M_x \\ M_y \\ M_{xy} \end{Bmatrix} \tag{3.5}$$

where $[D_{ij}]$ and $[d_{ij}]$ are the flexural stiffness matrix and flexural compliance matrix of the specimen, respectively. M_x, M_y and M_{xy} are applied moments (according to the definition in [58], M_x is the moment about y-axis and M_y is the moment about x-axis). κ_x, κ_y and κ_{xy} are the middle surface curvatures. Assuming M_y is present due to improper loading and M_x, M_{xy} are all zero, the bending curvature κ_y is found from

$$\kappa_y = d_{22} M_y \tag{3.6}$$

Because the component d_{26} is not zero, there is coupling between bending and twisting. The twisting curvature κ_{xy} is determined by

$$\kappa_{xy} = d_{26} M_y \tag{3.7}$$

The ratio of $\kappa_{xy}/\kappa_y = d_{26}/d_{22}$ characterizes the twisting caused by a bending moment M_y. On the other hand, if only a twisting moment is involved in the improper loading and M_x, M_y are all zero, the flexural and twisting curvatures are found from

$$\kappa_y = d_{26} M_{xy} \tag{3.8}$$

and

$$\kappa_{xy} = d_{66} M_y \tag{3.9}$$

The ratio of d_{26}/d_{66} characterizes the bending caused by a torque. Note since the unidirectional specimen is a lamina, the components of $[D_{ij}]$ and $[d_{ij}]$ are proportional to the components of the transformed stiffness and compliance matrices of the lamina, $[\overline{C_{ij}}]$ and $[\overline{S_{ij}}]$, respectively. Therefore, the ratios of d_{26}/d_{22} and d_{26}/d_{66} only depend on the lamina properties as well as the fiber orientation.

The variations of normalized flexural compliance d_{22} and d_{66}, the ratios of d_{26}/d_{22} and d_{26}/d_{66} with the fiber angle (the angle between the fiber orientation and loading axis) are shown in Fig. 3.37 and Fig. 3.38, respectively. As seen in Fig. 3.37, the flexural compliance d_{22} is small when the fiber is oriented close to the loading axis, and the value of d_{22} increases as θ increases. The maximum value of d_{22} is achieved when the fiber orientation is perpendicular to the loading direction. While d_{66} achieves the maximum value at $\theta = 0°$ and $\theta = 90°$, indicating when θ is either small, close to 0°, or large, close to 90°, the specimen is easy to deform in twisting. In Fig. 3.38, it is seen that for this composite material (AS4/3502) the gradient of d_{26}/d_{22} is very high from $\theta = 0°$ to $\theta = 15°$, and d_{26}/d_{22} achieves its maximum value when θ is close to 15°. Then it decreases as θ decreases. The curve of d_{26}/d_{66} is more flat, compared with that of d_{26}/d_{22}. The maximum value of d_{26}/d_{66} occurs at $\theta = 35°$. Based on these curves, it is seen that when θ is small, the flexural deformation of the specimen is small for a given bending moment. However, the bending-twisting coupling is significant so that a small amount of flexural deformation may be accompanied by a large amount of twisting deformation. In addition, since the twisting compliance is large, a small undesirable torque will also result in large twisting deformation. On the other hand, when θ becomes larger, the coupling between bending and twisting becomes small, but the specimen is more easy to deform in flexure due to the large flexural compliance. In other words, the twisting induced by improper loading may be significant for specimens of both small and large fiber angles. Therefore, the twisting effect on the measurement of shear properties by an off-axis tensile specimen should not be ignored.

(b) Global Nonuniformity

It is shown in [6], as mentioned above, that the end constraint can induce nonuniformity in the stress/strain fields within the test section of an off-axis tensile specimen. Subsequently, the analytical model proposed in [6] was employed to calculate a correction factor for the determination of shear modulus [4]. For an off-axis tensile specimen with fiber oriented at an angle θ to the loading axis, the correction factor is defined as

$$CF = \frac{G_{12}}{G_{12}^*} = \frac{\tau_{12}}{\tau_{12}^*} = \frac{1 - \dfrac{\beta(\cos^2\theta - \sin^2\theta)}{\sin\theta\cos\theta}}{(1 - \frac{2}{3}\eta)} \tag{3.10}$$

where τ_{12}^* is the apparent shear stress obtained by equation (2.1), τ_{12} is the shear stress at the center of the specimen obtained from the analytical model, β and η are parameters defined as

$$\beta = -\frac{6\,(\frac{h}{L})^2(\frac{\overline{S_{16}}}{\overline{S_{11}}})}{1 + 6\,(\frac{h}{L})^2(\frac{\overline{S_{66}}}{\overline{S_{11}}})} \tag{3.11}$$

$$\eta = \frac{6\,(\frac{h}{L})^2(\frac{\overline{S_{16}}}{\overline{S_{11}}})^2}{1 + 6\,(\frac{h}{L})^2(\frac{\overline{S_{66}}}{\overline{S_{11}}})} \tag{3.12}$$

where h and L are the half-width and length of the specimen, respectively, $\overline{S_{ij}}$ are the components of the reduced transformed compliance matrix of the specimen. In Fig. 3.39, the correction factor obtained from (3.10) is plotted against θ, the angle between the fiber orientation and loading axis. The material considered in this calculation is AS4/3502. The value of h is 0.64 cm, and two different values are used for L, that is, L = 23.3 cm and L = 15.67 cm. The former is the length of the specimen and the latter is the length between two grips. The effective length, the length between constraints at two ends of a real specimen, should be between these two values. It is seen that the degree of nonuniformity of the shear strain field decreases as θ increases. The correction factors are about 0.97 and 1.003 for 15° and 45° specimens, respectively. It should be noted here

that the second term in the numerator in equation (3.10) represents the correction for the induced shear force and only the denominator represents the correction for the nonuniformity [4]. In our cases, the denominators are 0.98 and 0.997 for 15° and 45° specimen, respectively, indicating the stress/strain fields are essentially uniform. Thus the correction factor is primarily effective in correcting the error due to the induced shear force rather than the nonuniformity. The situation is the same for 10° specimen, as discussed in section 3.2.6. It is clear then that the end constraint effect predicted by the analytical model [4,6] only induces a very small amount of global nonuniformity in the stress/strain field when the specimen aspect ratio is large, as in our cases.

It is known from the discussion above that besides the end constraint effect, there may also exist undesirable out-of-plane bending and twisting due to improper loading and bending-twisting coupling. Their effect on the global nonuniformity of the in-plane strain fields has not been identified yet, which needs further investigation.

(c) Local Nonuniformity

The significant nonuniformity observed in the strain fields, which can not be predicted by the existing analytical and numerical models, and the coincidence of the orientation of the bands occurring in the strain fields with the orientation of the fiber all implies that the nonuniform deformation may be associated with the material inhomogeneity. It should be emphasized here that the determination of the strains in the full-node hybrid analysis is merely the differentiation of the input displacement fields and no assumptions of material homogeneity are made. Therefore, the full-node hybrid method is able to capture, if there is any, the localized nonuniformity caused by material inhomogeneity.

In order to examine the material inhomogeneity, two samples were sectioned from the 10° off-axis specimen and 45° off-axis specimen used in the moiré experiments, respectively. The samples were cut through the gage section, in the location of grating where the photographs of fringe pattern were taken. The samples were then mounted and polished. The 1.0 micron alpha alumina powders were used for final polishing. The micrographs shown in Fig. 3.40 were taken from the polished samples using an optical microscope with magnification of 20X. The micrographs are cross-sectional view of full width of the specimen with the grating on the surface ply at the bottom edge. In Fig. 3.40a, obvious material inhomogeneity is revealed. The resin rich regions are found here

and there, not only between but also within the layers. It is considered that the observed material inhomogeneity may be responsible for the significant nonuniform deformation in 10° off-axis specimen captured by moiré interferometry. In Fig. 3.40b, the material of this examined sample appears more uniform. No obvious material inhomogeneity can be seen by eyes around the surface. Since the distribution of fiber density along the width of the specimen can not be determined from the micrographs, the degree of material homogeneity for this sample is not well understood yet. However, the observation that the 45° off-axis specimen exhibited less nonuniformity in deformation than the 10° specimen indicates the degree of nonuniformity of deformation is associated with the degree of material homogeneity. Recall that these two samples were made of two different composites, AS4/3501-6 and AS4/3502. The difference between the degree of material uniformity of these two samples may result from the difference between the material themselves or from the difference in the manufacture processing of the prepregs.

(d) Significance of Nonuniformity on the Measurement of Mechanical Properties

In an off-axis tensile test, the strains in the body coordinate system (x-y plane), ε_x, ε_y, and γ_{xy}, are either measured or calculated directly by the strain gages. If the strain fields are uniform, the local strains measured over a tiny area will represent the value for the whole field, regardless the size and the location of the strain gage. However, as is seen in Fig. 3.23, Fig. 3.25 and Fig. 3.27, all the strain component fields in the x-y coordinate system are nonuniform with some evidence of bands of deformation occurring in each field. The average variation in the strain values between the peaks and valleys is about 13%, and in some fields, the variations in the strain values between peaks and valleys may even reach 18%. The presence of nonuniformity may result in inconsistency in the measurement of shear properties. Since the nonuniformity is seen in the strain distributions across a width of only 12 mm, small variations of the location of the strain gage, from specimen to specimen, relative to the nonuniform bands may lead to different measurements of strain values. In addition, the nonuniformity may vary from specimen to specimen. Thus, the inconsistency in the determination of the shear property by an off-axis tensile test is anticipated.

The nonuniformity in the strain fields also influences the determination of engineering properties of the specimen. Originally, the engineering properties, E_x, E_y, υ_{xy}, G_{xy}, $\eta_{xy,x}$ and $\eta_{xy,y}$, are defined to characterize the mechanical behaviors of a laminate in the

loading coordinate system. As properties of a laminate, they should be constants over the whole laminate. However, because of the presence of nonuniformity, these quantities will have different values when measured at different positions. For instance, for the 10° specimen, within the analyzed region (area = 2.7 cm^2) the values of the coefficient of mutual influence, $\eta_{xy,y} = \gamma_{xy} / \varepsilon_y$, range from 2.21 to 2.4, and the values of υ_{xy} range from 0.30 to 0.33. Thus, these quantities would be more like point-properties rather than field-properties.

(e) Effects of Nonuniformity on the Failure Prediction

Usually, failure criteria are established based on the assumptions of material homogeneity and uniform state of stress/strain fields, and the critical stresses used in the criteria are obtained as the ultimate forces average a cross-section. When the stress/strain fields in the 1-2 coordinate system are not uniform, errors might be induced in the failure prediction, which can be shown in the following example.

The distributions of strains along the horizontal center line of the 10° off-axis specimen, which are normalized with respect to their critical values given in [59], are shown in Fig. 3.41. It should be noted here that since it is difficult to measure the ultimate strains directly, the critical values given in [59] are obtained in an indirect way, that is, $(\varepsilon_1)_{cr} = (\sigma_1)_{cr} / E_1$, $(\varepsilon_2)_{cr} = (\sigma_2)_{cr} / E_2$, and $(\gamma_{12})_{cr} = (\tau_{12})_{cr} / G_{12}$. As is seen in Fig. 3.40, at this load level, the average longitudinal normal strain ε_1 is about 6% of its critical value, the average transverse normal strain ε_2 is about 3% of its critical value, and the average shear strain γ_{12} is about 25% of its critical value. However, because of the presence of nonuniformity, higher values are reached at some points. For instance, in the shear strain field, the highest value reached is about 27% of its critical value, which is about 8% higher than its average. In addition, because of the banded nature of the shear strain field, the higher values in the whole field will appear not at individual points, but in the form of a band. Therefore, failure may occur along this band before the average shear strain reaches its critical value.

3.3 Nonuniform Deformation in Laminated Fiber Composite

3.3.1 Material and Specimen Preparation

Two ± 45° specimens were studied in the present investigation. One was machined from a 24 cross-ply graphite/epoxy panel (AS4/3502). This panel was made of commercial prepreg manufactured by Hercules and cured according to the manufacturer's instruction. This specimen has dimensions of 25.4 cm x 2.54 cm (length x width). It was tested by the conventional strain gage measurement. Three strain gage rosettes (Micro Measurements EA-13-125-TV350) were mounted on the specimen in the same way shown in Fig. 3.1. Each rosette consists of two elements: one is oriented in 0°(x) direction and the other is oriented in 90°(y) direction. The instrumented specimen was tested in two test machines: the screw-driven test machine Tinius Olsen and the hydraulic test machine Instron 4206. The other specimen was made of AS4/3501-6. This specimen has been previously tested with moiré interferometry in [53]. In this study, only the moiré fringe patterns of the specimen, obtained in [53], were analyzed by the full-node hybrid method.

3.3.2 Stress-Strain Curves

The ± 45° tensile specimen has been tested in the Tinius Olsen test machine for four times and the in the Instron 4206 test machine for another four times differing in positions of the specimen relative to the test machine as described in section 3.2.3. The longitudinal normal stress-strain curves are shown in Fig. 3.42 and Fig. 3.43. It is seen that the difference between the curves obtained at rosette 2 and rosette 3 are relatively small, compared with that observed in the off-axis tensile specimens, indicating the out-of-plane bending is not significant for a ± 45° tensile specimen. The shear stress-strain curves in 1-2 plane are shown in Fig. 3.44. Since the ratio of d_{26}/d_{22} of this ± 45° specimen is 0.036 and $d_{66}/(d_{66})_{0°}$ is 0.123, neither undesirable bending moment nor torque can cause significant twisting deformation. Hence only a slight difference between the curves obtained from front and back faces of the specimen is seen in these figures. From the resistance to twisting induced by improper loading point of view, thus, ± 45° tensile specimen is better than any of the off-axis tensile specimens. In addition, that the curve obtained at rosette 1 is always above that obtained at rosette 2 reveals the nonuniformity of the shear strain field within the test section.

3.3.3 Strain Fields

The full-node hybrid method was employed to obtain the strain fields from the moiré fringe patterns for a ± 45° tensile specimen, obtained in [53]. The finite element mesh used in the localized hybrid analysis is shown in Fig. 3.45. This square region is about 23 x 23 mm and divided into 196 rectangular thin shell elements. A pair of fringe pattern is shown in Fig. 3.46. In the u displacement field, lines of nonuniformity at 45° to the loading direction can be seen clearly. By differentiating the displacement fields, strain fields were obtained using the full-node hybrid method. The strain contours in the material coordinate system, 1-2 plane, are shown in Fig. 3.47. Bands of nonuniformity, as observed in the strain fields of unidirectional specimens, also occur in the laminated specimen, and the orientation of the bands is in the 45° direction.

As mentioned above, the ± 45° tensile specimen has much stronger resistance against the twisting caused by improper loading than the off-axis tensile specimen. If the twisting does have some effect on the global nonuniformity of in-plane deformation, the effect is supposed to be much smaller for the ± 45 tensile specimen than for the off-axis specimen. However, the nonuniformity in the strain fields of the ± 45° specimen is still significant. Considering the moiré fringe patterns are the contour maps of displacement on the surface of the specimen, the nonuniformity may also be associated with the material inhomogeneity.

3.4 Nonuniform Deformation in Hybrid Fabric Composite

3.4.1 Material and Specimen Preparation

The material tested is a new industrial grade thermoplastic composites, glass/PETP (PETP=Polyethylen Terephtalats), developed by DSM (Dutch State Mines). Iosipescu specimens of dimensions shown in Fig. 3.48 were cut from two 30 x 21 cm panels of glass/PETP. These panels were supplied by DSM and labeled as 90/10 material, which indicates that 90% of the fibers are in one direction and 10% of the fibers are in the plane of the panel at 90° to the principal fiber direction. Specimens were prepared with 90% of the fibers either parallel or perpendicular to the specimen longitudinal axis and designated as 0° and 90° specimens, respectively. The nominal thickness of the specimens is 1.9 mm. A diamond-tipped end mill was used in cutting the V-notches. Note that the notch

angle in these specimens was 110°. Each specimen was then ground flat on the long edges.

Two Iosipescu specimens of different material orientations, i.e. 0° and 90°, were investigated with the moiré interferometry technique. A two-element strain gage rosette, oriented at ± 45° to the specimen longitudinal axis, was applied on one face of the Iosipescu specimen, and a crossed-line diffraction grating was applied to the opposite face. The specimen grating had a frequency of 1200 lines per mm, and covered the width of the specimen, extending approximately 10 mm on each side of the notches. The instrumented specimens were inserted in the modified Wyoming fixture. The side of the specimen with strain gage rosette faced the back of the fixture and the side with specimen grating faced the front. The specimen and the fixture were installed in the universal testing machine. A three-mirror interferometer [56] was positioned in front of the fixture. Before the load was applied to the specimen, the interferometer was tuned to give no-load (null-field) fringe patterns. Load was then applied to the specimen until a predetermined value was reached. While under constant loading, longitudinal (u) and transverse (v) displacement fringe patterns were recorded photographically. Three sets of fringe patterns were obtained during each test.

3.4.2 Moiré Fringe Patterns

A pair of typical moiré fringe pattern for the 0° specimen configuration is shown in Fig. 3.50. The nonuniformity can be readily detected in the u-field, where dense and relatively less dense fringe bands are observed. It is considered that the nonuniformity is caused by the material inhomogeneity.

3.4.3 Finite Element Analysis

It has been shown the shear stress field in the test section of the Iosipescu specimen is nonuniform and that inconsistencies between the apparent shear moduli of unidirectional 0° and 90° specimens have been widely documented [4, 25, 53, 60-63]. To evaluate the nonuniformity of the shear stress field in the test section of the 90/10 hybrid composite and its effect on the shear modulus measurement, a linear-elastic 2-D finite element analysis was performed.

The Iosipescu specimen of both 0° and 90° configurations was modeled, as shown in Fig. 3.49, with 1495 constant strain elements using the ABAQUS finite element code. A refine mesh was used in the vicinity of the notch roots. The input elastic constants are E_x = 30.8 GPa, E_y = 14.8 GPa, υ_{xy} = 0.21, G_{xy} = 4.0 GPa, which are the values obtained from the preliminary tensile and shear tests, respectively. A trial-and-error iterative approach [26] was employed and the finite element models corresponding to the 0° and 90° specimens were obtained where the criteria of no displacement interference and no tensile force along the specimen long edges were satisfied. Finite element models for 0° and 90° specimen configurations are shown in Fig. 3.51.

3.4.4 Discussion

The shear strain distributions along the center line between notches of the 0° and 90° specimens obtained from moiré fringe patterns are shown in Fig. 3.52a and Fig. 3.52b, respectively, together with those obtained from finite element analysis for comparison. The differences between the strain distributions obtained from the finite element analysis and moiré data are important. The former is smooth and symmetric about the center line of y = 0 because of the assumption of material homogeneity and the application of ideal boundary conditions. In contrast, the strain distribution obtained experimentally is neither smooth nor symmetric. Since glass/PETP material system is a hybrid of unidirectional fibers and fabric rather than a homogeneous material, it is not surprising that the strain distribution curve is not smooth so that the strain distributions reflect the different local responses at fiber bundles and resin rich regions. Furthermore, the real boundary conditions may not be exactly antisymmetric, as applied in finite element analysis, due to the uncertainty of load points [25], which is also observed in the non-symmetric strain distribution obtained from the moiré experiments. The fact that the strain distributions at different load levels are essentially superposed indicates that within a certain load range the load level has no effect on the shear strain distributions. Moreover, similar fluctuations apparent at different load levels confirms that the local responses are resolved experimentally and correspond to the material architecture.

It can be seen from Fig. 3.52, that the strain distribution curves obtained from moiré experiments oscillate around the numerically predicted strain distributions. Thus, the numerical results provide the global "average" for the local responses. Based on this observation, it is concluded that the 2-D finite element analysis is still valid for prediction

of the global (smeared property) shear strain distribution and calculation of the correction factors for the hybrid fabric composite material system. It should be emphasized here that the numerical solution is only valid for the assessment of global nonuniformity but not for the failure prediction. Since at the peaks of shear strain distribution obtained from moiré test the value may be 25% above the average value obtained from finite element analysis, the failure prediction based on numerical solution will be an underestimate.

CHAPTER 4. NONLINEAR SHEAR RESPONSE

4.1 Introduction

It has been recognized since the fiber reinforced plastics were first developed that when the load is applied transverse to the fiber direction, the composite exhibits physically nonlinear behavior. Nonlinearity has been widely documented in transverse tension and shear responses. Since the degree of nonlinearity in shear is much higher than that in transverse tension, the issue of nonlinearity is primarily associated with shear behavior. In addition, it has been found from the experimental observations that for fiber reinforced plastic composites no yield point can be well defined in the shear stress-strain response. The nonlinearity arises almost from the beginning of the stress-strain curve. Therefore, the shear behavior of fiber composites can not be well understood without accounting for nonlinearity.

When dealing with a material with nonlinear behavior, the first problem is how to describe its stress-strain relationship. In the past twenty years, lots of effort has been made on analytical approaches and a number of constitutive models has been proposed to simulate and predict the nonlinear shear response. However, experimental data on the actual shear behavior of various fiber composites, especially those recently developed composites, is not sufficient. Experimental study is necessary not only for the analysis and design of composite structures but also for the validation of the proposed response functions. Moreover, it is well known that the nonuniformity in the stress/strain field is a common problem for most of the shear test methods. In order to take into account the effect of global nonuniformity in the specimen test section, the use of correction factor is suggested in the determination of shear properties. Theoretically, the correction factors, calculated either analytically as for the off-axis tensile specimen or numerically as for the Iosipescu specimen, are valid only in the linear range because all the calculations are based on linear elasticity theory. However, for most fibrous composites, the shear response is mainly, if not entirely, nonlinear. The question is then posed that if the correction factors used in the linear range could also be used in the nonlinear range. The answer is affirmative only when there is no significant change in the global nonuniformity under the effect of material nonlinearity. Therefore, the judgment of the validity of correction factors in the nonlinear range requires an experimental investigation of nonlinear shear strain distribution.

In this chapter, shear behavior of various fiber composites obtained from the Iosipescu shear tests are described and the characterization of nonlinear shear response is discussed. Further, the shear strain distribution in nonlinear range is examined by moiré interferometry as well as strain gage measurement. Finally, the issue of the determination of shear strength is addressed.

4.2 Characterization of Nonlinear Shear Behavior

4.2.1 Shear Stress-Strain Curves

Four different composite materials, AS4/3502, AS4/LaRC-TPI, AS4/PEEK (APC-2) and glass/PETP, were tested by Iosipescu shear tests. These composites can be categorized into three classes: aerospace grade thermoset composite (AS4/3502), aerospace grade thermoplastic composite (AS4/LaRC-TPI, AS4/PEEK) and industrial grade thermoplastic composite (glass/PETP). The typical shear stress-strain curve of these composite material systems obtained from Iosipescu 90° specimen are shown in Fig. 4.1. It is seen that all the curves are not linear. Since shear behavior is matrix-dominated, the degree of nonlinearity of a composite material system is primarily related to the mechanical behavior of the matrix. Consequently, the graphite/epoxy composites, AS4/3502, AS4/LaRC-TPI and AS4/PEEK, of same fiber but different matrix materials (and possibly different interface/interphases) exhibit different shear responses. Moreover, the shear response of glass/PETP, based on commodity resin, is quite different from that of the graphite/epoxy material system.

To describe the nonlinear shear stress-strain response, curve fitting technique is employed. The polynomial function is found to provide a convenient fit to all the shear stress-strain curves shown in Fig. 4.1. The general form of the curve fit equation is

$$\tau = A_1 \gamma - A_2 \gamma^2 + A_3 \gamma^3 + A_4 \gamma^4 \tag{4.1}$$

Differentiating equation (4.1) will give an expression for the tangential shear stiffness, that is:

$$G_{tan} = d\tau / d\gamma = A_1 - 2.0 \times A_2 \gamma + 3.0 \times A_3 \gamma^2 + 4.0 \times A_4 \gamma^3 \tag{4.2}$$

where A_1 represents the initial shear modulus. It can be seen from equation (4.2) that the nonlinearity of shear response induces a reduction in shear stiffness as the shear strain

increases and the degree of nonlinearity is determined by the combination of A_2, A_3 and A_4. Among the four composites shown in Fig. 4.1, only glass/PETP requires a fourth order polynomial to fit its shear stress-strain curve. For AS4/PEEK, the fitting function is of third order. While for AS4/3502 and AS4/LaRC-TPI, a polynomial of second order is sufficient for good fitting. In such cases, the degree of nonlinearity is evaluated by the value of A_2 only. Choosing a polynomial as the fitting function has an advantage that one of the coefficients represents the initial shear modulus. It is shown that by using the curve fitting technique, the nonlinear shear response can be approximated by an analytical expression, which is needed for the stress analysis and structure design.

4.2.2 Shear Stiffness

Shear stiffness is one of the basic properties used for characterization of a material. The conventional definition of shear stiffness is the ratio of shear stress to corresponding shear strain, that is

$$G = \tau / \gamma \tag{4.3}$$

For a linear elastic material, the shear stiffness defined as above is a constant throughout the response so that it is meaningful. For a nonlinear material, however, the ratio of shear stress and shear strain will vary as a function of shear stress level. The definition given in equation (4.4) is, hence, no longer suitable for representing the shear stiffness. Secant shear modulus is a widely used definition for initial shear modulus, which is defined as

$$G_{sec} = \frac{\tau - \tau_0}{\gamma - \gamma_0} \tag{4.4}$$

where τ_0 and γ_0 are corresponding to the origin of the τ - γ coordinates. Geometrically, it represents the secant of the curve at a given point. For the linear case, the secant of a curve at a given point is identical with the tangent of the curve as well as the curve itself. For the nonlinear case, however, beyond certain point of a curve, the secant will deviate from the tangent of the curve and the curve itself so that the secant shear modulus becomes physically meaningless. An alternative definition of shear modulus is the tangential shear modulus, defined as

$$G_{tan} = \frac{d\tau}{d\gamma} = \frac{\Delta\tau}{\Delta\gamma} \tag{4.5}$$

This definition is more rational since it represents approximately the slope of the curve. It is identical with the secant shear modulus at the origin of the shear stress-strain curve and is reduced to the traditionally defined shear modulus in the linear case. Thus, the tangential shear modulus presents itself as an appropriate definition for shear stiffness in the nonlinear case. Nevertheless, in practice, an arbitrary determination of the increments of τ and γ might result in an inconsistency in the determination of G_{tan}. Then, the curve fitting technique proves to be an effective tool for eliminating the subjectivity in the determination of G_{tan}. By using this technique, determining tangential shear modulus is equivalent to differentiating the curve equation obtained by the curve fit, as shown in equation (4.2). Since a unique derivative exists for a given polynomial, the determination of G_{tan} can be carried out objectively.

In Fig. 4.2, the tangential shear moduli of the tested composite materials, obtained from the curve function by equation (4.2), are plotted as function of the shear strain. This figure provides a clear picture of how the shear stiffness varies under the effect of different degree of nonlinearity. For instance, it is seen that the starting points of curves for AS4/3502 and for AS4/PEEK are very close, which means the values of initial shear modulus of these two composites are almost identical (for AS4/3502, G_{ini} = 5.15 GPa; for AS4/PEEK, G_{ini} = 4.95 GPa). However, the curve for AS4/PEEK is then much lower than that for AS4/3502, indicating that the reduction of shear stiffness for AS4/PEEK is much faster than that for AS4/3502 (e.g. for AS4/3502, $G_{1.0\%}$ = 3.74 GPa; for AS4/PEEK, $G_{1.0\%}$ = 2.71 GPa) because of the higher degree of nonlinearity. Another interesting observation is the comparison between the shear stiffness of AS4/LaRC-TPI and AS4/PEEK at different strain levels. The initial shear modulus of AS4/PEEK is 4.95 GPa, which is about 25% higher than that of AS4/LaRC-TPI, 3.94 GPa. At γ = 1.0%, the shear stiffness of AS4/PEEK reduces to 2.71 GPa, while the shear stiffness of AS4/LaRC-TPI is 3.1 GPa. The former is about 13% lower than the latter. It is obvious then that using the initial shear modulus as the only parameter of stiffness for the evaluation of shear behavior of composite materials is inadequate due to the presence of nonlinearity. It is suggested that other coefficients in the fitting polynomial function, which describe the degree of nonlinearity, being considered together with the initial shear modulus. Particularly, when the shear stress-strain curve is fitted by a second order polynomial, two-parameter evaluation is effective and convenient, in which one parameter shows the shear stiffness in the initial stage, the other one characterizes the rate of shear stiffness reduction.

4.3 Nonlinear Effect on Shear Strain Distribution

4.3.1 Strain Gage Experiment

In order to examine the effect of nonlinearity on the shear strain distribution, strain gage experiments of Iosipescu specimen were performed. The material tested was AS4/3502. It has been observed from preliminary Iosipescu shear tests of this material that shear response of 0° configuration exhibited more nonlinearity and the failure occurred at much higher strain level than that of the 90° configuration. In addition, the shear responses obtained from the front and back faces of the 0° specimen were almost identical. Therefore, the 0° Iosipescu specimen was chosen for the examination. The notch angle of the 0° specimen is 90°. In order to record shear strain at different locations, one strain gage rosette was mounted at the center of the specimen as usual, the other one on the opposite side was bonded above the center and close to one of the notch tips. A scheme of the arrangement of strain gage rosettes on both sides of the specimen is shown in Fig. 4.3. Shear stress-strain curves obtained at these two gage rosettes were shown in Fig. 4.4. It is seen that the strain measured at the middle of the specimen is always smaller than that measured at the edge due to the global nonuniformity. From the observations during the tests, it was found that the discontinuity point in the curve appearing close to $\gamma = 2.0\%$ corresponds to the occurrence of first crack at one of the notch tips. In Fig. 4.5, shear strain measured at the edge of the specimen was plotted against that measured at the middle of the specimen. It is seen that there is a straight line with constant slope until the occurrence of discontinuity, which also corresponds to the initiating of the first crack. This observation implies that before the appearance of the first crack, there is no change in the ratio of shear strains measured at different locations even though the curve is in obviously nonlinear range. When a crack initiated at one of the notch tips, the loading is released within the vicinity of the crack. Consequently, the strain decreases in that region and the shear strain in the whole test section is redistributed.

A numerical analysis by using linear elastic finite element method was performed to assess the global nonuniformity in the linear range for 0° Iosipescu specimen. The mesh used in the analysis was the same as shown in Fig. 3.48 and the determination of boundary conditions followed the procedure described in section 3.4.3. The normalized shear strain distribution along the notch axis, obtained from finite element analysis, is shown in Fig. 4.6. It can be seen that the shear strain at the center is less than the average and increases

gradually when the location is away from the center. The peak is reached at areas close to the notch tips. If the finite element mesh in the vicinity of the notch tip is fine enough, the shear strain is expected to drop to zero to satisfy the free edge boundary condition. From the shear strain distribution curve, the ratio of the shear strain at the location of edge rosette to that at the location of middle rosette can be determined, which is 1.10. The same ratio obtained from Fig. 4.5 is about 1.17. Since the shear strain distribution of a 0° Iosipescu specimen is sensitive to the location of the load points [25], it is not surprising that the ratio obtained from numerical analysis, where an ideal antisymmetric boundary condition is applied, is not exactly the same as that obtained from a real test.

4.3.2 Moiré Interferometry

A moiré experiment was performed on a 0° Iosipescu specimen of graphite/epoxy composite AS4/3502 to examine the shear strain distribution in the nonlinear range of the shear response. In the setup with a high frequency grating, the specimen is usually tested in a shear strain range below 1% so that a reasonable number of fringes can be easily distinguished. In order to record information up to a shear strain level of 1.5% or higher, a modification was made on the conventional test procedure. Instead of loading the specimen from an initial null field, a certain amount of shear strain component, which has a sign opposite to the real shear strain, was added to the measurement, in which the status is set as the initial reference. In the present investigation, a strain component of 1% was added. With the help of this modification, moiré fringe patterns could be analyzed up to a shear strain level of 1.7%, at which a crack had already occurred at one of the notch tips.

A pair of fringe patterns at γ_{avg} = 1.1% is shown in Fig. 4.8. The zig-zag nature of the u displacement field, as documented in [25] for composite AS4/3501-6, has been observed again, which is considered to be the result of material inhomogeneity. The normalized shear strain distributions along the notch axis at different shear strain levels are shown in Fig. 4.7. The finite element result is also plotted in Fig. 4.7 for comparison. Note since the gradient of shear strain near the notch tips is very high, by using manual differentiation of the displacement field to get the shear strain is unable at the notch tips to reflect the significant variation in those areas so that zero shear strain can not be seen at the ends of the curves. It is seen that the shear strain distributions at different strain levels are all similar and generally close to the linear elastic result except the one obtained after the first crack has occurred. This observation indicates that material nonlinearity has no effect on the shear

strain distribution for the tested material, which further confirms the observation in strain gage experiments.

From the above observations, the following conclusions can be drawn. First, the global nonuniformity in the shear strain field of Iosipescu specimen predicted by the numerical analysis has been verified by both the strain gage and moiré experiments. In addition, the global nonuniformity shown in the linear range is not to change when the material becomes nonlinear. Accordingly, the correction factor based on a linear elastic calculation can also be used in the nonlinear range for the determination of shear properties.

4.4 Determination of Shear Strength

One of the challenges for the composites community is the determination of shear strength. Since virtually none of the existing shear test methods is able to offer a pure shear state in the specimen test section, it is difficult to determine the shear strength experimentally. The apparent failure shear stress obtained by experiments is popularly used for defining the shear strength. However, the apparent failure stress is test-method dependent. One of the reasons is that specimens of the same material but tested by different test methods usually fail in different modes. For the Iosipescu shear test, inconsistency of the apparent failure shear stresses was also found in different specimen configurations, as reported in [25].

In addition to the failure mode, failure strain should be another factor of concern. As discussed before, the shear behavior of a composite is dominated by the mechanical properties of the matrix material as well as the interfacial bond strength. Accordingly, the improvements of the property of matrix material and interface are expected to induce some changes in the shear performance of the composite. The shear behavior of recently developed composites do show some features differing from the shear behavior of the traditional thermoset composites. One of the changes is the increase of failure shear strain. For instance, it has been documented in [5,25] that the shear response of 90° Iosipescu specimen was of relatively brittle nature and the failure of 90° Iosipescu specimen always occurred at very low strain level. These features are, however, less seen in the shear behavior of 90° Iosipescu specimen of thermoplastic composites. For all the thermoplastic composites tested in the present investigation, including those discussed in Chapter 5, the 90° Iosipescu specimens also exhibited obviously nonlinear shear response. The degree of

nonlinearity varies with composite material systems. For some composite materials, the degree of nonlinearity is fairly high. In addition, the 90° Iosipescu specimen can sustain shear strain beyond 2%, sometimes even beyond the range of strain gage. When the degree of nonlinearity is very high, such as for glass/PETP, the tested specimen deformed continuously as the load was gradually increased, and none of the specimen fractured in tests. Even though a load drop was observed, the corresponding deformation was already beyond the range of strain gage. Therefore, from the stiffness point of view, failure shear stress corresponding to a high failure shear strain, no matter the failure is defined as specimen fracture or a load drop, is not adequate to be used as shear strength of a composite.

A characteristic shear stress is then needed for defining the shear strength. One possibility is employing the offset method, which is analogous to that used to define a quasi-yield point for metals without a distinct yield point. According to this so-called 0.2-percent offset method, a line is drawn through a strain of 0.2% with a slope of the initial stiffness. The intersection of this line with the stress-strain curve defines the shear strength. For metals, the variation of initial stiffness is very small, e.g. the variation of Young's modulus of commonly used steels is about 7%. Consequently, the strains corresponding to the defined yield stress for different steels would be very close. On the contrary, the range of initial shear modulus for composites is fairly large. For instance, the initial shear moduli of the composites tested in the present study range from 3.6 GPa to 6.2 GPa. The shear strain corresponding to the intersection can be determined analytically from

$$A_1 (\gamma - 0.2) = A_1 \gamma - A_2 \times \gamma^2 + A_3 \times \gamma^3 + A_4 \times \gamma^4 \qquad (4.6)$$

The range of the corresponding shear strain for the composites tested in this study is found from 0.9% to 1.3%. Besides, this definition is merely conventional and physically meaningless.

In practice, shear strength is required not only for structure design as a critical value but also for comparison of shear behavior of different materials. From the comparison point of view, it is suggested that the capability of carrying load at certain shear strain level be used as a criterion. In order to establish such a criterion, a shear strain level should be selected. By studying the shear behavior of various composites tested in this investigation, it was found that for most thermoplastic composites the failure shear strain is higher than 3.0%.

For such composites, shear stress at some intermediate shear strains, e.g. from $\gamma = 1.5\%$ to $\gamma = 2.5\%$, can be used as a characteristic shear stress. As an example, the shear stress at $\gamma = 2.0\%$ together with the ultimate shear stress for the Iosipescu specimens of AS4/PEEK (APC-2) are shown in Fig. 4.9. It can be seen that the difference between the ultimate shear stress for 0° and 90° specimens are relatively large due to different failure modes. The 0° specimens failed with cracks occurring at the notch tips and propagating along the fiber direction; while the failure of 90° specimens was a fracture of specimen caused by the propagation of a crack close to the notch axis and parallel to the fiber direction. When different specimen configurations are compared with shear stress at the same strain level, $\gamma = 2.0\%$, the values of this characteristic stress for 0° and 90° are more close. If a correction factor is applied to take into account of the global nonuniformity in the shear strain fields, the value of shear stress at $\gamma = 2.0\%$ for 0° specimen will be decreased while that for 90° specimen will be increased. Consequently, a good agreement is expected to be achieved. Another example is shown in Fig. 4.10, where the shear stress at $\gamma = 2.0\%$ for Iosipescu specimens of glass/PETP is presented. Here, the values of shear stress at $\gamma = 2.0\%$ for different specimen configurations, 0° and 90°, are also quite consistent. From these examples, it is seen that shear stress at certain shear strain level, for instance, $\gamma = 2.0\%$, can be used as an alternative for defining shear strength from an engineering point of view.

CHAPTER 5. SHEAR RESPONSE OF NOVEL COMPOSITES

5.1 Introduction

PEEK (polyetheretherketone) composites have been an area of great interests for the composite community in recent years because the PEEK composites possess several significant advantages over the epoxy composites. These include improved toughness, better impact resistance, infinite prepreg shelf life, ease of repair and reduced sensitivity to water. There are several methods of producing PEEK prepreg and composites, one of which is suspension prepregging. In this method, a binder is used to hold the prepregs together before consolidation. Since the binder can form a high performance polymer upon consolidation, the question is posed that if the binder has any effect on the mechanical properties of the composites. In this chapter, AS4/PEEK material system with immiscible binder (LaRC-TPI PAA) and miscible binder (BisP-BTDA PAA), together with APC-2 as the reference, were investigated by Iosipescu shear test method to evaluate the effect of binders on the shear response of the composites.

Another area that has received considerable attention recently is the reinforcement of thermoplastics with thermotropic liquid crystalline polymers (LCPs). Under certain processing conditions, the LCPs can develop a fibrillar morphology within the thermoplastic matrix. These fibrils display a high degree of orientation so that the blends exhibit anisotropic behavior similar to the fiber reinforced composites. Since the reinforcing LCP fibrils are formed during a melt processing of blends of the matrix and LCP and a high degree of extensional flow is involved in the processes, these blends are sometimes referred to as in-situ composites. The LCP reinforced composites have the potential to meet some special requirements for cost/performance composites, which can not be satisfied by glass and carbon fiber reinforced composites, including recyclability, better surface appearance, reduced viscosity and lower physical wear on processing equipment. An in-situ composite, PEKK/HX1000, has been developed by Professor Donald Baird of the Virginia Tech NSF S&TC. The improvement in tensile performance of the PEKK matrix polymer due to the addition of HX1000 has been shown in [64]. In this chapter, the shear response of PEKK/HX1000 system was investigated. Since PEKK/HX1000 is a novel anisotropic material system, the shear property measurement requires special care. Among the most popularly employed shear test methods for high

modulus fiber composites, the 10° off-axis tensile test, ± 45° tensile test and Iosipescu shear test, only the Iosipescu test method is the means of test available. Accordingly, the PEKK/HX1000 material system was tested by the Iosipescu test method. In this investigation, the conventional strain gage measuring technique is employed combined with full-field moiré interferometry.

5.2 AS4/PEEK System

5.2.1 Material and Specimen Preparation

The AS4/PEEK system, APC-2, AS4/PEEK+LaRC-TPI and AS4/PEEK+BisP-BTDA, were manufactured and provided by Professor Richey Davis of the Virginia Tech NSF S&TC. Details of material fabrication can be found in [65]. The in-plane dimension of the panels is 76 x 76 mm. Three standard Iosipescu specimens with dimensions shown in Fig. 2.3 were cut from each panel. The nominal thickness was 2.1 mm for APC-2 specimens, 1.9 mm for AS4/PEEK+LaRC-TPI specimens and 2.0 mm for AS4/PEEK+BisP-BTDA specimens. For each material, three specimens were prepared with the fibers in 0° and three with fibers in 90° fiber orientation. All the Iosipescu specimens were instrumented with back-to-back two-gage rosettes. The strain-gage Iosipescu tests were performed according to the procedure proposed by Ho et al. [63].

5.2.2 Shear Stress-Strain Curves

The shear stress-strain curves obtained from the strain gage measurements for the AS4/PEEK composites are shown in Fig. 5.1 to Fig. 5.3. Shear responses of 0° Iosipescu specimens and 90° specimens are plotted together for comparison. It can be seen that all the specimens display nonlinear shear behavior. A polynomial of third order is required to fit the shear stress-strain curves for both 0° and 90° specimens, that is

$$\tau = A_1 \gamma - A_2 \times \gamma^2 + A_3 \times \gamma^3 \qquad (5.1)$$

The coefficients of the fitting function, i.e. A_1, A_2 and A_3, for these three materials are presented in Table 1. The gap between the curves of 0° and 90° specimen is believed to be attributed to the nonuniformity of the shear strain fields. The average shear stress-strain curve, as presented by the dashed line in each figure, is then plotted as a representative of

the shear response for the material. In Fig. 5.4, the average shear stress-strain curves for the three materials are shown together. No significant difference is seen between the three curves.

As compared with the shear response of traditional thermoset composites, as documented in [25], the shear behavior of AS4/PEEK material system presents the following differences: (a) It has been observed that, for AS4/3501-6, the shear response of 0° Iosipescu specimen varied from specimen to specimen due to the sensitivity of 0° specimen to load points; while the shear stress-strain curves obtained from different 0° specimens of AS4/PEEK composites appear quite consistent; (b) The shear response of 90° specimen of thermoset composites displayed less nonlinearity than that of the 0° specimen, however, for AS4/PEEK composites, the fitting functions for 0° and 90° specimens are of the same order, indicating the degree of nonlinearity in shear for 0° and 90° specimens are the same; (c) The 90° Iosipescu specimen of thermoset composites always failed at very low shear strain levels. In contrast, the 90° specimen of AS4/PEEK composites can sustain shear strain beyond 4.0%.

5.2.3 Shear Stiffness

The initial shear moduli of the three materials tested are presented in Table 2 and is plotted in Fig. 5.5. After being normalized with respect to the fiber volume fraction, the values of initial modulus for AS4/PEEK+LaRC-TPI and AS4/PEEK+BisP-BTDA are very close to each other, and both are slightly lower than that of APC-2.

By differentiating equation (5.1), the tangential shear modulus is obtained as

$$G_{tan} = d\tau / d\gamma = A_1 - 2.0 \times A_2 \gamma + 3.0 \times A_3 \gamma^2 \qquad (5.2)$$

In Fig. 5.6, the tangential shear modulus is plotted against the shear strain for the three materials. The curves of AS4/PEEK+LaRC-TPI and AS4/PEEK+BisP-BTDA are very similar in shape and both are higher than the curve of APC-2, indicating the nonlinearity in shear for the two materials with binders are slightly improved, even though the initial shear moduli of them are relatively lower than that of APC-2.

5.2.4 Shear Strength

As is seen in Fig. 5.1 to Fig. 5.3, both the 0° and 90° specimens can sustain shear strain beyond 4.0%. The failure modes of 0° specimens and 90° specimens of AS4/PEEK system are similar to those of the 0° and 90° specimens of AS4/3501-6, that is, the 90° specimens fractured at the middle of the specimen along the fiber orientation and the 0° specimens failed when cracks were initiated at both notch tips and propagated along the fiber direction. The apparent failure shear stress, the failure load averaged over the cross-section between notch tips, for the three materials are shown in Fig. 5.7. It is seen that the apparent failure shear stresses of AS4/PEEK+LaRC-TPI and AS4/PEEK+BisP-BTDA are 7 - 10% higher than that of ASP-2 for both 0° and 90° specimens. But, there is about 20 - 24% differences between the values of ultimate shear stress for 0° and 90° specimens due to different failure modes for all the three materials. In addition, the failure stresses were all obtained at shear strains beyond the range of strain gage. According to the suggestion given in section 4.4, the shear stress at $\gamma = 2.0\%$ is compared in Fig. 5.8 for the three materials. It can be seen in Fig. 5.8 that the APC-2 has the highest capability of carrying load at shear strain level of 2.0%, then followed by AS4/PEEK+LaRC-TPI. The same capability for AS4/PEEK+BisP-BTDA appears to be the lowest. The difference between shear stress at $\gamma = 2.0\%$ for 0° and 90° specimens is reduced to 12 - 14% for the three materials. After applying a correction factor to take the nonuniformity of strain field into account, the values of shear stress at $\gamma = 2.0\%$ for 0° and 90° specimens are expected to be much more close. Hence, this characteristic shear stress can be used as an alternative of shear strength for the AS4/PEEK system.

5.3 PEKK/HX1000 System

5.3.1 Material and Specimen Preparation

PEKK/HX1000 system was fabricated and supplied by Professor Donald Baird of the Virginia Tech NSF S&TC. Iosipescu specimens of dimensions shown in Fig. 2.3 were cut from eight 76 x 76 mm panels with eight different HX1000 concentrations. Three PEKK/HX1000 specimens for each percentage of HX1000 content were tested. The specimens, except the neat PEKK specimens, were prepared with the LCP fibrillar orientation perpendicular to the specimen longitudinal axis. The nominal thickness of the

specimens is about 1.7 mm. Three Iosipescu specimens, neat PEKK, neat HX1000 and PEKK/HX1000 20/80, were instrumented with a two-gage rosette on one face and moiré grating on the opposite face, and were investigated by the moiré interferometry. The procedure of moiré experiments is the same as described in section 3.2.2. All other Iosipescu specimens were instrumented with two-gage rosette in the back-to-back fashion and tested by strain gage measurement technique.

5.3.2 Shear Stress-Strain Curves

The typical shear stress-strain curves obtained from strain gage experiments for the eight different blends of PEKK/HX1000 are shown in Fig. 5.9. It should be noted here that for some blends of PEKK/HX1000, such as PEKK/HX1000 50/50, 70/30 and neat PEKK, the stress-strain curves of different specimens are nearly coincident and the shear response of the specimen is highly reproducible; while for other blends the curves lie apart to a certain extent, the neat HX1000 being the worst case.

It can be seen from Fig. 5.9 that all these materials exhibit nonlinear shear response. A quadratic function was found to provide a convenient fit to these shear stress-strain curves. The general form of curve fit equation for the PEKK/HX1000 system is

$$\tau = A_1\gamma - A_2\gamma^2 \tag{5.3}$$

As discussed in sections 4.2 and 4.3, A_1 represents the initial shear modulus, A_2 characterizes the degree of nonlinearity. The values of A_1 and A_2 for the eight different blends are presented in Table 3. It is seen that the degree of nonlinearity of shear response depends on the percentage of HX1000 content, with neat PEKK as the lowest one and neat HX1000 as the highest one.

5.3.3 Shear Strain Field

Three pairs of typical moiré fringe patterns for neat PEKK, neat HX1000 and PEKK/HX1000 20/80, respectively, are shown in Fig. 5.10 to Fig. 5.12. It is seen that the fringes in the region far away from the notches are quite uniform for all three materials, indicating that these materials are relatively homogeneous, compared to unidirectional graphite/epoxy composites [63].

By differentiating the data from the u- and v- moiré fringe patterns, the shear strain distributions at the surface of the Iosipescu specimens were obtained, as shown in Fig. 5.13. It is seen that for all the three materials the strain distribution on the center line between notches are not uniform as would occur in the ideal isotropic case, and the value of shear strain at the center of the line, which is the value measured by the strain gage, is greater than the average shear strain along notch-root axis. The shape of the curves is similar to that observed in the unidirectional 90° Iosipescu specimen [25].

5.3.4 Shear Stiffness

The initial shear modulus may be calculated directly from the strain gage test data, that is,

$$G = \tau_{avg} / \gamma_{avg} \tag{5.4}$$

where γ_{avg} is the average shear strain along notch-root axis. However, as is mentioned above, the shear strain distribution across the notches is not uniform for the Iosipescu specimen of PEKK/HX1000 composites so that the shear strain γ, measured by the strain gage, is not equal to the average shear strain γ_{avg}. To account for the nonuniformity in the calculation of the shear modulus, it is necessary to apply a correction factor (CF) which is defined by

$$CF = \gamma / \gamma_{avg} \tag{5.5}$$

Hence, the shear modulus can be expressed as

$$G = \tau_{avg} / \gamma_{avg} = \tau_{avg} / \gamma \times CF = CF \times G^* \tag{5.6}$$

where $G^* = \tau_{avg} / \gamma$ is called the apparent shear modulus. It has been shown that the correction factor depends on the material orthotropic ratio, i.e. the ratio of E_x to E_y [25]. Since for different HX1000 concentration, the longitudinal and transverse tensile moduli are different, the correction factors are then different also. For neat PEKK, neat HX1000 and PEKK/HX1000 20/80, the correction factors are obtained from the moiré data, while for other materials of the PEKK/HX1000 material system tested, the correction factors are calculated approximately by an empirical formula given in [25]

$$CF = 1.036 - 0.125 \log (E_x / E_y) \tag{5.7}$$

Correction factors for the PEKK/HX1000 material system are presented in Table 4 along with the corrected values of the initial shear moduli. The longitudinal and transverse tensile moduli, E_x and E_y, used for calculating correction factors are obtained from injection molded plaques tensile tests. It is seen from Table 4 that the shear moduli are improved by increasing the concentration of HX1000, but the improvement is not as much as that in the tensile moduli [64], an observation which is not surprising since shear response is matrix-dominated.

The corrected initial shear moduli are also plotted against the HX1000 concentration, as shown in Fig. 5.14, along with the theoretical values predicted by simple micromechanics of composites model. With the help of the micromechanics model, the mechanical properties of a composite can be predicted on the basis of the mechanical properties and the relative volumes of the constituents. The relationship between the shear moduli of a composite and its constituents for the ideal series spring model is:

$$G_{com} = G_m G_f / (v_m G_f + v_f G_m) \tag{5.8}$$

where v_m and v_f are volume fractions of the matrix material and fiber material, respectively. G_{com}, G_m, G_f are the shear moduli of the composite, the matrix material and the fiber material, respectively. In the present study, G_m is the shear modulus of PEKK, which is measured in the Iosipescu shear test, and G_f is the shear modulus of the reinforcing phase, that is, HX1000. In order to give a more accurate estimation of G_f, the value of G_f is determined by equation (5.8), instead of using the value obtained from test data of neat HX1000. The determination of G_f is as follows: first, choose a blend of PEKK/HX1000, say, 20/80, as a reference, which shear modulus and relative volume of constituents are all known and should satisfy the equation (5.8). Then, G_f, as the only unknown in equation (5.8), is determined by

$$G_f = G_{com} v_f G_m / (G_m - G_{com} v_m) \tag{5.8}$$

When G_f is determined, the theoretical values of G_{com} for different blends of PEKK/HX1000 can be obtained by equation (5.8). From Fig. 5.14, it is seen that the experimental and theoretical values of G_{12} are in good agreement with each other, indicating that the initial shear modulus for most blends of PEKK/HX1000 composite can be well predicted by the micromechanics of composites approach. It might be observed in [64] that, with the exception of the (bulk) 100% HX1000, a rule of mixtures type model

also gives a good prediction of the tensile modulus, with an apparent HX1000 fiber modulus of about 21 GPa.

It has been shown in Fig. 5.9 that all the PEKK/HX1000 composites exhibit nonlinear shear behavior. Therefore the shear stiffness will decrease as the shear strain increases. A comparison of shear moduli at different shear strain levels is shown in Fig. 5.15, where the solid lines are fitted curves. It can be seen that the rate of shear stiffness reduction depends on the HX1000 concentration which leads to different degree of nonlinearity. As the percentage of HX1000 content increases, the shear moduli decrease more and more rapidly. When the shear strain reaches 2.0%, G_{12} of neat HX1000 is even lower than that of neat PEKK.

5.3.5 Shear Strength

For the PEKK/HX1000 material system, different failure modes were observed for different blends. Two typical failure modes are shown in Fig. 5.16, which are for neat HX1000, PEKK/HX1000 10/90, 20/80, 50/50, and 70/30, respectively. When the HX1000 concentration is lower than 30%, such as PEKK/HX1000 80/20, 90/10 and neat PEKK, no fracture of specimen was observed. Instead of being broken, the specimen continued to carry load to large deformation beyond the range of strain gage. In such cases, the test was stopped when a load drop was observed.

The apparent failure shear stress of different blends of PEKK/HX1000 material system is shown in Fig. 5.17 as a function of HX1000 concentration, where the failure shear stress is obtained by averaging the ultimate load, corresponding to either the fracture of a specimen or a load drop, over the cross-section between notches. Apparently, the failure shear stress of blends with lower HX1000 concentration is greater than that of the blends with higher HX1000 concentration. However, since different blends of PEKK/HX1000 fail in different modes, it may be questioned as to whether the comparison is meaningful. In addition, for most of the test specimens, the shear strain corresponding to the ultimate shear stress is higher than 3.0%, therefore, it is not suitable to use the ultimate shear stress as the shear strength from the stiffness point of view. Moreover, for most of the blends, the standard deviation of the ultimate shear stress is great, as shown in Fig. 5.17, it is also not good for defining a proper shear strength of a composite material. Another characteristic shear stress proposed in section 4.4 is then employed, which is the shear

stress corresponding to a selected shear strain level. In Fig. 5.18, the shear stress at γ = 2.0% is plotted against the percentage of HX1000 content. The shear stresses of different blends of PEKK/HX1000 are now compared at the same shear strain level. The comparison indicates that at the shear strain level of 2.0%, the capability of carrying load for a blend of PEKK/HX1000 is improved by increasing the HX1000 concentration. It can be seen from Fig. 5.18 that the values of the shear stress at γ = 2.0% are quite consistent for each blend of PEKK/HX1000 and the corresponding shear strain is also practically acceptable. Therefore, it is shown that the shear stress at γ = 2.0% is more appropriate than the apparent failure shear stress for defining the shear strength for PEKK/HX1000 material system.

CHAPTER 6. CLOSURE

6.1 Conclusions

The conclusions can be summarized as follows:

(1). The nonuniformity of shear deformation has been identified in different specimen configurations by both strain gage and moiré experiments. The nonuniformity shown in either displacement or strain fields exhibit a banded nature, not only for hybrid fabric composites but also for unidirectional and laminated fibrous composites. For off-axis tensile specimens, the orientation of the bands varies with the fiber angles and is apparently coincident with the fiber orientation. The degree of nonuniformity observed in the strain fields of off-axis tensile specimens is fairly high, even though the specimen dimensions were chosen to achieve a nearly uniform field. Neither the banded nature nor the significant nonuniformity can be predicted by the existing analytical and numerical models. It appears that the nonuniformity is localized. From the micrographs of the 10° off-axis specimen, obvious material inhomogeneity is revealed. It is considered that the nonuniformity is attributed mainly to the material inhomogeneity. The presence of the nonuniformity in the strain fields will influence both the measurements of the mechanical properties and the failure prediction.

(2). By performing the off-axis tensile tests on different test machines with different grip systems, it is detected that improper loading is a common problem for off-axis tensile test. Undesirable out-of-plane bending usually exists, which in turn induces specimen twisting due to the bending-twisting coupling effect. Different shear strain values may be obtained from different sides of the specimen, which will then lead to inconsistency in the calculated shear properties if strain gage is applied only on one side of the specimen. However, by measuring strains at both sides of the specimen and averaging the values, the twisting effect on the determination of shear properties can be eliminated. Consequently, applying back-to-back strain gage on an off-axis tensile specimen is recommended for obtaining accurate shear properties.

(3). In order to characterize the nonlinear shear stress-strain response obtained experimentally, a curve fitting technique has been employed, which can yield an analytical

expression for the nonlinear shear behavior. The polynomial function is found to provide a convenient fit for all the composite material systems tested in the present investigation. By differentiating the fitting function, the tangential shear modulus can be determined analytically, which proved to be an appropriate definition of shear stiffness for nonlinear case. Because of the effect of nonlinearity, the tangential shear modulus will decrease as the shear strain increases. The rate of the reduction depends on the degree of nonlinearity. Therefore, it is suggested that all the coefficients of the fitting polynomial, one of which represents the initial shear modulus and the others characterize the degree of nonlinearity, being used together as parameters for evaluation of the shear behavior of a composite material.

(4). The effect of material nonlinearity on shear strain distribution within the test section of the Iosipescu specimen has been investigated by strain gage and moiré experiments. No significant change is detected in the global nonuniformity when the material becomes nonlinear, confirming the validity of using correction factor, obtained from linear elastic solution, in the nonlinear range.

(5). It is found from the present study that shear behavior of thermoplastic composites demonstrates higher degree of nonlinearity than that of traditional thermoset composites. In addition, the failure shear strain is also increased, up to 3.0% or higher, not only for the 0° Iosipescu specimens but also for the 90° Iosipescu specimens. From the stiffness point of view, failure shear stress corresponding to high shear strain is not adequate to be used as shear strength. Furthermore, Iosipescu specimens of different materials may fail in different modes, which raises the question as to whether the comparison of failure shear stress between different composites is meaningful. Different failure modes for 0° and 90° specimen configurations also lead to an inconsistency in the values of shear strength for the tested composite. It is suggested then that shear stress at certain shear strain level be used as an engineering definition of shear strength. This definition can be interpreted as the capability of carrying load at a selected shear strain level so that the comparison of this characteristic shear stress between different composites has a clearly physical meaning. For composites with highly nonlinear shear behavior, shear stress at an intermediate shear strain level, e.g. $\gamma = 2.0\%$, can be used. By applying correction factors to account for the global nonuniformity of shear strain fields, consistent value of this characteristic shear stress obtained from different specimen configurations, 0° and 90°, is expected to be gained.

(6). The study of shear response of the AS4/PEEK system with different binders has shown that there is no significant difference between the shear responses of these materials. The initial shear moduli of AS4/PEEK composites with binders are relatively lower than the reference material, APC-2, but the degree of nonlinearity of the former appears to be slightly improved as compared with that of the latter.

(7). The application of Iosipescu shear test method in the measurements of shear properties of in-situ composite, PEKK/HX1000, has been demonstrated to be successful. It is shown that the initial shear stiffness is improved by increasing the HX1000 concentration. Because of the nonlinear shear response the shear stiffness will reduce as the shear strain increases and the reduction depends on the percentage of HX1000 content. The shear stress at $\gamma = 2.0\%$ has proved again to be a practical alternative for defining shear strength of PEKK/HX1000 material system.

6.2 Suggestions for Future Work

Based on the summary given above, some suggestions are made for future work.

(1) Because of the practically unavoidable existence of improper loading involved in the off-axis tensile specimen, the effect of out-of-plane bending and twisting on the in-plane deformation of the specimen should be further investigated. 3-D numerical analysis appears necessary for simulating the boundary conditions and assessing the global nonuniformity of the strain fields.

(2). Further experimental studies are needed to confirm the argument that the significant nonuniformity revealed in the strain fields of off-axis specimen is mainly a consequence of material inhomogeneity.

(3). More experimental data for the shear response of various composite material systems will be useful for further verifying the rationality of defining the shear stress at $\gamma = 2.0\%$ as shear strength for composites with highly nonlinear shear behavior.

REFERENCES

1. I. M. Daniel and T. Liber, "Lamination Residual Stresses in Fiber Composites," IIT Research Institute Report IITRI-D6073-1, 1975.

2. C. C. Chamis and J. H. Sinclair, "Ten-deg Off-Axis Test for Shear Properties in Fiber Composites," Experimental Mechanics, Vol. 17 (9), pp339-346, 1977.

3. S. W. Tsai, "A Test Method for the Determination of Shear Modulus and Shear Strength," Air Force TR AFML-TR-66-372, Air Force Laboratory, 1967.

4. M. J. Pindera and C. T. Herakovich, "Shear Characterization of Unidirectional Composites with Off-Axis Tension Test," Experimental Mechanics, Vol. 26 (1), pp103-112, 1986.

5. M. J. Pindera, G. Choksi, J. S. Hidde and C. T. Herakovich, "A Methodology for Accurate Shear Characterization of Unidirectional Composites," Journal of Composite Materials, Vol. 21 (12), pp1164-1184, 1987.

6. N. J. Pagano and J. C. Halpin, "Influence of End Constraint in the Testing of Anisotropic Bodies," Journal of Composite Materials, Vol. 2 (1), pp18-31, 1968.

7. R. R. Rizzo, "More on the Influence of End Constraints on Off-Axis Tensile Tests," Journal of Composite Materials, Vol. 3, pp202 - 219, 1969.

8. G. L. Richards, T. P. Airhart and J. E. Ashton, "Off-Axis Tensile Coupon Testing," Journal of Composite Materials, Vol. 3, pp586-589, 1969.

9. J. Canas, F. Paris and J. C. Marin, "Numerical Analysis of 'Off-Axis Tension Test' for Unidirectional Graphite-Epoxy Composites," Proceedings ICCM VIII, Vol. 4, 36-F-1, Hawaii, USA, 1991.

10. C. C. Chiao, R. L. Moore and T. T. Chiao, "Measurement of Shear Properties of Fiber Composites, Part 1. Evaluation of Test Methods," Composites, Vol. 8 (3), pp161-169, 1977.

11. Y. T. Yeow and H. F. Brinson, "A Comparison of Simple Shear Characterization Methods for Composite Laminates," Composites, Vol. 9 (1), pp49-55, 1978.

12. P. H. Petit, "A Simplified Method of Determining the In-Plane Shear Stress/Strain Response of Unidirectional Composites," Composite Materials: Testing and Design, ASTM STP 460, pp83-93, American Society for Testing and Material, Philadelphia, 1969.

13. B. W. Rosen, "A Simple Procedure for Experimental Determination of the Longitudinal Shear Modulus of Unidirectional Composites," Journal of Composite Materials, Vol. 6, pp552-554, 1969.

14. H. T. Hahn, "A Note on Determination of the Shear Stress-Strain Response of Unidirectional Polymer Matrix Composites," Journal of Composite Materials, Vol. 7, pp383 - 386, 1973.

15. G. Terry, "A Comparative Investigation of Some Methods of Unidirectional, In-Plane Shear Characterization of Composite Materials," Composites, October, pp233-237, 1979.

16. ASTM Standard D3518/D3518M-91, "Standard Practice for In-Plane Shear Stress-Strain Response of Unidirectional Polymer Matrix Composites," Annual Book of ASTM standards, Vol.15.03, American Society for Testing and Material, Philadelphia, PA, 1991 (or current printing).

17. S. Kellas and J. Morton, "Strength Scaling in Fiber Composites," NASA Contractor Report 4335, November 1990.

18. S. Kellas, J. Morton and K. E. Jackson, "An Evaluation of the ±45° Tensile Test for the Determination of the In-Plane Shear Strength of Composite Materials," Proceedings ICCM VIII, 36-M-1, Hawaii, 1991.

19. N. Iosipescu, "New Accurate Procedure for Single Shear Testing of Metals," Journal of Materials, Vol. 2 (3), pp537-566, 1967.

20. D. E. Walrath and D. F. Adams, "The Iosipescu Shear Test as Applied to Composite Materials," Experimental Mechanics, Vol. 23 (1), pp105-110, 1983.

21. M. Arcan, "The Iosipescu Shear Test as Applied to Composite Material - Discussion," Experimental Mechanics, Vol. 24 (1), pp66-67, 1984.

22. D. E. Walrath and D. F. Adams, "Analysis of the Stress State in an Iosipescu Shear Test Specimen," Report No. UWME-DR-301-102-1, Department of Mechanical Engineering, University of Wyoming, USA, 1983.

23. D. E. Walrath and D. F. Adams, "Verification and Application of Iosipescu Shear Test Method," Report No. UWME-DR-401-103-1, Department of Mechanical Engineering, University of Wyoming, USA, 1984.

24. D. F. Adams and D. E. Walrath, "Further Development of the Iosipescu Shear Test Method," Experimental Mechanics, Vol. 27 (2), pp113-119, 1987.

25. J. Morton, H. Ho, M. Y. Tsai and G. L. Farley, " An Evaluation of the Iosipescu Specimen for Composite Materials Shear Property Measurement," Journal of Composite Materials, Vol. 26 (5), pp708-750, 1992.

26. H. Ho, M. Y. Tsai, J. Morton and G. L. Farley, "Numerical Analysis of the Iosipescu Specimen for Composite Materials," Composite Science and Technology, Vol 46, pp115-128, 1993

27. J. L. Sullivan, B. G. Kao and H. Van Oene, "Shear Properties and a Stress Analysis obtained from vinyl-ester Iosipescu Specimen," Experimental Mechanics, Vol. 24 (3), pp223-232, 1984.

28. D. E. Walrath and D. F. Adams, "Iosipescu Shear Properties of Graphite fabric/Epoxy Composite Laminates," Report No. UWME-DR-501-103-1, Department of Mechanical Engineering, University of Wyoming, NASA Grant No. NAG-1-272, 1985.

29. J. A. Barnes, M. Kumosa and D. Hull, "Theoretical and Experimental Evaluation of the Iosipescu Shear test," Composite Science and Technology, Vol. 28, pp251-268, 1987.

30. M. Kumosa and D. Hull, "Mixed-Mode Fracture of Composites Using Iosipescu Shear Test," International Journal of Fracture, Vol 35, pp83-102, 1987.

31. D. F. Adams and D. E. Walrath, "Iosipescu Shear Properties of SMC Composite Materials," Composite Materials: Testing and Design (6th Conf.), ASTM 787. pp19-23, American Society for Testing and Materials, Philadelphia, 1982.

32. D. C. Phillips and J. M. Scott, "The Shear Fatigue of Unidirectional Composites," Composites, Vol.8, pp233-236, 1977.

33. S. N. Chatterjee, E. C. J. Wung, C. F. Yen, V. Ramnath, J. A. Kessler and D. F. Adams, "Composite Specimen Design Analysis, Vol. I: Analytical Studies, Vol. II: Experimental Effort," MTL TR 91-5, 1991.

34. M. Arcan Z. Hashin and A. Voloshin, "A Method to Produce Uniform Plane-Stress States with Application s to Fiber-Reinforced Materials," Experimental Mechanics, Vol. 18, pp141-146, 1978.

35. H. G. Bush and T. Weller, "A Bi-Axial Method for In-Plane Shear Testing," NASA TM 74070, 1978.

36. M. F. Duggan, J. T. McGrath and M. A. Murphy, "Shear Testing of Composite Materials by a Combined Loading Technique," Proceeding of AIAA/ASME SDM Coference, pp311-319, 1978.

37. R. A. Elkin, G. Fust and D. P. Hanley, "Characterization of Graphite Fiber/Resin Matrix Material," ASTM STP 460, pp321-335, 1969.

38. C. W. Bert, "Experimental Characterization of Composites," in Composite Materials, L. J. Broutman and R. H. Krock, Editors, Vol.8, pp95, 1974.

39. C. L. Browning F. L. Adams and J. M. Whitney, "A Four Point Shear Test for Graphite Epoxy Composites," ASTM STP 797, pp54-74, 1983.

40. J. M. Whitney and J. C. Halpin, "Analysis of Laminated Anisotropic Tubes under Combined Loading," Journal of Composite Materials, Vol. 2, pp360-367, 1968.

41. N. J. Pagano and J. M. Whitney, "Geometric Design of Composite Cylindrical Characterization Specimens," Journal of Composite Materials, Vol. 4, pp360-378, 1970.

42. R. R. Rizzo and A. A. Vicario, "A Finite Element Analysis for Stress Distribution in Gripped Tabular Specimens," ASTM STP 497, pp68-88, 1972.

43. S. R. Swanson, G. R. Toombes and S. W. Beckwith, " In-Plane Shear Properties of Composite Using Torsion Tests of Thin Walled Tubes," Proceeding of 29th SAMPE Symposium, pp567-577, 1984.

44. S. R. Swanson, M. Messick and C. R. Toombes, "Comparison of Torsion Tube and Iosipescu In-Plane Shear Test Results for a Carbon Fiber Reinforced Epoxy Composite," Composites, Vol. 16, pp220-224, 1985.

45. G. A. Foley, M. E. Poylance and W. W. Houghton, "Use of Torsion Tubes to Measure In-Plane Shear Properties of Filament Wound Composites," ASTP STP 1003, pp208-223, 1989.

46. R. Bucinell, "Interim JANNAF Test Method for In-Plane Shear Properties of Unidirectional Fiber/Resin Composite Cylinders," Interim Report for MIL-HDRK-17, AMTL Contract DAAL04-89-C-0023, 1991.

47. ASTM Standard D4255-83, "Standard Guide for Testing In-plane Shear Properties of Composite Laminates," Annual Book of ASTM standards, Vol. 15.03, American Society for Testing and Material, Philadelphia, PA, 1992 (or current printing).

48. J. M. Whitney, D. L. Stansbarger and H. B. Howell, "Analysis of the Rail Shear Test - Applications and Limitations," Journal of Composite Materials, Vol. 5, pp24-34, 1971.

49. H. W. Berger, J. G. Davis and C. T. Herakovich, "Analysis of Shear Test Methods for Composite Laminates," Report VPI-E-77-14, Virginia Polytechnic Institute and State University, 1977.

50. R. Garcia, T. A. Weisshaar and R. R. McWithey, "An Experimental and Analytical Investigation of the Rail Shear-Test Method as Applied to Composite Materials," Experimental Mechanics, Vol. 20 (8), pp273-279, 1980.

51. P. A. Lockwood, "Results of the ASTM Round-Robin on the Rail Shear Test for Composites," Composites Technology Review, Vol. 3 (2), pp83-86, 1981.

52. S. Lee and M. Munro, "Evaluation of In-Plane Shear Test Methods for Advanced Composite Materials by the Decision Analysis Technique," Composites, Vol. 17 (1), pp13-22, 1986.

53. H. Ho, M. Y. Tsai, J. Morton and G. L. Farley, "A Comparison of Three Popular Test Methods for Determining the Shear Modulus of Composite Materials," Composites Engineering, Vol. 3 (1), pp69-81, 1993.

54. ASTM Standard D3039-76, "Standard Test Method for Tensile Properties of Fiber-Resin Composites," Annual Book of ASTM standards, Vol. 15.03, American Society for Testing and Material, Philadelphia, PA, 1991 (or current printing).

55. J. Guild, "The Interference Systems of Crossed Diffraction Gratings; Theory of Moiré Fringes," Oxford: Clardendon Press, 1956.

56. R. Czarnek, "Moiré Interferometry," Structure Testing, Society of Experimental Mechanics, Vol. 30 (2), pp195-200, 1991.

57. M. Y. Tsai and J. Morton, "New Developments in the Localized Hybrid Method of Stress Analysis," Experimental Mechanics, Vol. 31 (4), pp298-305, 1991.

58. R. M. Jones, "Mechanics of Composite Materials," Scripta Book Compony, 1975

59. S. T. Tsai, " Composites Design," (4th edition), Think Composites, 1988

60. D. F. Adams and D. E. Walrath, "Current Status of Iosipescu Shear Test Method," Journal of Composite Materials, Vol. 21, pp497-507, 1987.

61. M. G. Abdallah and H. E. Gascoigne, "The Influence of Test Fixture Design on the Iosipescu Shear Test for Fiber Composite Materials," ASTM STP 1003, pp231-260, ASTM 1989

62. W. R. Broughton, M. Kumosa and D. Hull, "Analysis of the Iosipescu Shear Test as Applied to Unidirectional Carbon-Fiber Reinforced Composites," Composite Science and Technology, Vol. 38, pp299-325, 1990.

63. H. Ho, M. Y. Tsai, J. Morton and G. L. Farley, "An Experimental Investigation of Iosipescu Specimen for Composite Materials," Experimental Mechanics, Vol. 31 (4), pp328-336, 1991.

64. K. J. Teh, J. Morton, J. P. de Souza and D. G. Baird, "Impact Damage Studies in AS4/PEEK and PEKK/HX1000," Proceedings of the Ninth International Conference on Composite Materials (ICCM-9), pp475-482, Madrid, July, 1993.

65. Alvaro Gonzalez-Ibarra, "The Effect of Polymeric Binders on the Processability and Properties of Composites Made by Suspension Prepregging," Master Thesis, Virginia Tech, 1993.

Table 1. Fitting Coefficients of AS4/PEEK System

Material	Specimen Configuration	A_1 (GPa)	A_2 (GPa)	A_3 (GPa)
APC-2	0°	6.5306	199.17	2164.4
	90°	5.2875	142.36	1394.3
AS4/PEEK +LaRC-TPI	0°	5.7224	154.70	1544.8
	90°	4.3659	94.45	787.46
AS4/PEEK +BisP-BTDA	0°	5.3061	134.30	1268.7
	90°	4.1933	89.48	728.57

Table 2. Normalized Initial Shear Moduli of AS4/PEEK System

Material	Specimen Configuration	Fiber Volume Fraction V_f (%)	Normalized G_{ini} (GPa)
APC-2	0°	61.1	6.351
	90°	61.0	5.155
	average		5.753
AS4/PEEK+LaRC-TPI	0°	59.5	5.808
	90°	55.1	4.901
	average		5.355
AS4/PEEK+BisP-BTDA	0°	54.5	6.036
	90°	54.4	4.780
	average		5.408

Table 3. Fitting Coefficients of PEKK/HX1000 System

HX1000 Concentration (%)	A_1 (GPa)	A_2 (GPa)
0	1.1143	5.7599
10	1.1673	7.4894
20	1.2116	8.3549
30	1.2764	9.3052
50	1.4309	13.135
80	1.5631	19.137
90	1.5576	18.288
100	1.8410	24.425

Table 4. Average Values of Apparent and Corrected Initial Shear Moduli of PEKK/HX1000 System

HX1000 Concentration (%)	Apparent Shear Moduli(GPa)	Correction Factors	Corrected Shear Moduli(GPa)
0	1.114	1.090	1.215
10	1.167	1.052	1.263
20	1.212	1.120	1.315
30	1.276	1.074	1.371
50	1.431	1.086	1.499
80	1.563	1.115	1.743
90	1.558	1.117	1.843
100	1.841	1.170	1.955

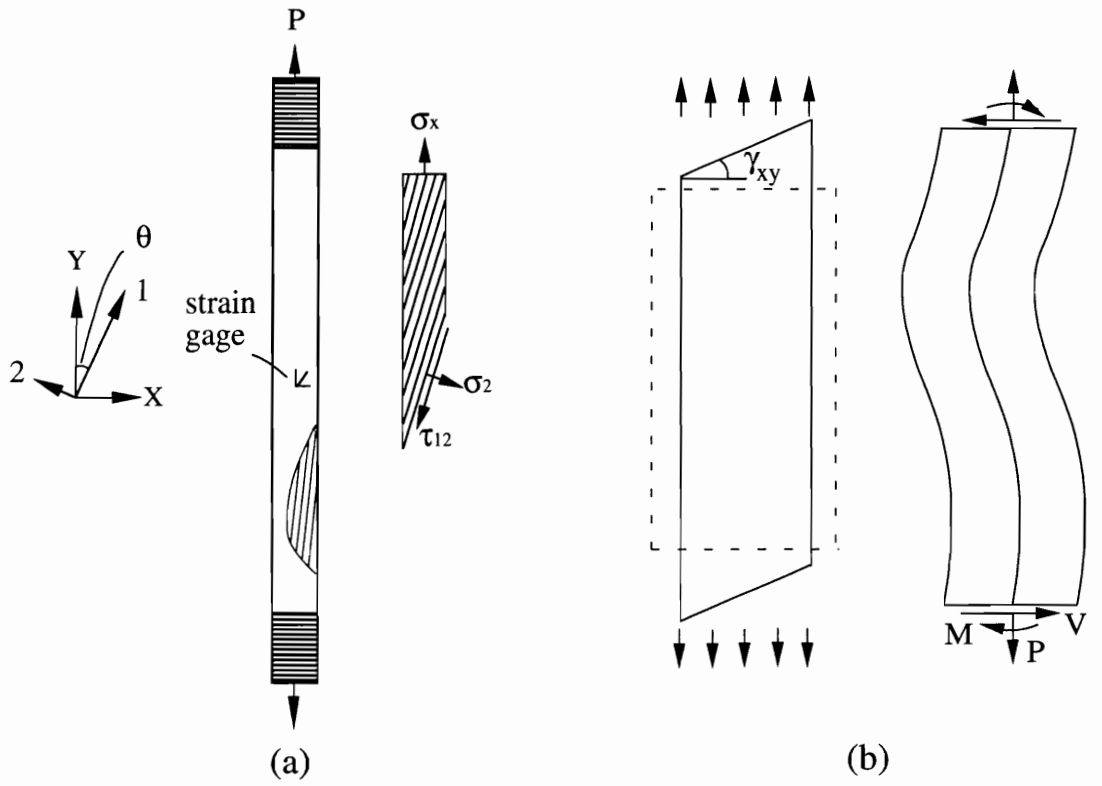

Fig. 2.1 (a) Off-Axis Tensile Specimen, (b) Unconstraint and Constraint Deformation in Off-Axis Specimen [6]

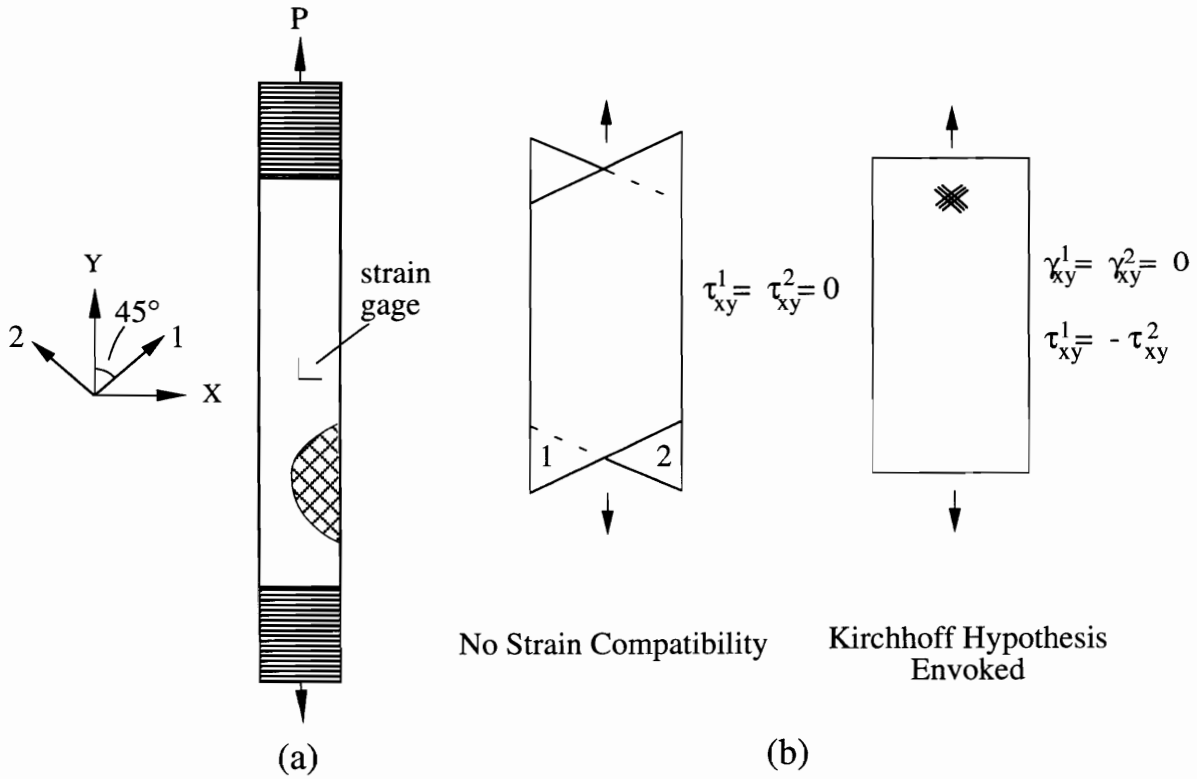

Fig. 2.2 (a) ± 45° Tensile Specimen, (b) Behavior of ± 45° Specimen [12]

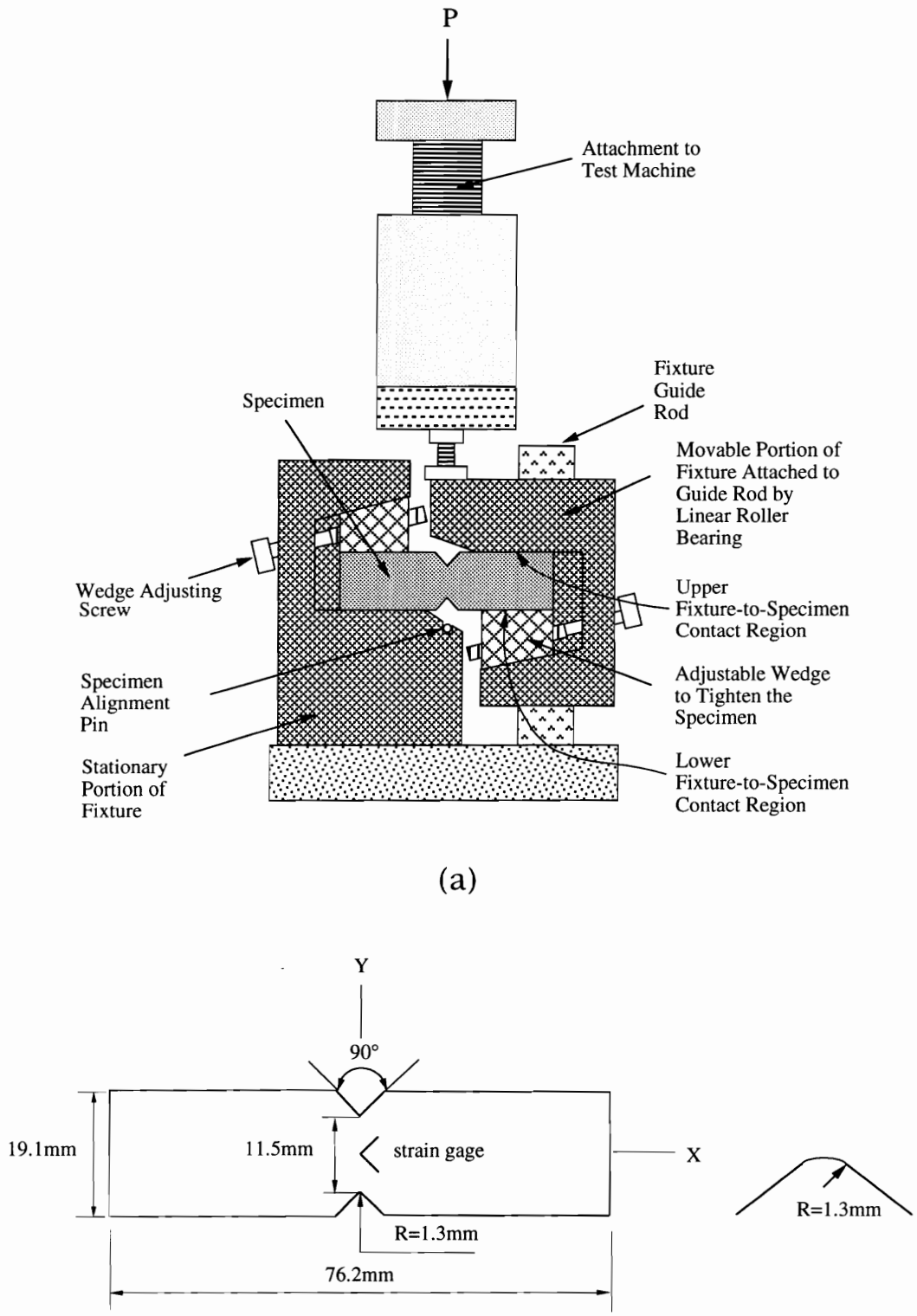

Fig.2.3 Modified Iosipescu Shear (a) Fixture, (b) Specimen [25]

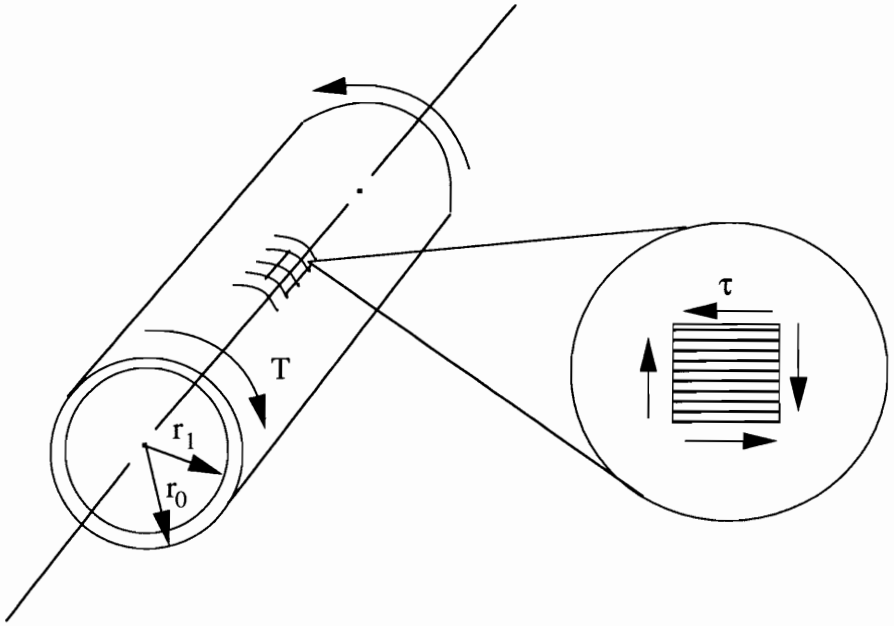

Fig. 2.4 Thin-Walled Torsion Tube [52]

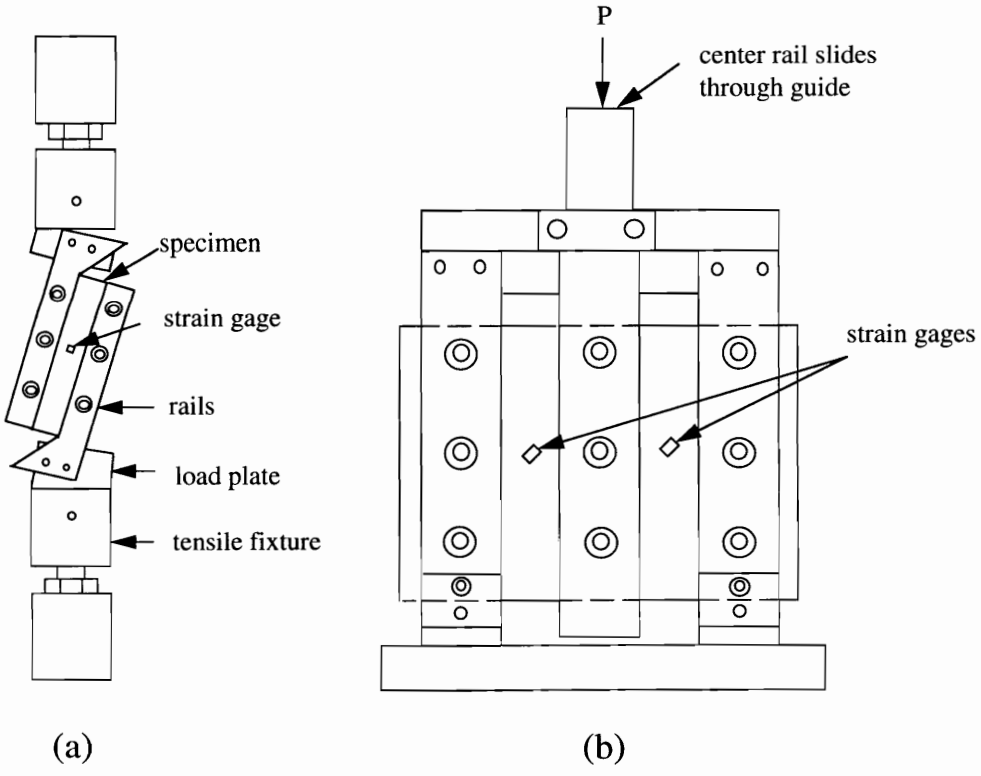

Fig. 2.5 (a) Two-rail, (b) Three-rail Shear Test Apparatus and Specimen [47]

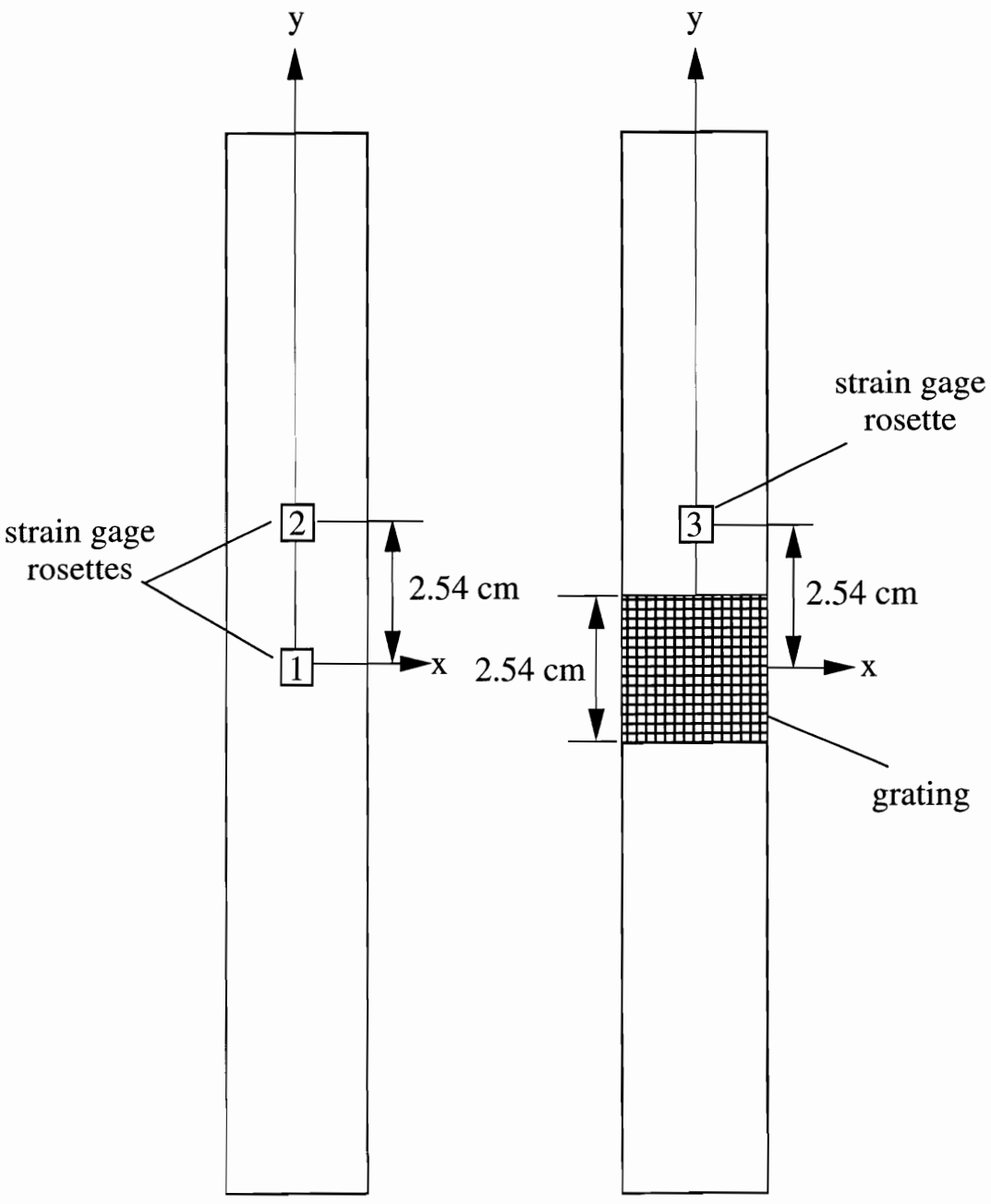

Fig. 3.1 Strain Gage Rosettes and Grating Arrangement for Tensile Specimen

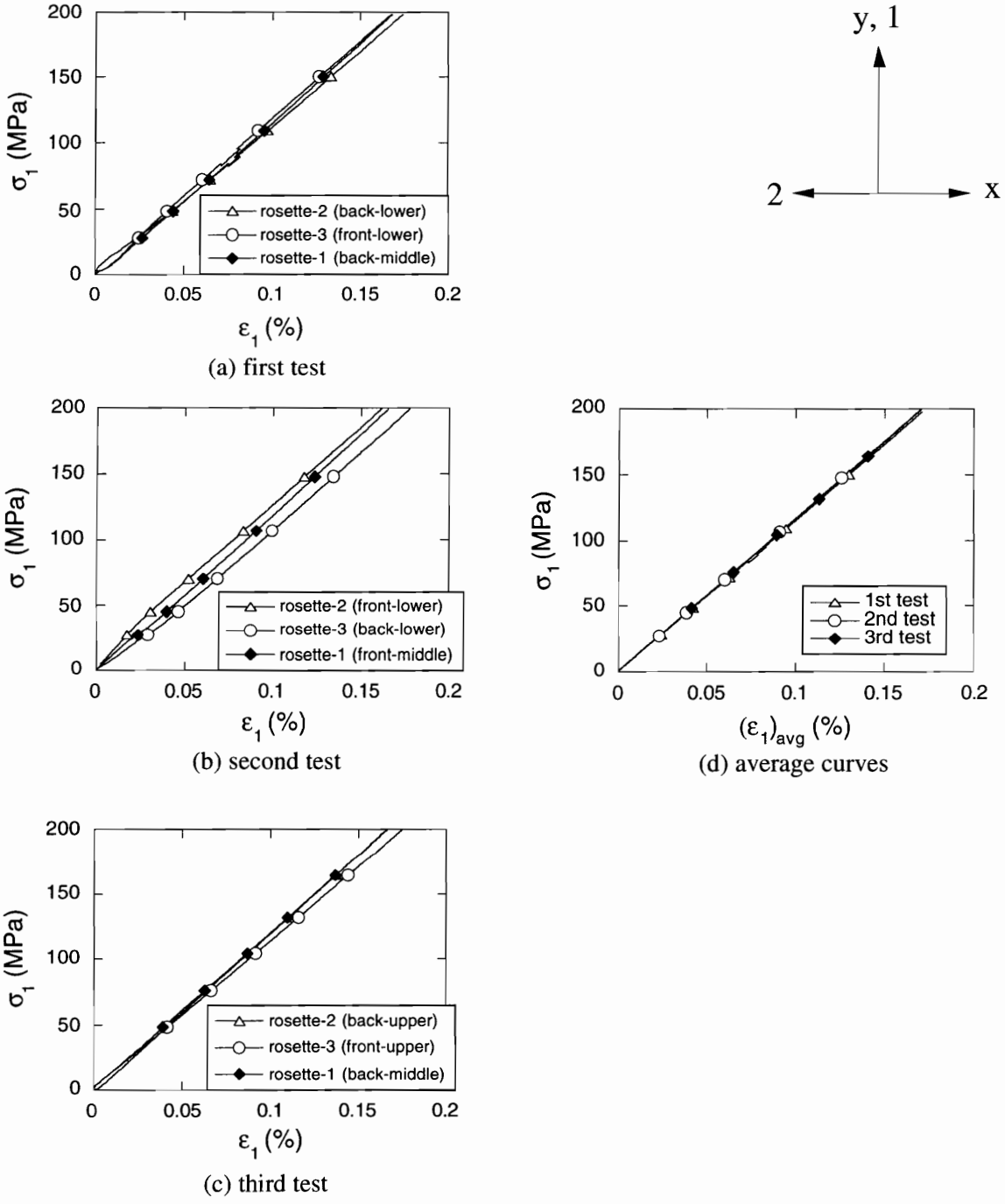

Fig. 3.2 Stress-Strain Curves of 0° Tensile Specimen

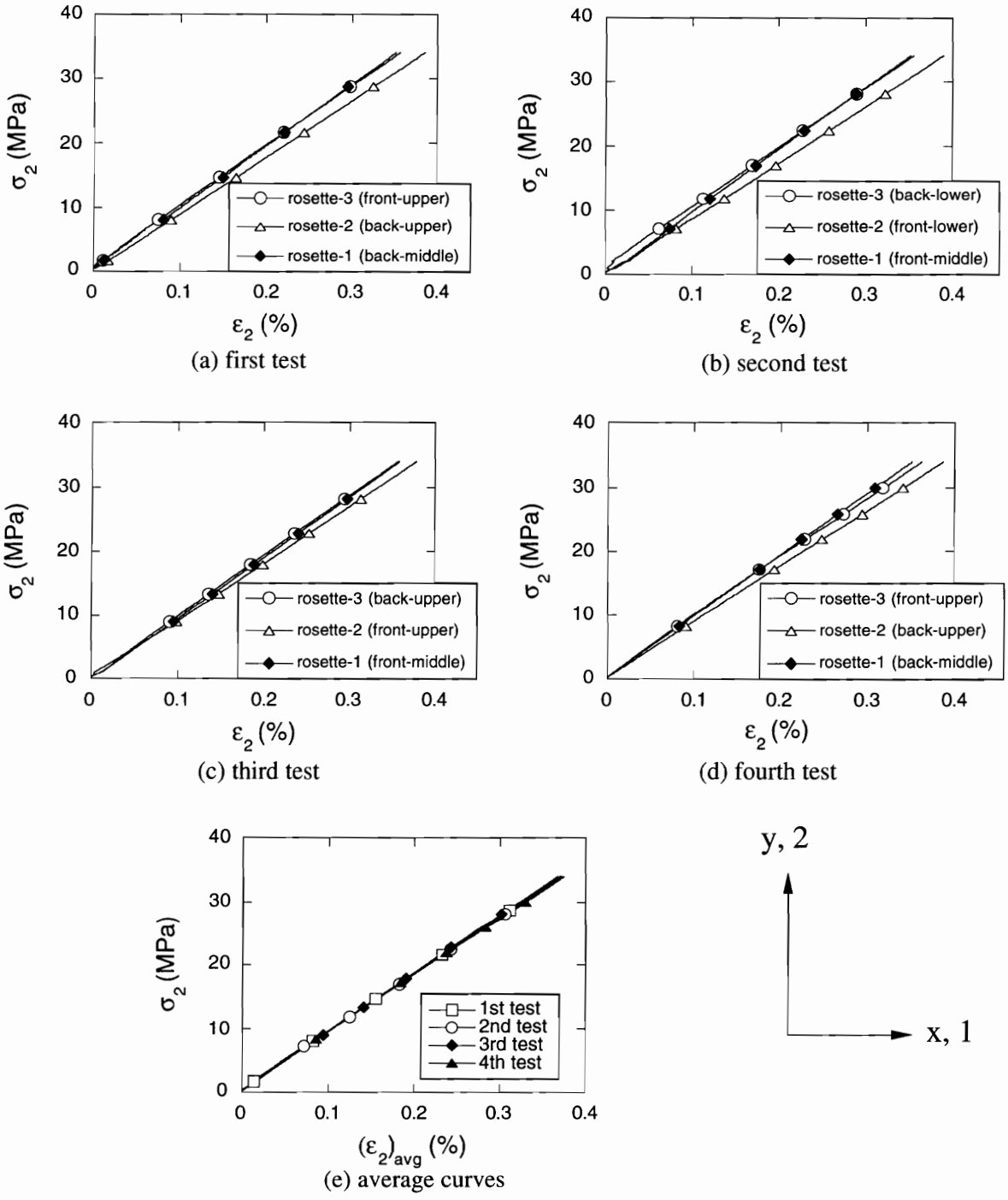

Fig. 3.3 Stress-Strain Curves of 90° Tensile Specimen

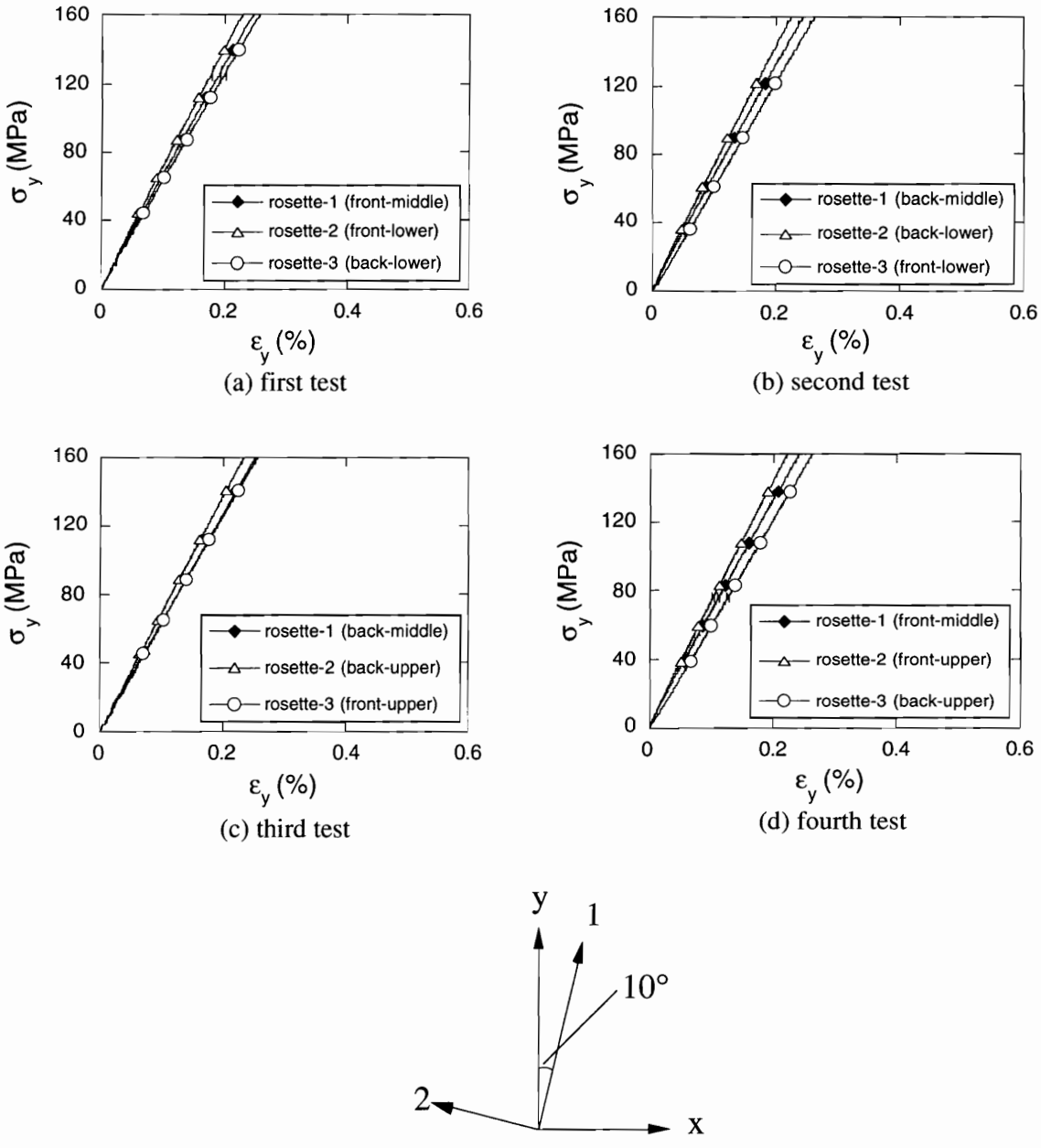

Fig. 3.4 Normal Stress-Strain Curves of 10° Off-Axis Tensile Specimen in x-y Plane
(Tested in Tinius Olsen Test Machine)

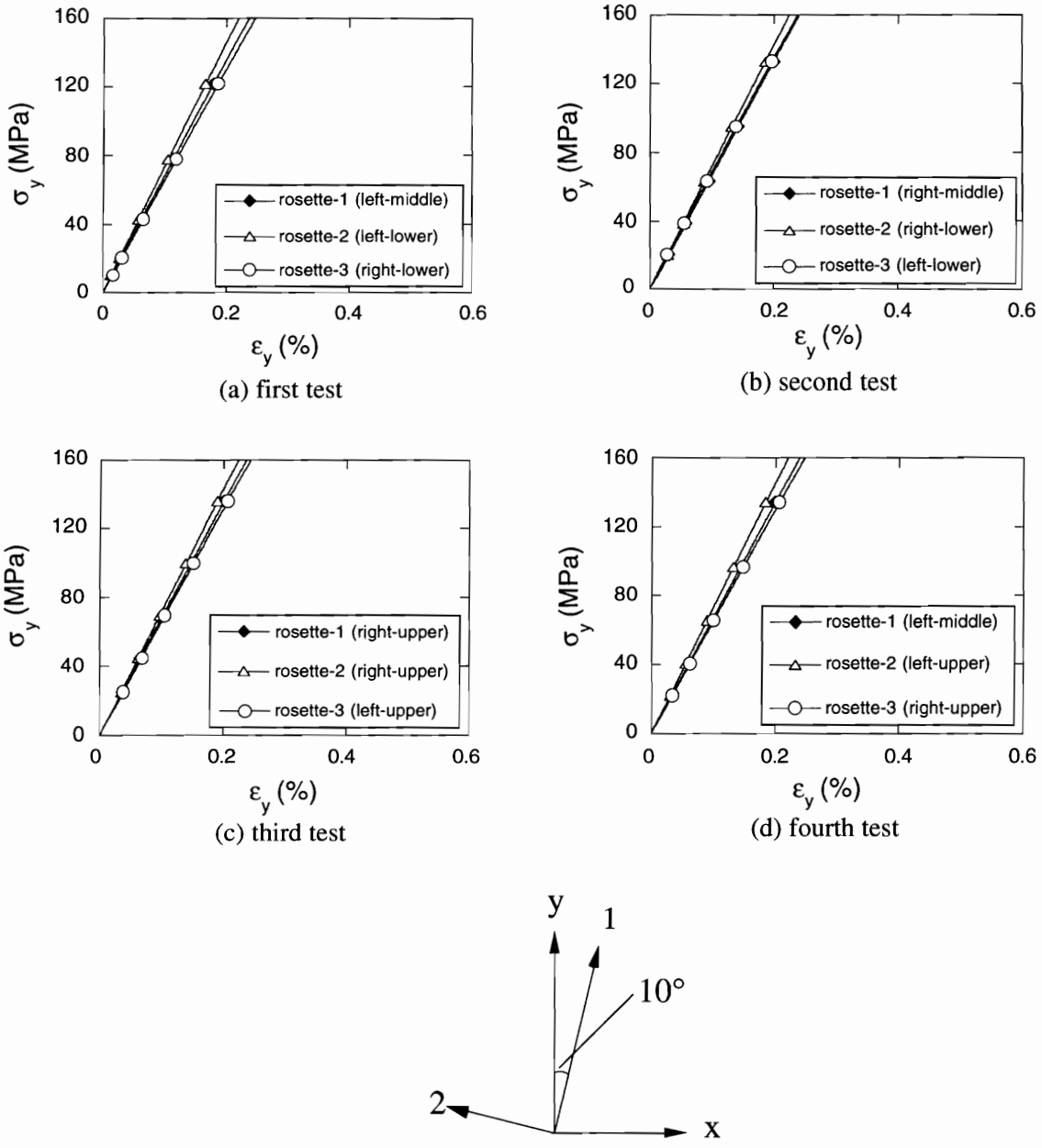

Fig. 3.5 Normal Stress-Strain Curves of 10° Off-Axis Tensile Specimen in x-y Plane
(Tested in Instron-4206 Test Machine)

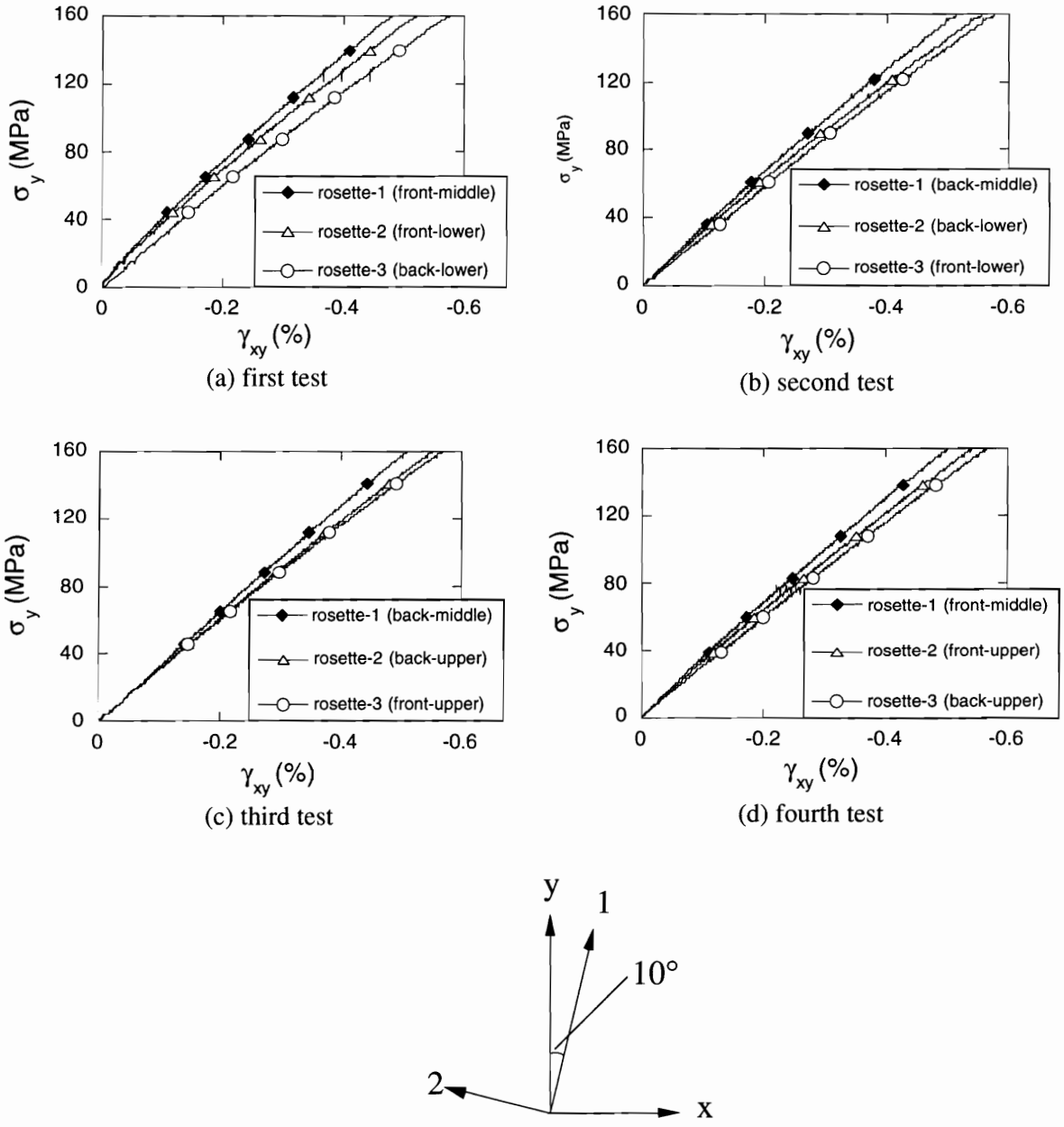

Fig. 3.6 Shear Strain vs Normal Stress Curves of 10° Off-Axis Tensile Specimen in x-y Plane
(Tested in Tinius Olsen Test Machine)

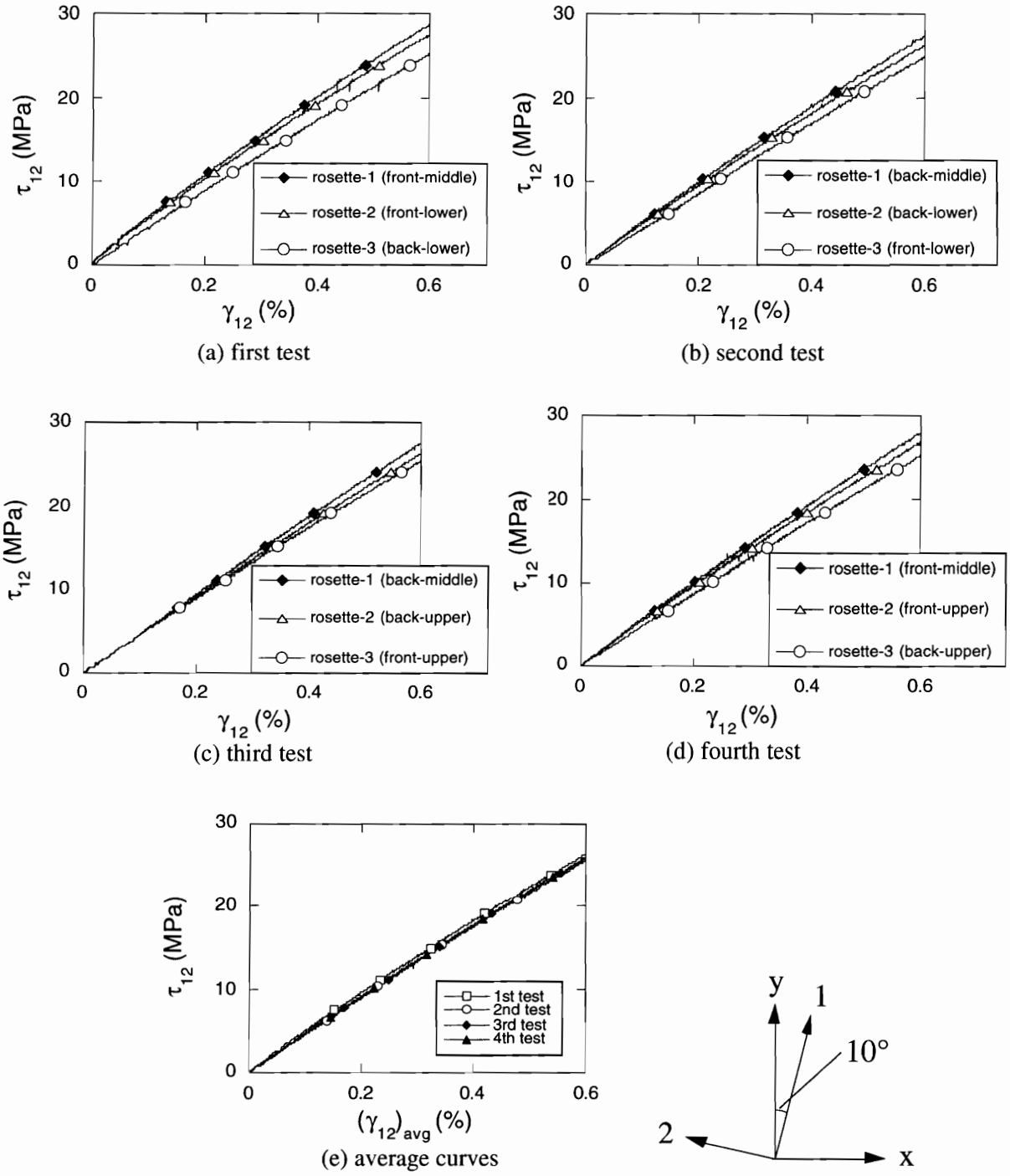

Fig. 3.7 Shear Stress-Strain Curves of 10° Off-Axis Tensile Specimen in 1-2 Plane
(Tested in Tinius Olsen Test Machine)

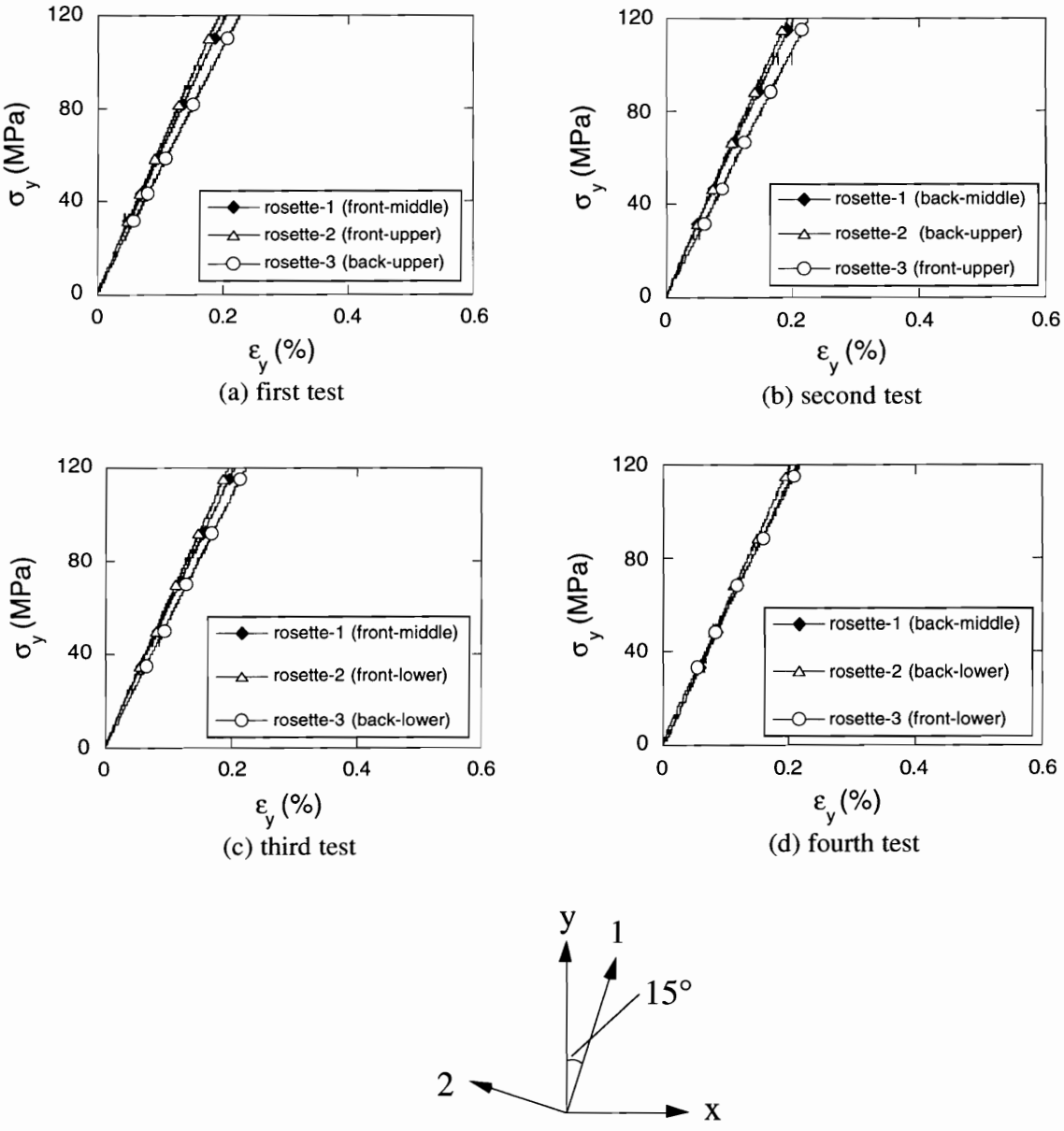

Fig. 3.8 Normal Stress-Strain Curves of 15° Off-Axis Tensile Specimen in x-y Plane
(Tested in Tinius Olsen Test Machine)

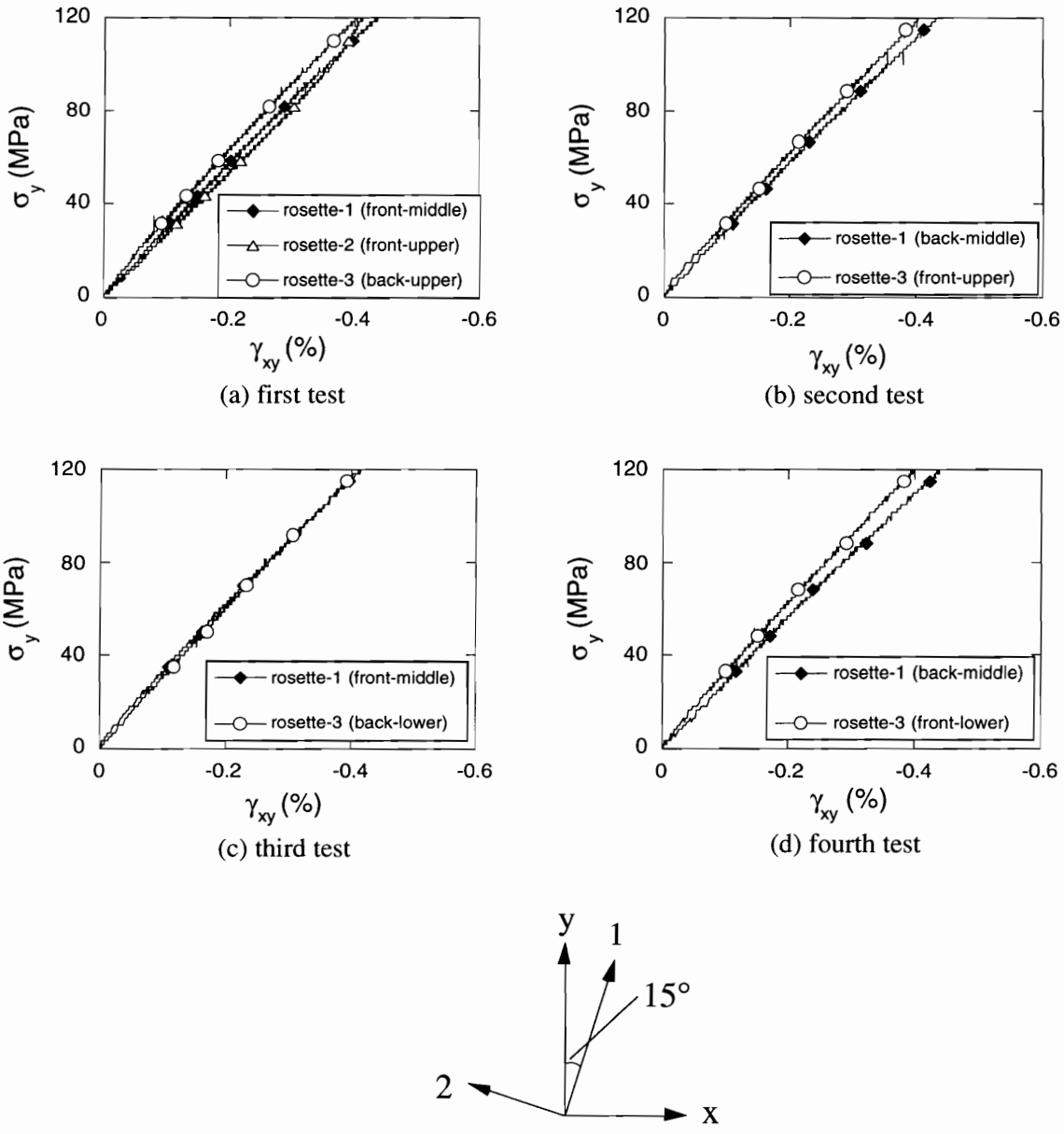

Fig. 3.9 Shear Strain vs Normal Stress Curves of 15° Off-Axis Tensile Specimen in x-y Plane
(Tested in Tinius Olsen Test Machine)

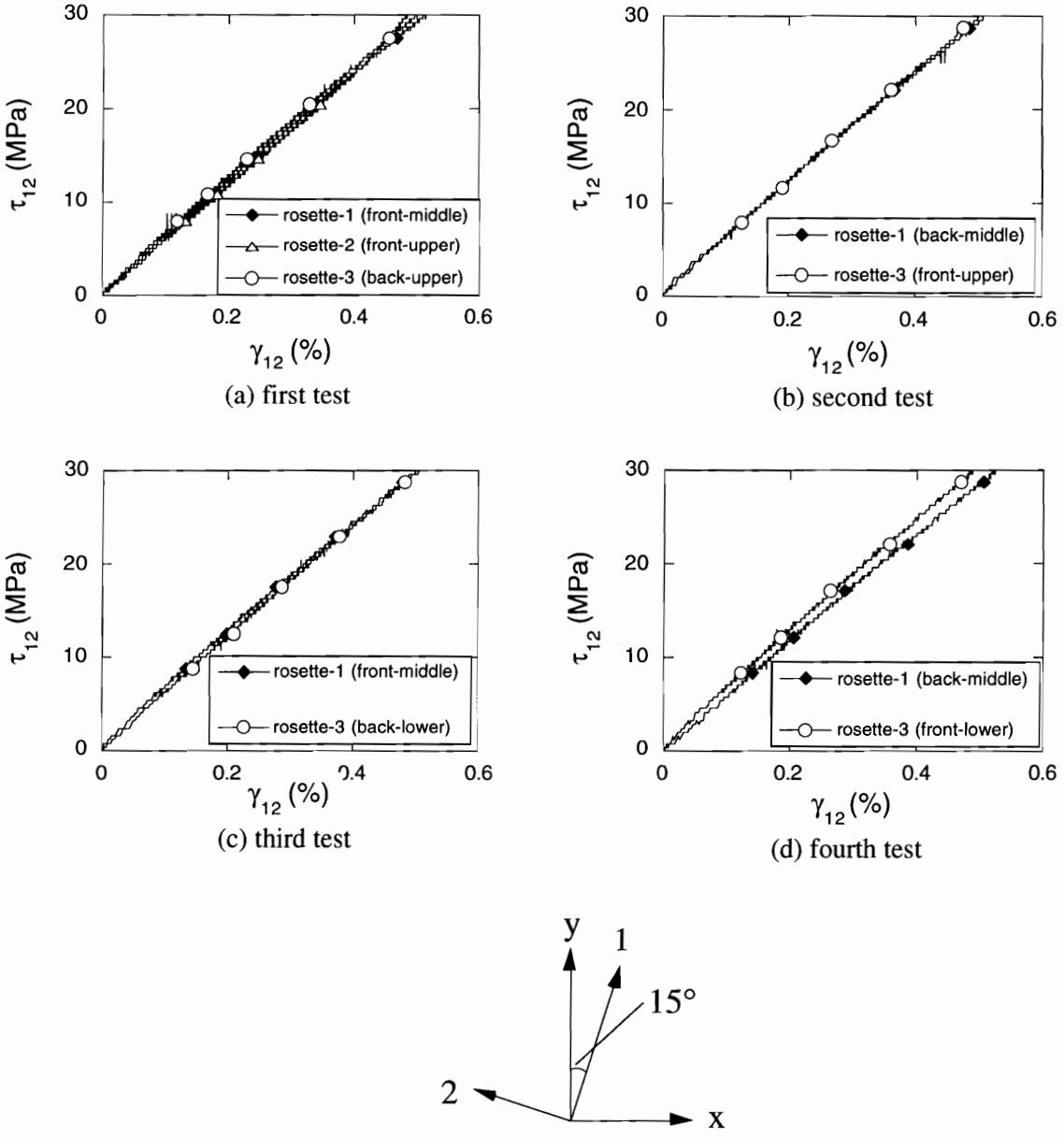

Fig. 3.10 Shear Stress-Strain Curves of 15° Off-Axis Tensile Specimen in 1-2 Plane
(Tested in Tinius Olsen Test Machine)

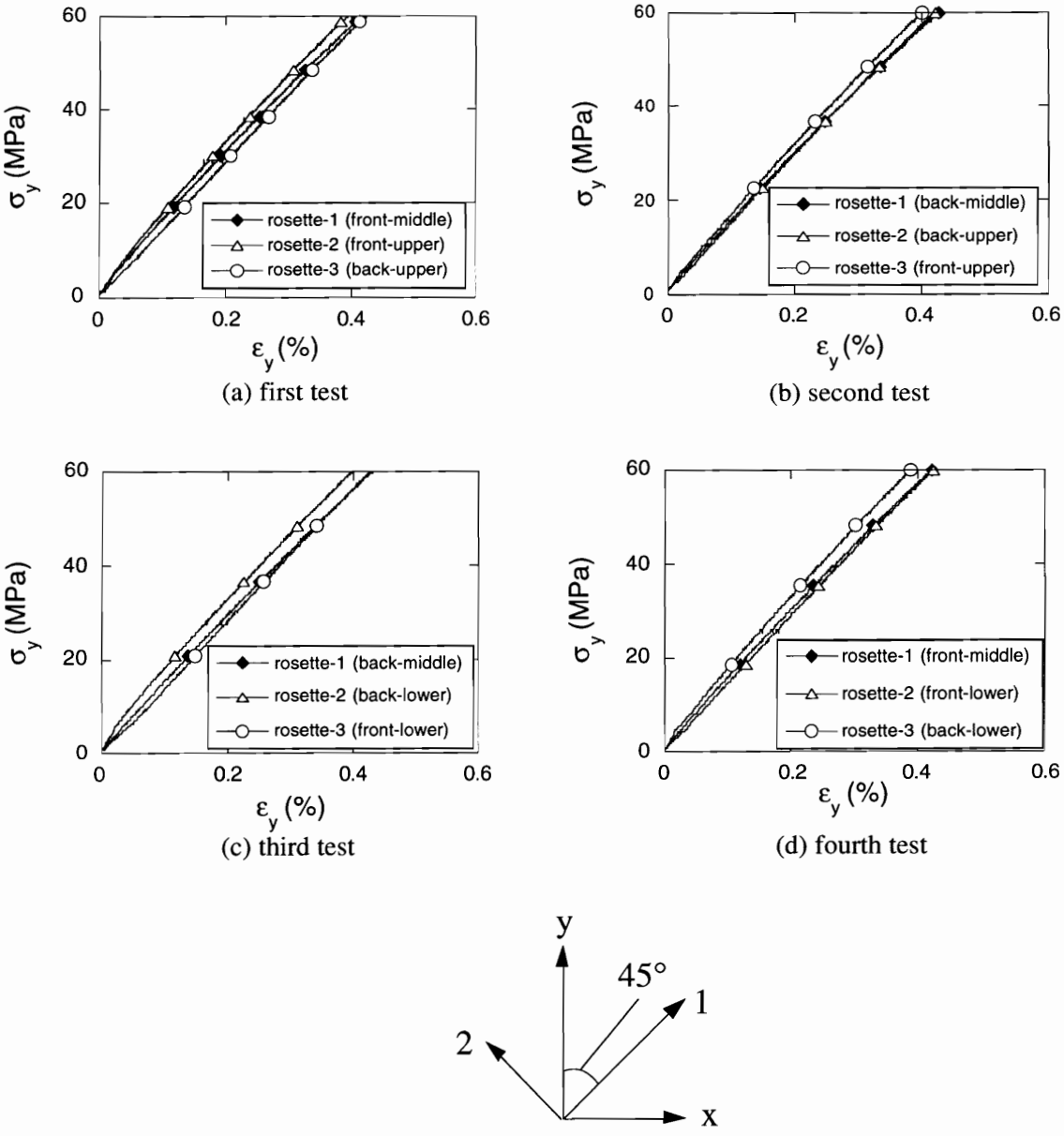

Fig. 3.11 Normal Stress-Strain Curves of 45° Tensile Specimen in x-y Plane
(Tested in Tinius Olsen Test Machine)

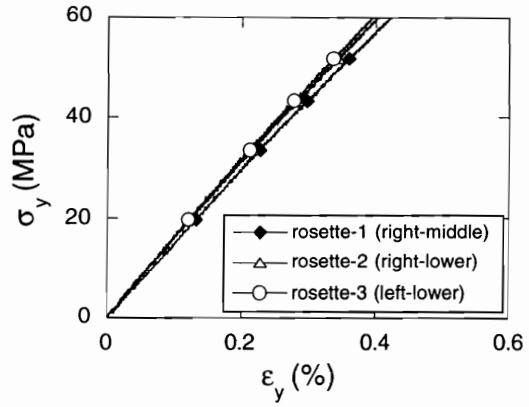

(a) Normal Stress-Strain Curves

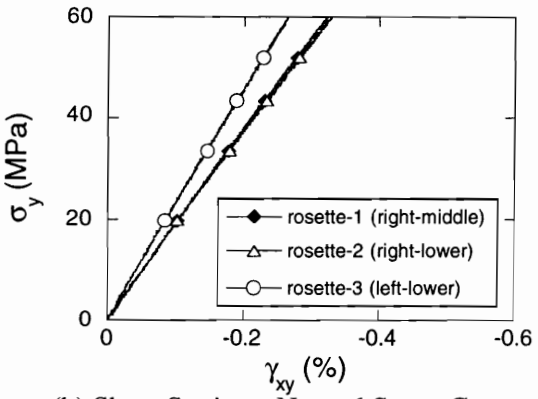

(b) Shear Strain vs Normal Stress Curves
(x-y plane)

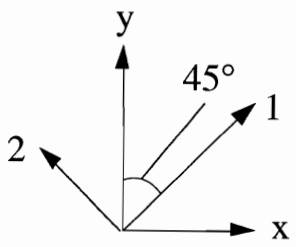

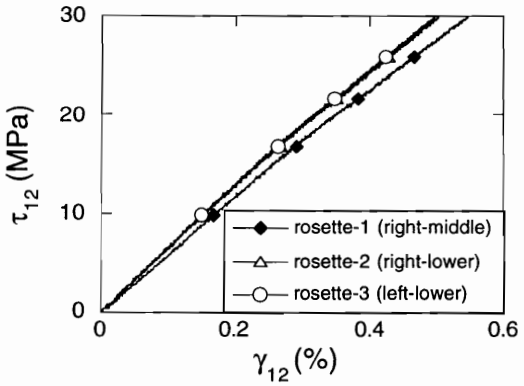

(c) Shear Stress-Strain Curves
(1-2 plane)

Fig. 3.12 Stress-Strain Curves of 45° Off-Axis Tensile Specimen
(Tested in Instron 4206 Test Machine)

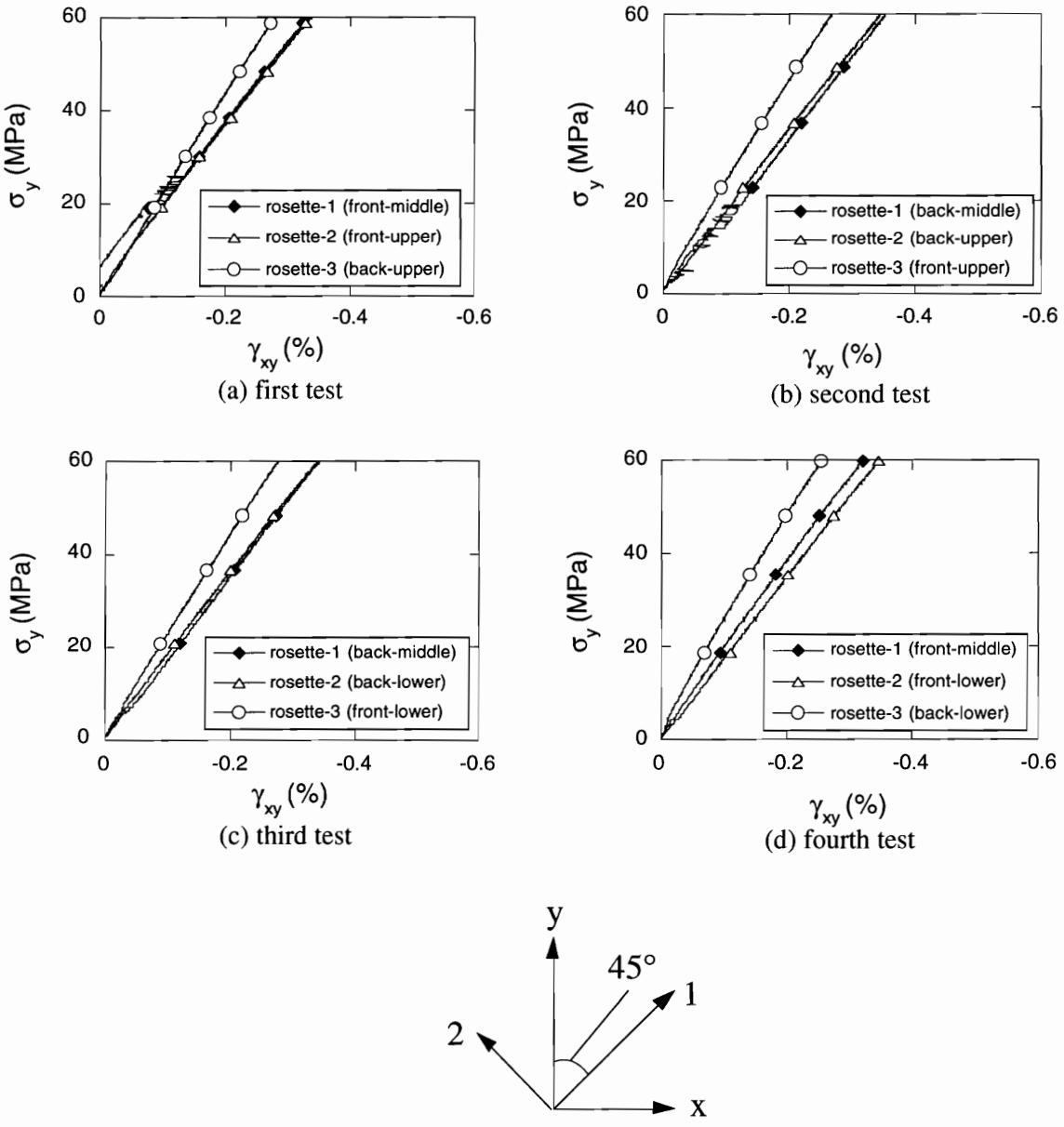

Fig. 3.13 Shear Strain vs Normal Stress Curves of 45° Off-Axis Tensile Specimen in x-y Plane (Tested in Tinius Olsen Test Machine)

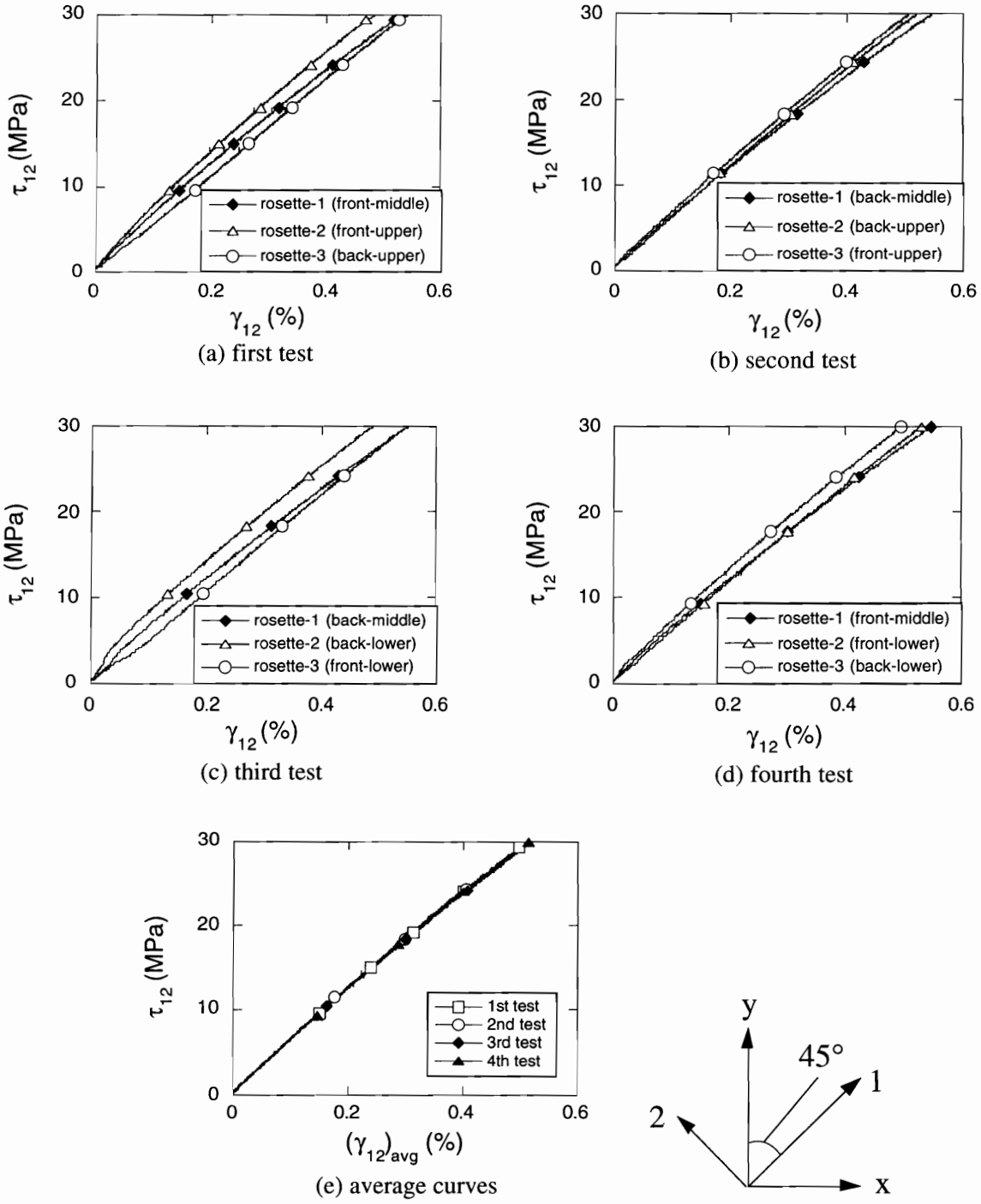

Fig. 3.14 Shear Stress-Strain Curves of 45° Off-Axis Tensile Specimen in 1-2 Plane
(Tested in Tinius Olsen Test Machine)

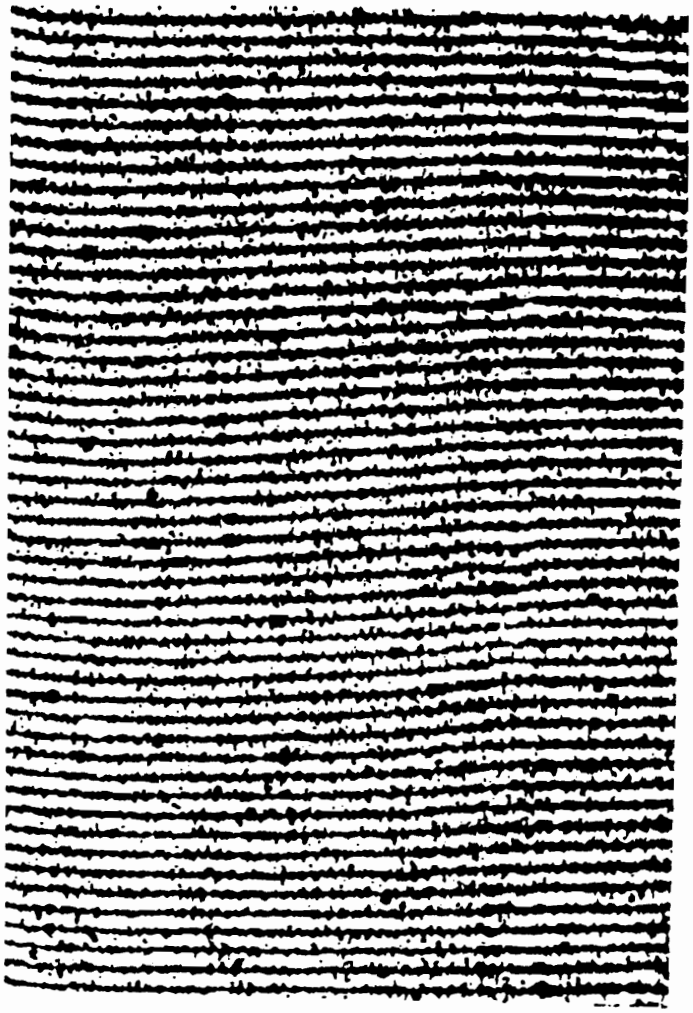

V - Field

Fig. 3.15 Moire Fringe Pattern of 0° Tensile Specimen
(P = 6.67 KN, σ_1= 206.8 MPa)

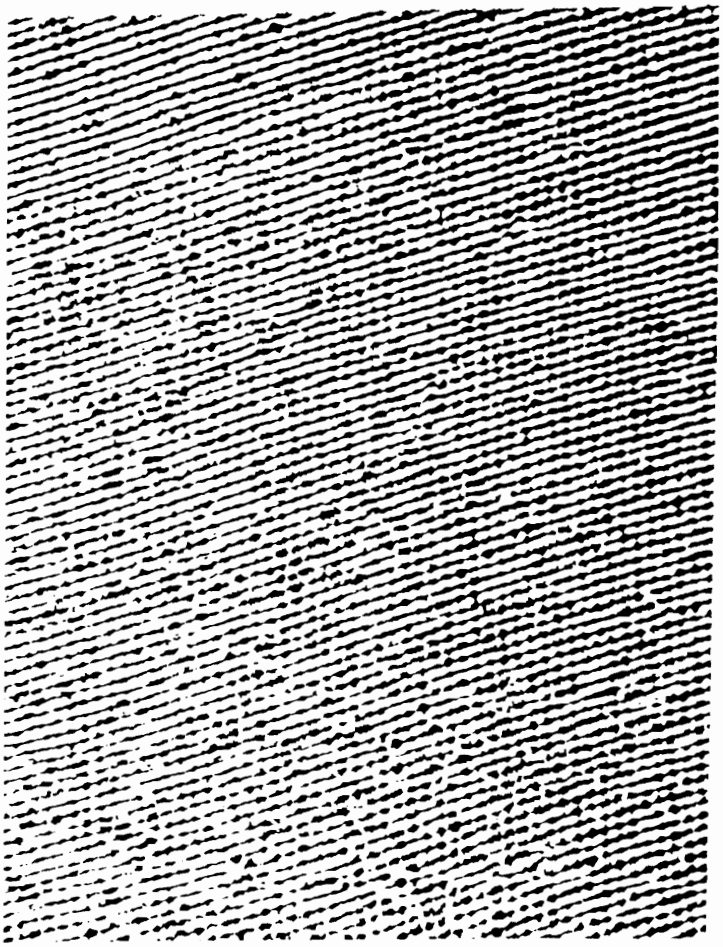

V - Field

Fig. 3.16 Moire Fringe Pattern of 90° Tensile Specimen
(P = 1.33 KN, σ_2 = 20.82 MPa)

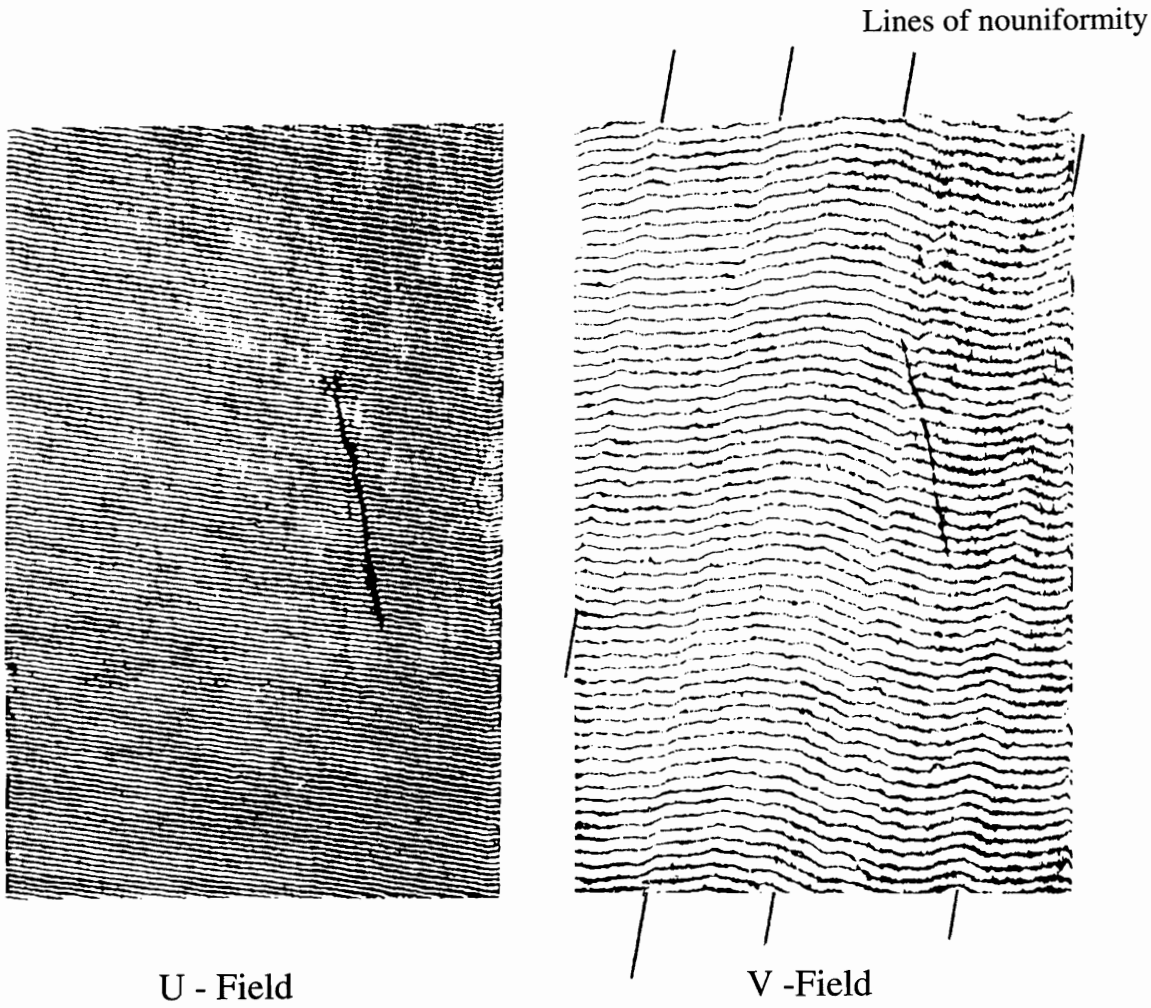

Fig. 3.17 Moire Fringe Patterns of 10° Off-Axis Tensile Specimen
(P = 3.56 KN, τ_{12}= 16.13 MPa)

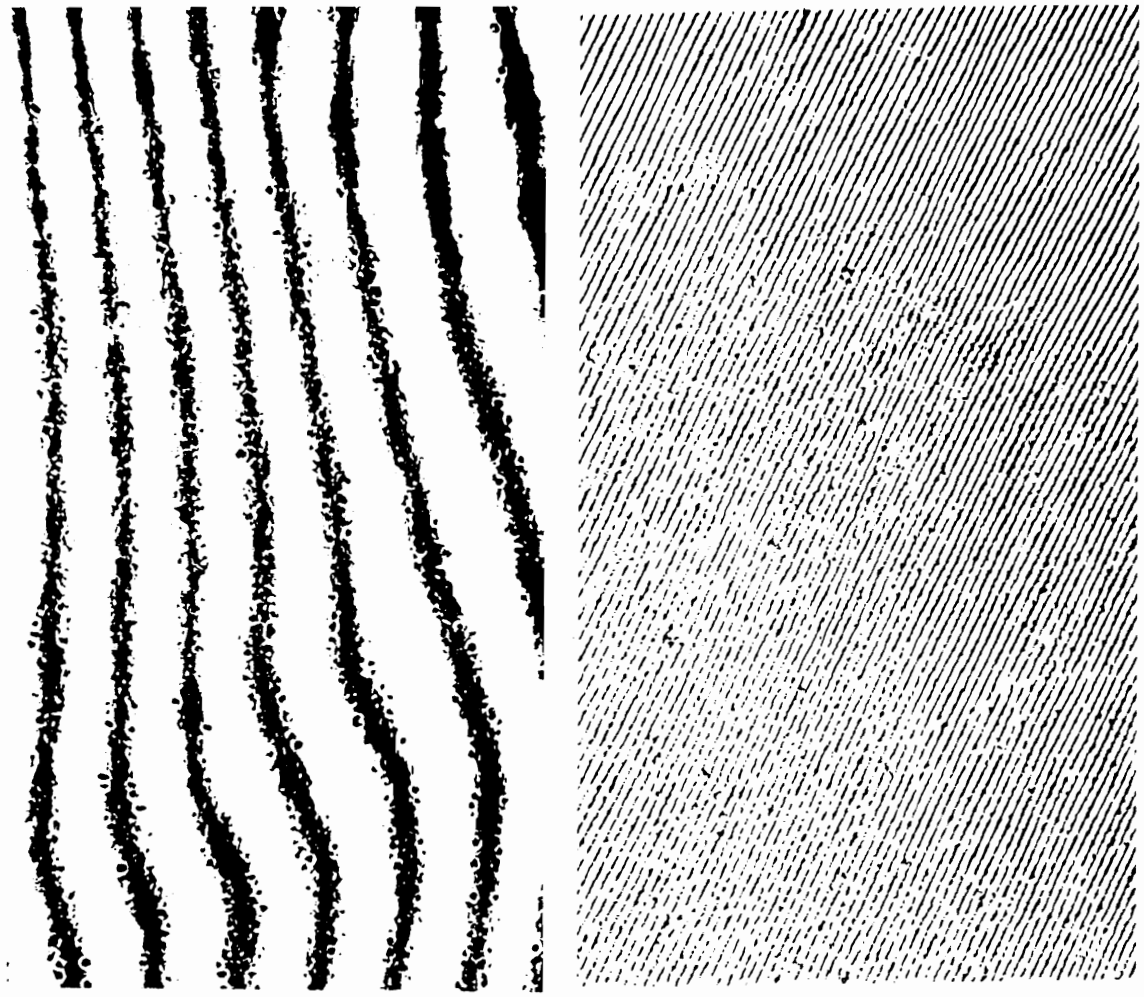

U - Field

V - Field

Fig. 3.18 Moire Fringe Patterns of 15° Off-Axis Tensile Specimen
(P = 2.56 KN, τ_{12}= 20.45 MPa)

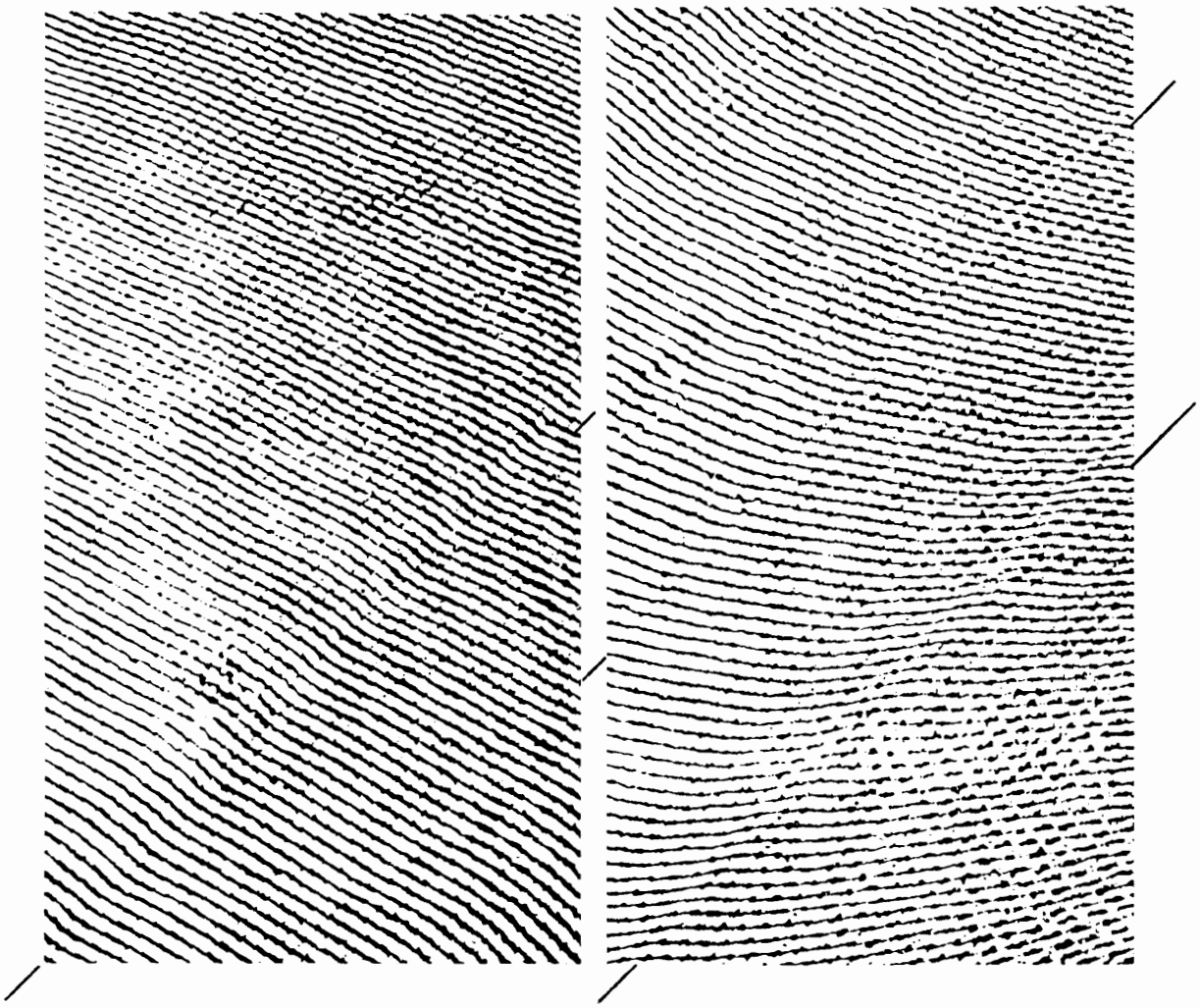

Fig. 3.19 Moire Fringe Patterns of 45° Off-Axis Tensile Specimen
(P = 1.21 KN, τ_{12}= 19.32 MPa)

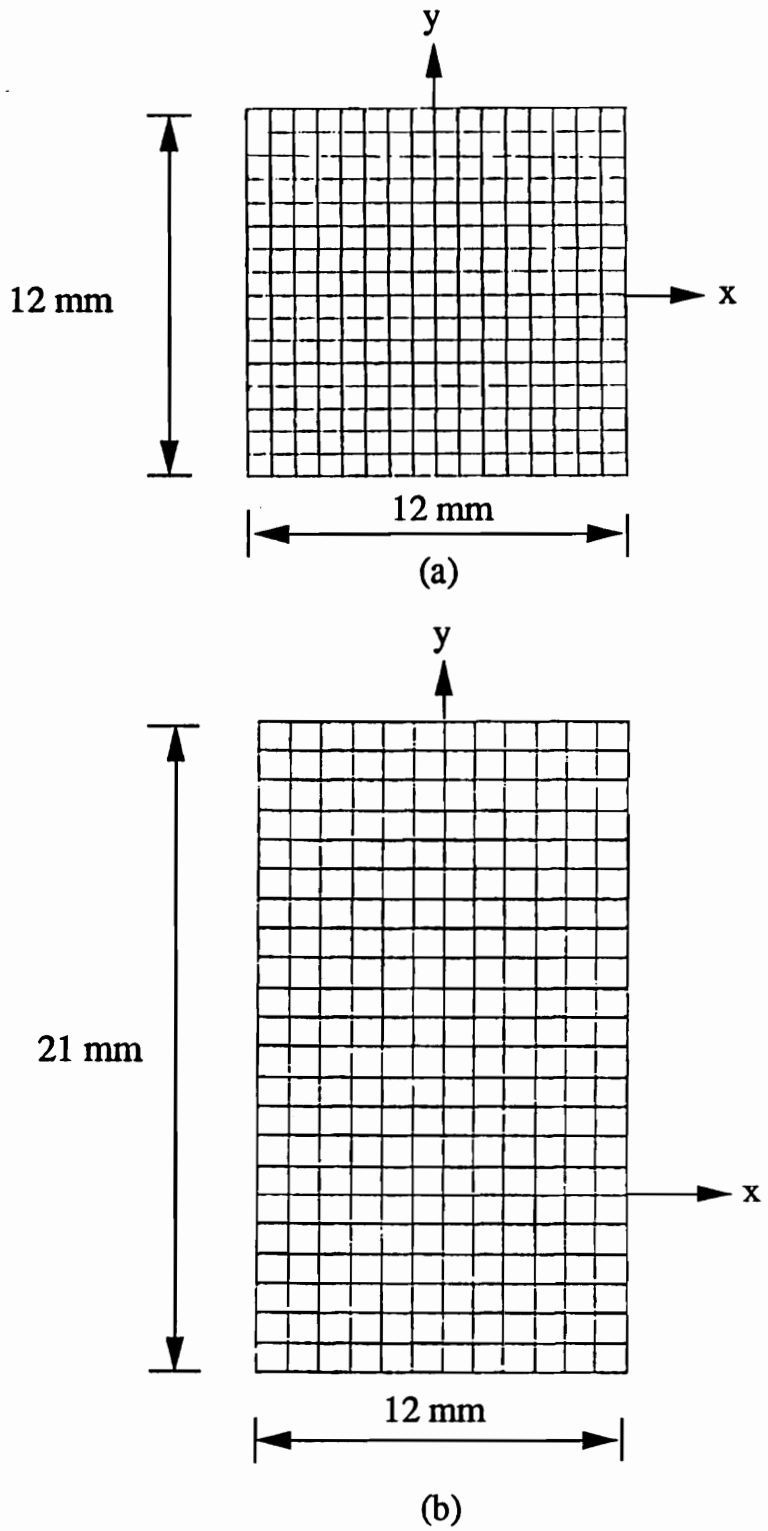

Fig. 3.20 Finite Element Meshes for Localized Hybrid Analysis
(a) 0°, 90°, 15° and 45° Specimens, (b) 10° Specimen

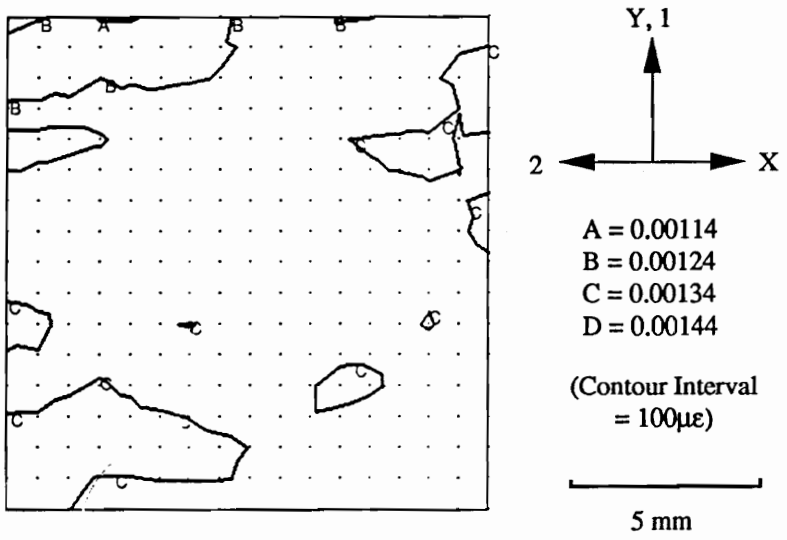

Fig. 3.21 Strain Contour of ε_1 of 0° Tensile Specimen

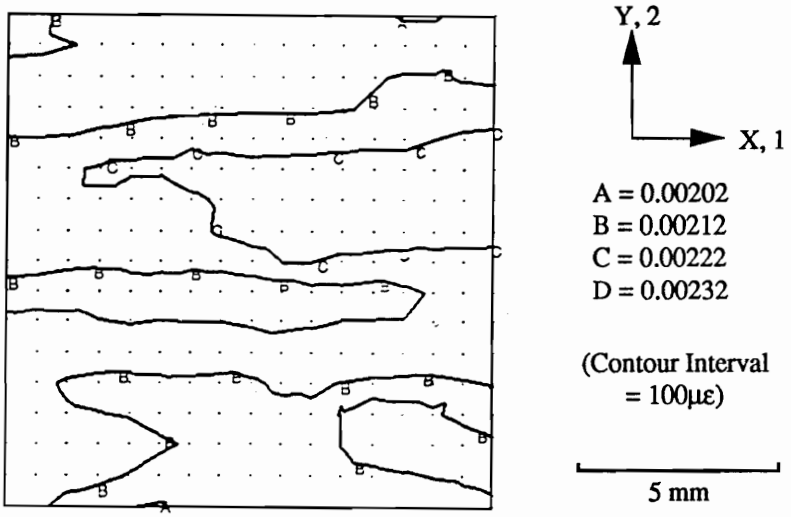

Fig. 3.22 Strain Contour of ε_2 of 90° Tensile Specimen

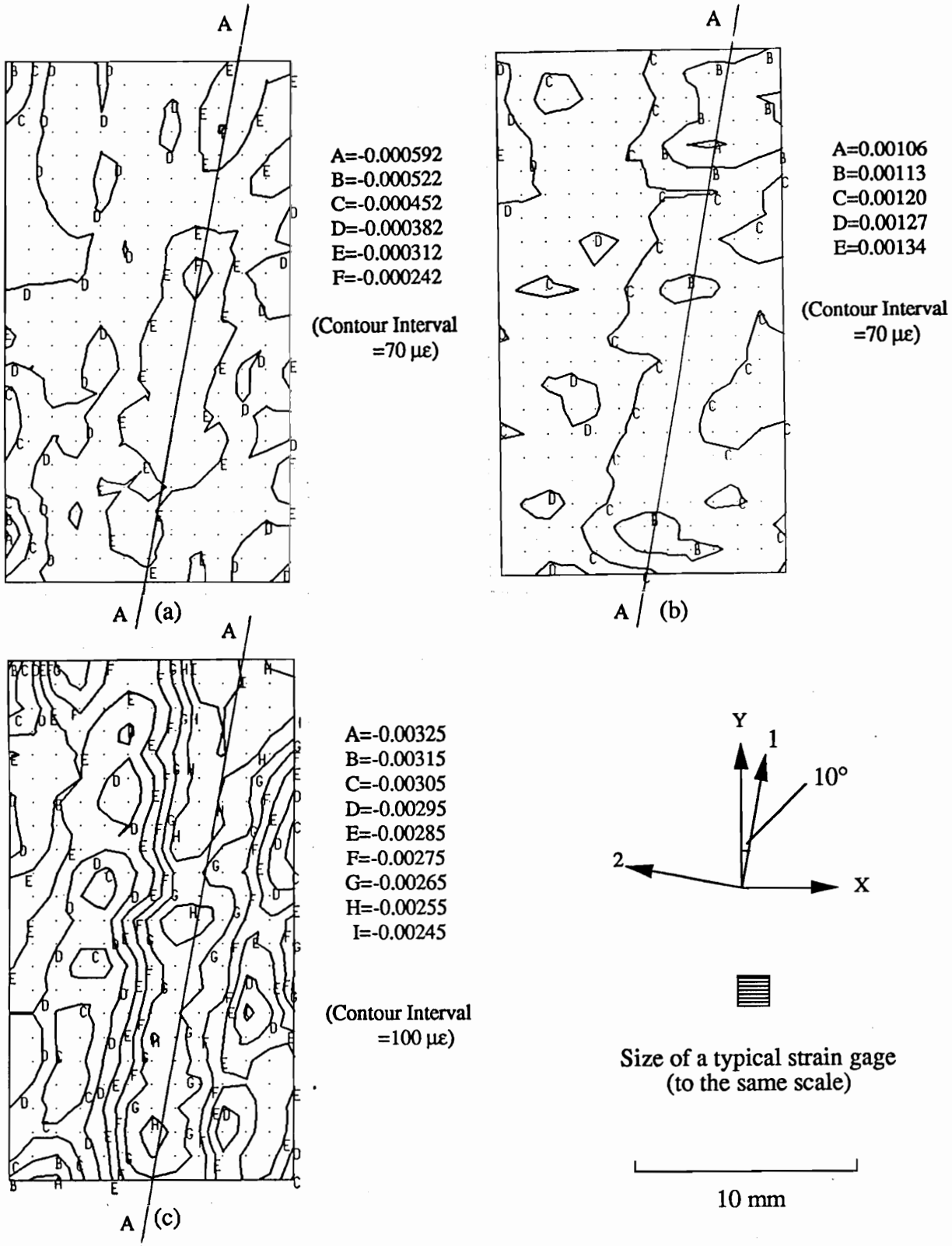

Fig. 3.23 Strain Contours in x-y Plane for 10° Off-Axis Tensile Specimen
(a) ε_x, (b) ε_y, (c) γ_{xy}

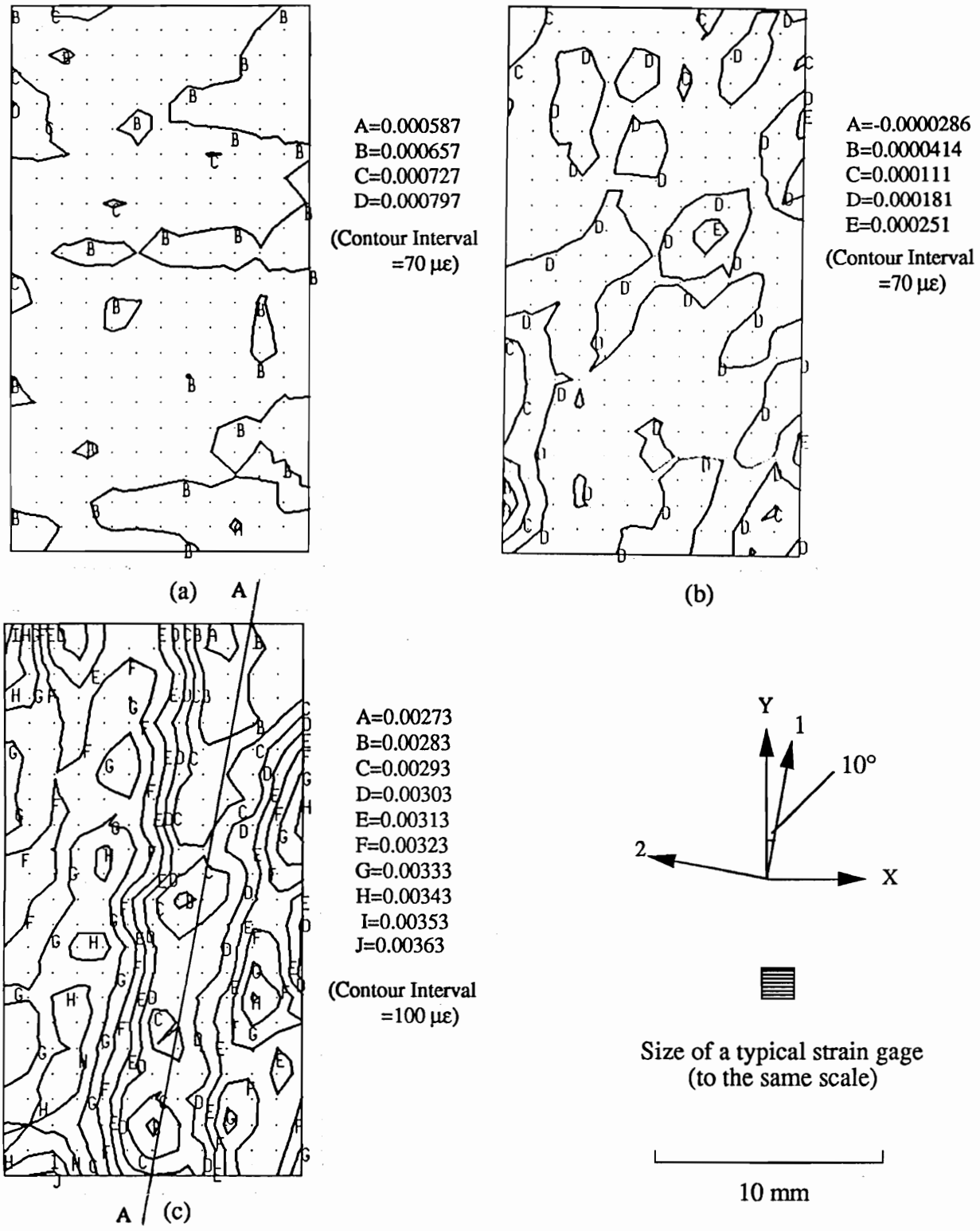

Fig. 3.24 Strain Contours in 1-2 Plane for 10° Off-Axis Tensile Specimen (a) ε_1, (b) ε_2, (c) γ_{12}

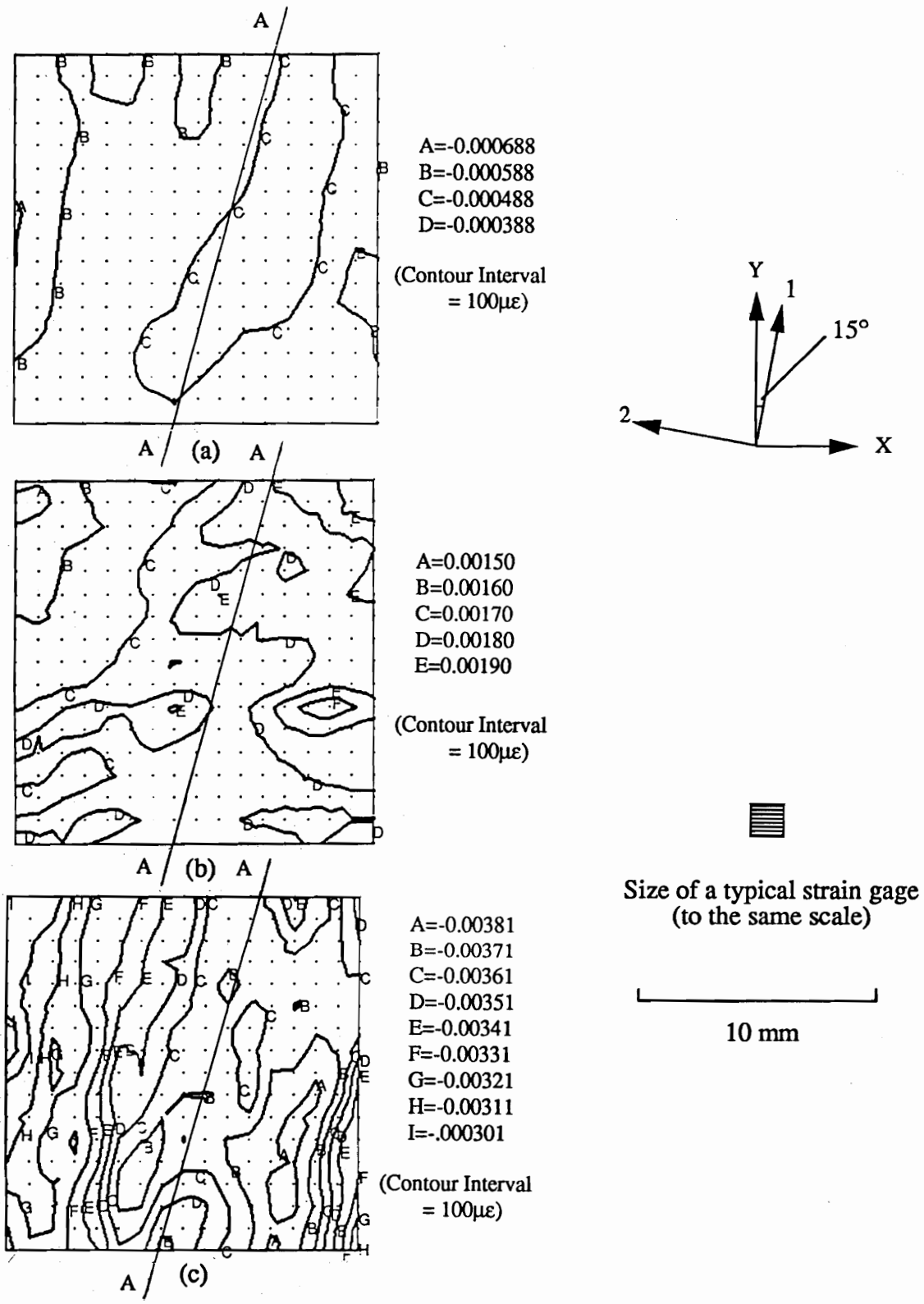

Fig. 3.25 Strain Contours in x-y Plane for 15° Off-Axis Tensile Specimen
(a) ε_x, (b) ε_y, (c) γ_{xy}

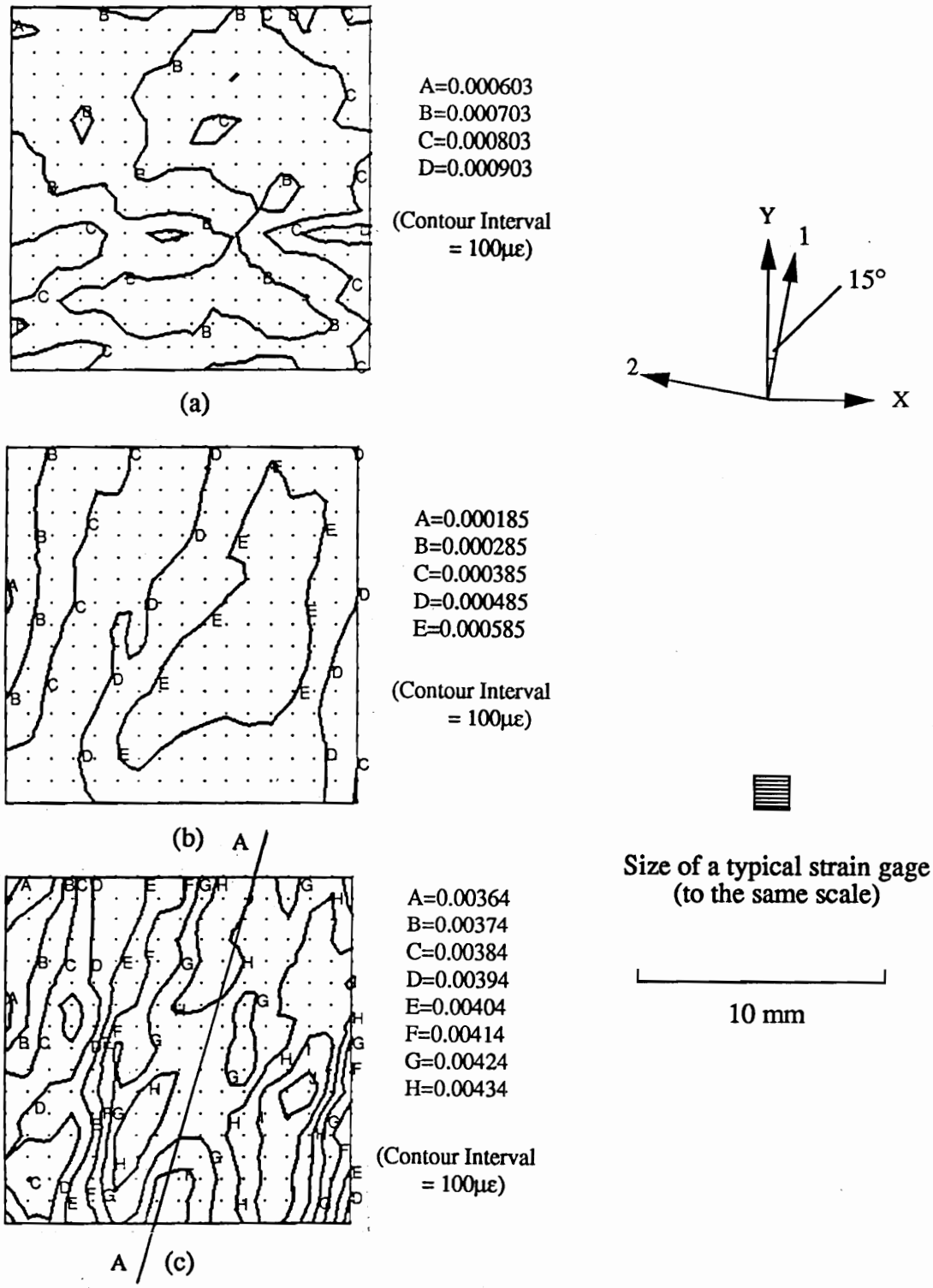

Fig. 3.26 Strain Contours in 1-2 Plane for 15° Off-Axis Tensile Specimen (a) ε_1, (b) ε_2, (c) γ_{12}

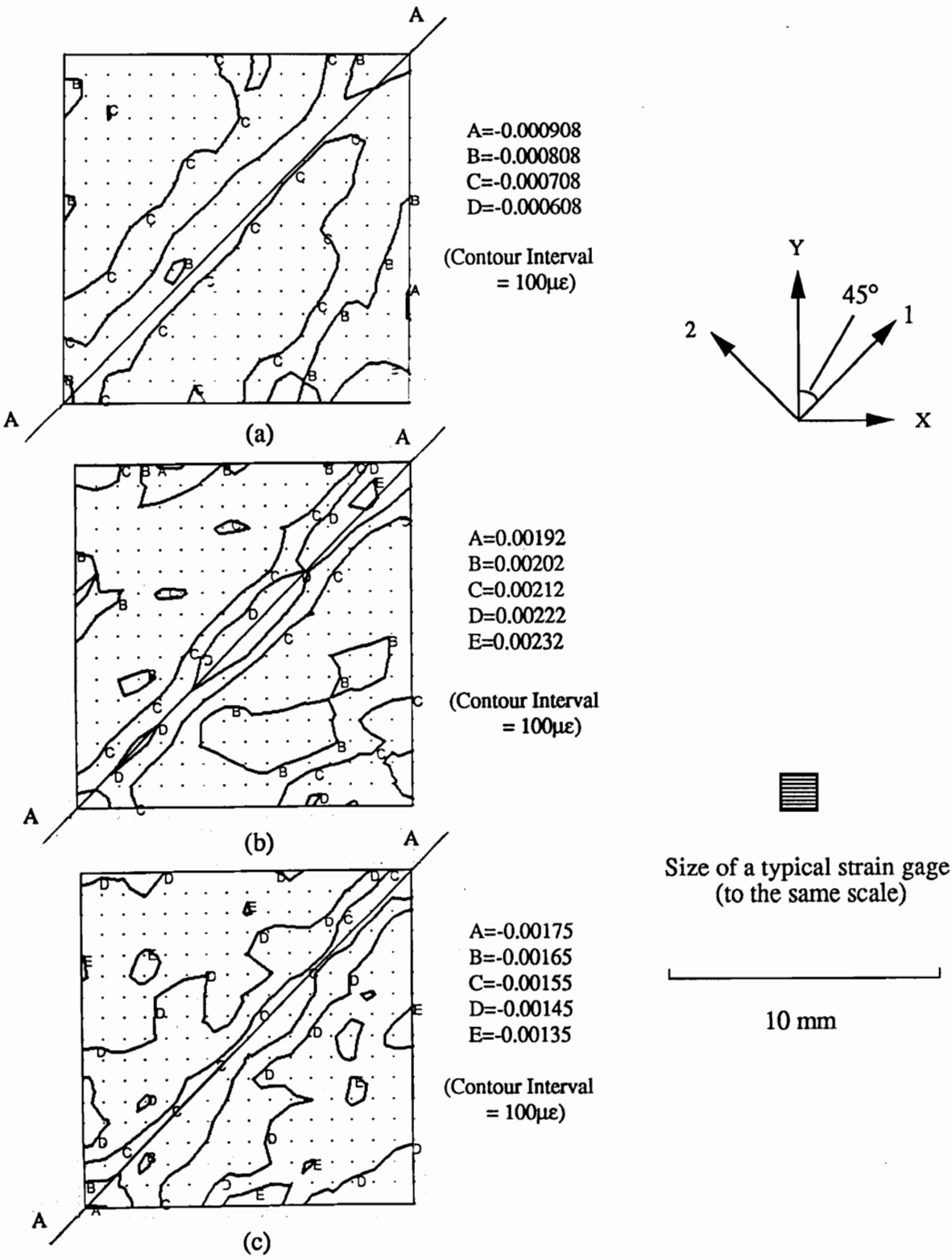

Fig. 3.27 Strain Contours in x-y Plane for 45° Off-Axis Tensile Specimen
(a) ε_x, (b) ε_y, (c) γ_{xy}

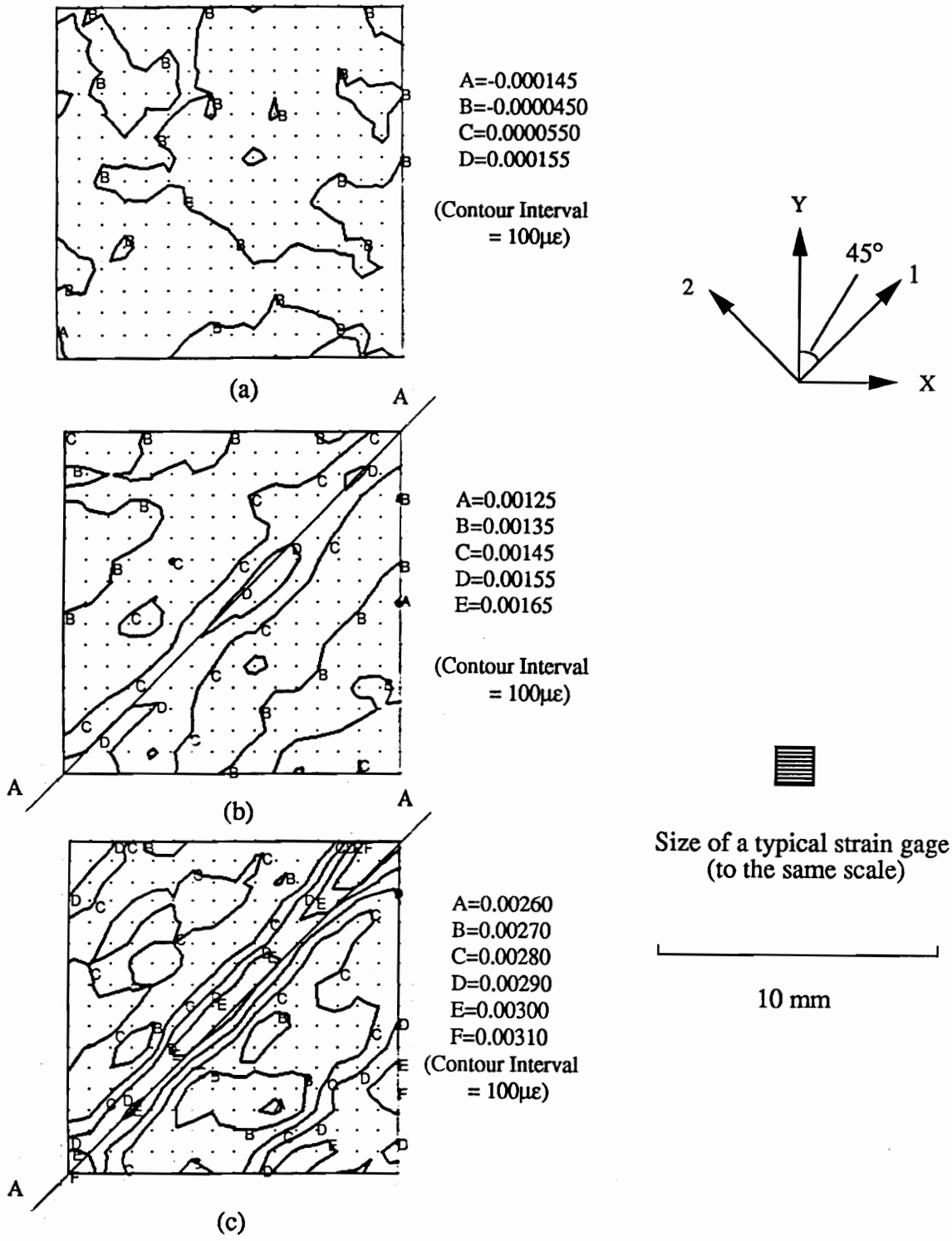

Fig. 3.28 Strain Contours in 1-2 Plane for 45° Off-Axis Tensile Specimen
(a) ε_1, (b) ε_2, (c) γ_{12}

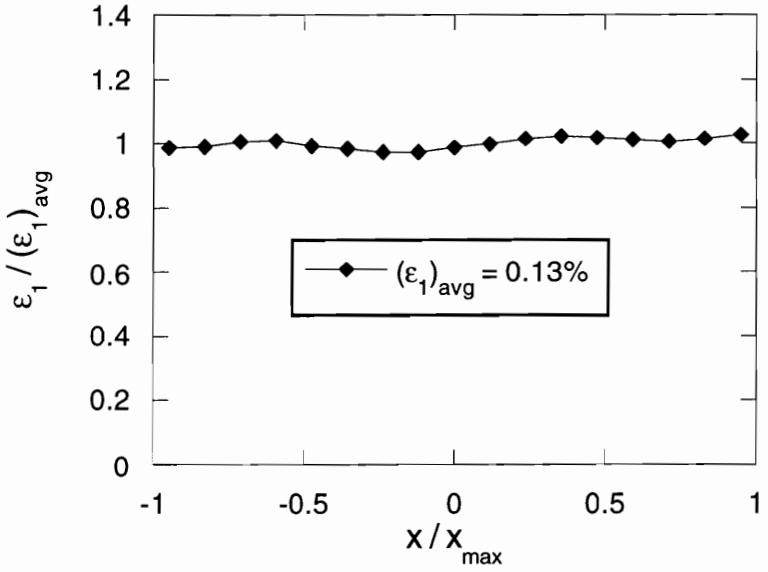

Fig. 3.29 Normalized Normal Strain Distribution along Center Line of 0° Tensile Specimen

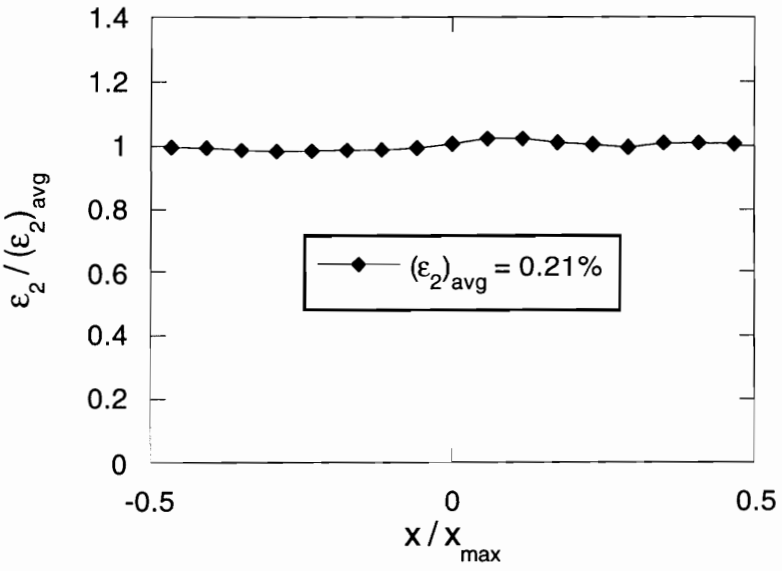

Fig. 3.30 Normalized Normal Strain Distribution along Center Line of 90° Tensile Specimen

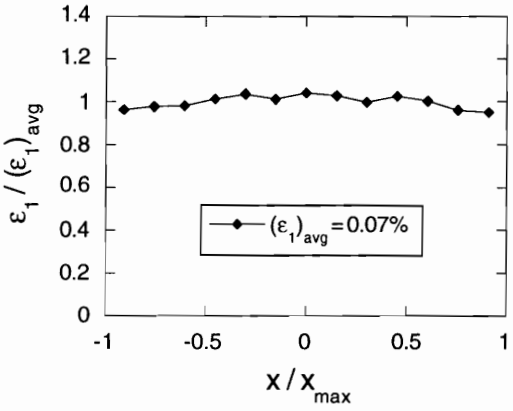

(a)

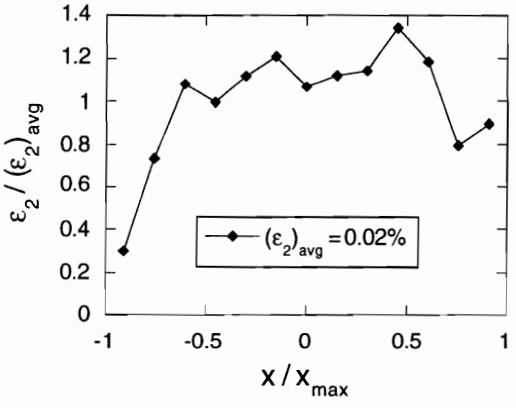

(b)

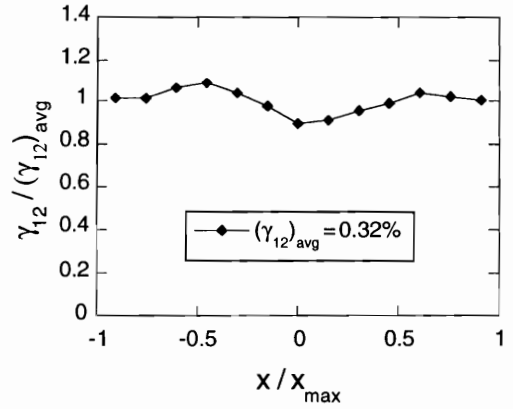

(c)

Fig. 3.31 Normalized Strain Distributions along Center Line of 10° Off-Axis Tensile Specimen: (a) $\varepsilon_1/(\varepsilon_1)_{avg}$, (b) $\varepsilon_2/(\varepsilon_2)_{avg}$, (c) $\gamma_{12}/(\gamma_{12})_{avg}$

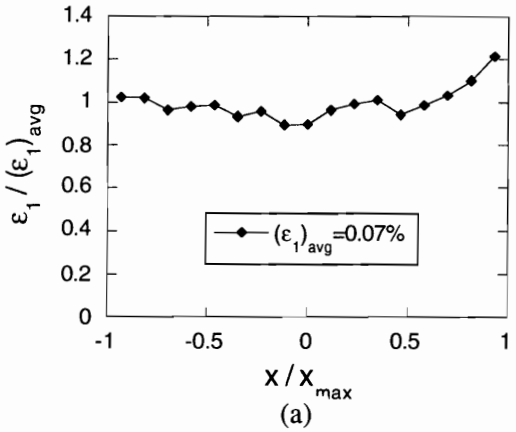

(a)

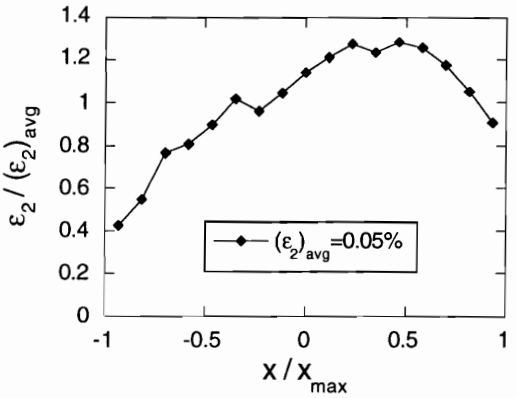

(b)

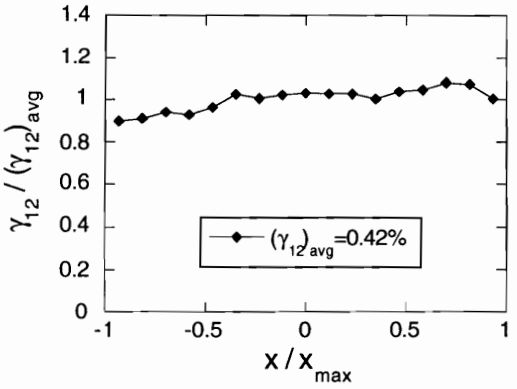

(c)

Fig. 3.32 Normalized Strain Distributions along Center Line of 15° Off-Axis Tensile Specimen: (a) $\varepsilon_1/(\varepsilon_1)_{avg}$, (b) $\varepsilon_2/(\varepsilon_2)_{avg}$, (c) $\gamma_{12}/(\gamma_{12})_{avg}$

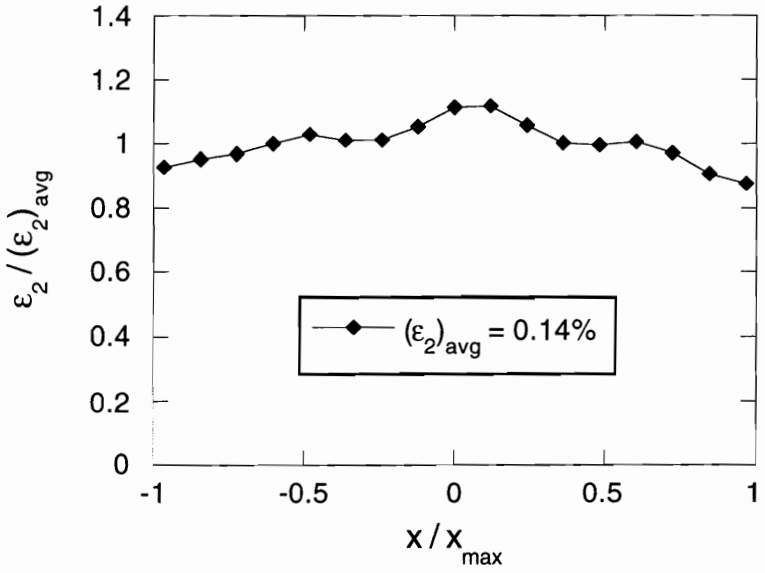

(a)

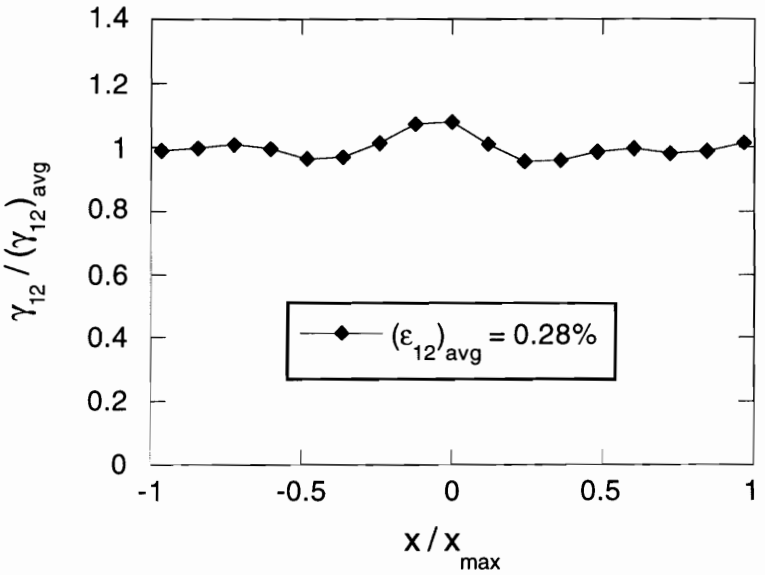

(b)

Fig. 3.33 Normalized Strain Distributions along Center Line of 45° Off-Axis Tensile Specimen: (a) $\varepsilon_2/(\varepsilon_2)_{avg}$, (b) $\gamma_{12}/(\gamma_{12})_{avg}$

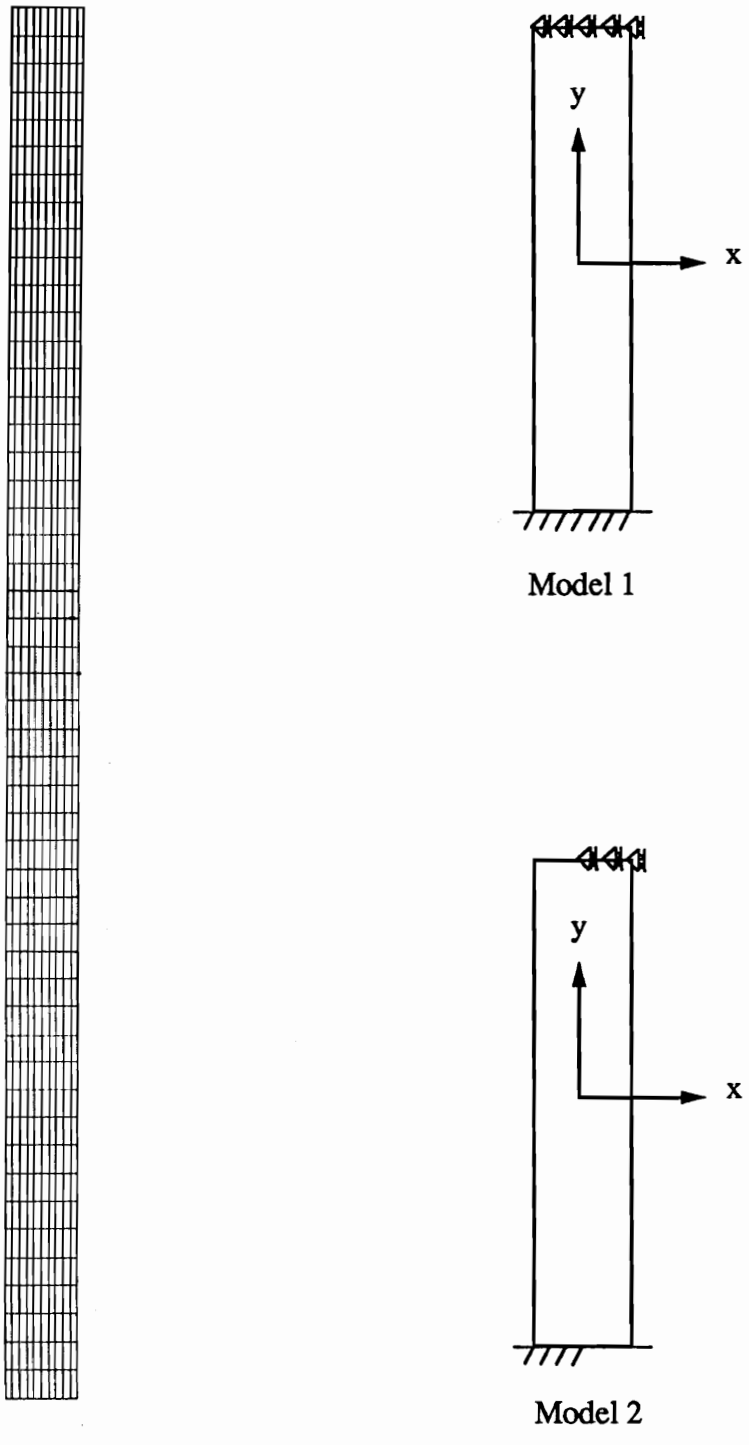

Fig. 3.34 Finite Element Models for 10° Off-Axis Tensile Specimen

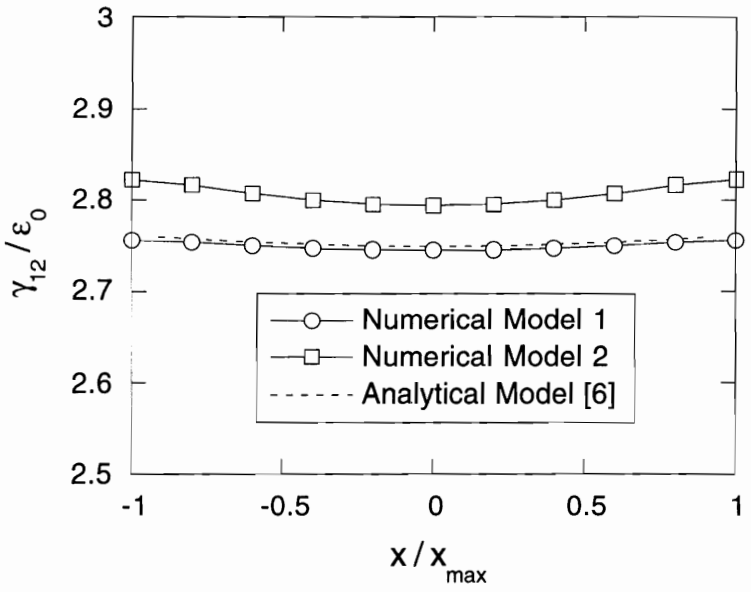

Fig. 3.35 Numerical Prediction of Shear Strain Distribution along Center Line of 10° Off-Axis Tensile Specimen

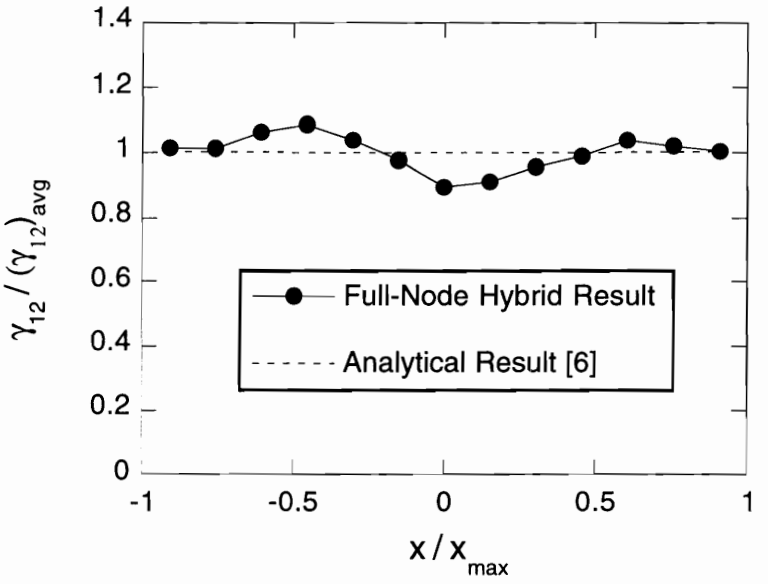

Fig. 3.36 Normalized Shear Strain Distribution along Center Line of 10° Off-Axis Tensile Specimen

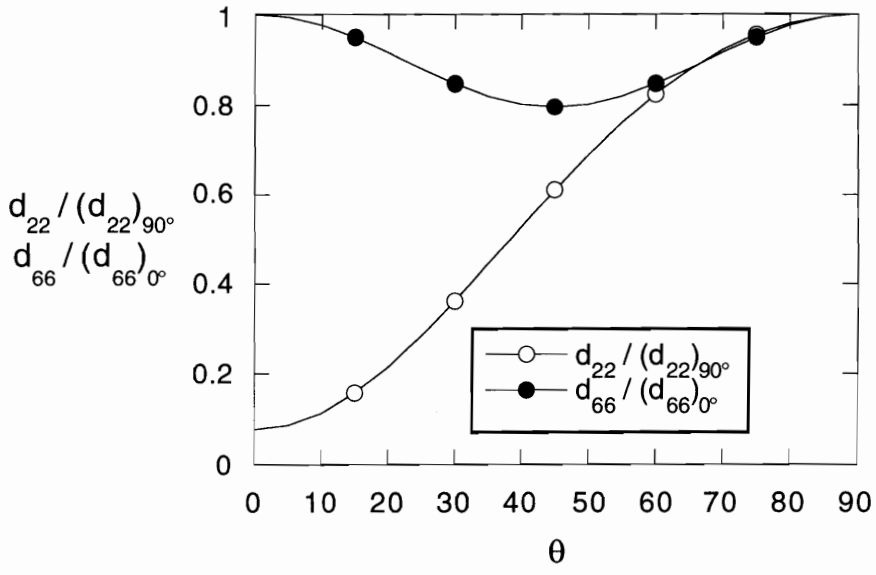

Fig. 3.37 Variation of Normalized Flexural Compliance with Fiber Orientation

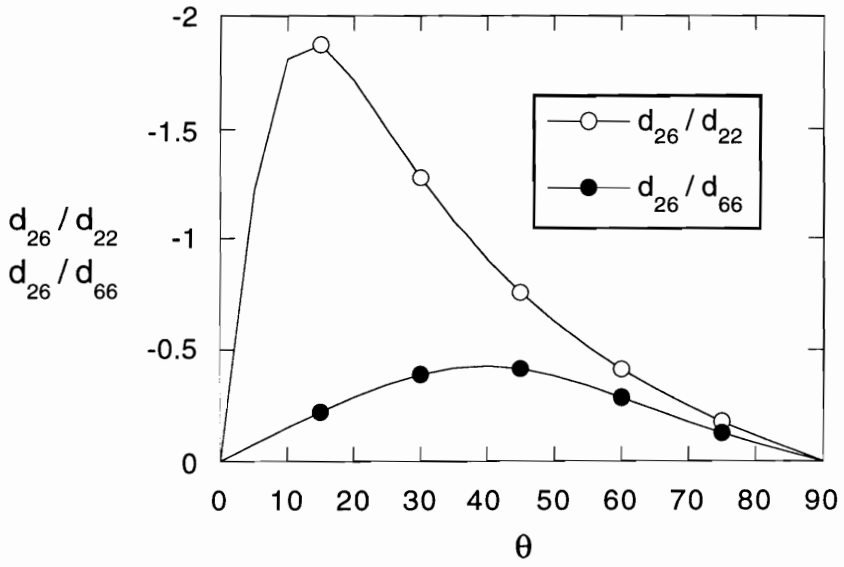

Fig. 3.38 Variation of Bending-Twisting Coupling with Fiber Orientation

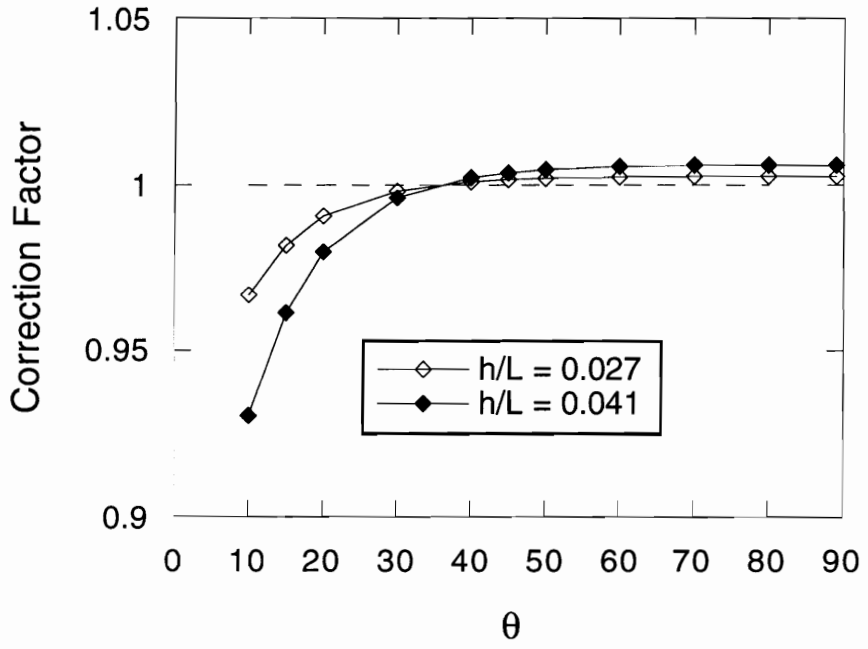

Fig. 3.39 Variation of Correction Factor with Fiber Orientation

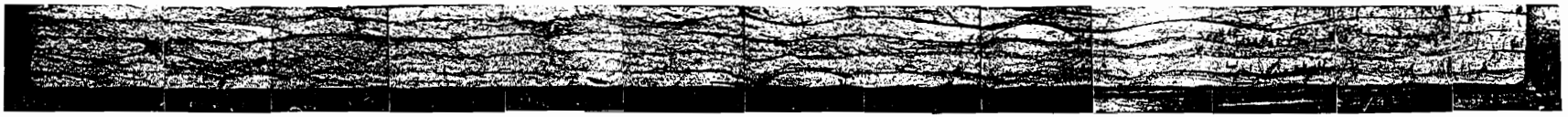

(a)

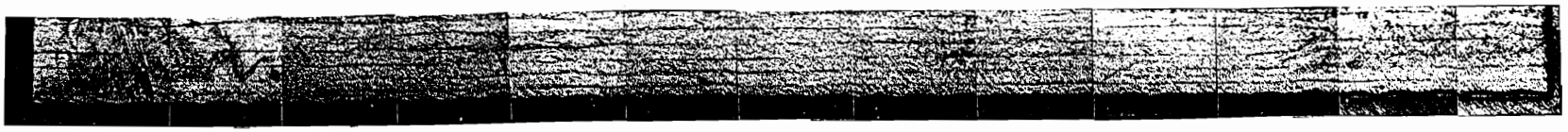

(b)

Fig. 3.40 Micrographs of Off-Axis Tensile Specimen (a) 10° Specimen of AS4/3501-6
(b) 45° Specimen of AS4/3502

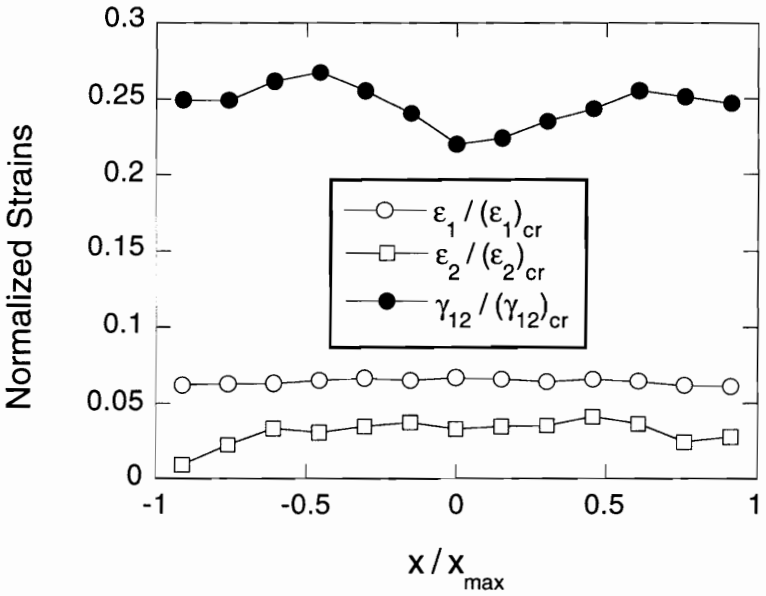

Fig. 3.41 Normalized Strain Distributions along Center Line of 10° Off-Axis Specimen

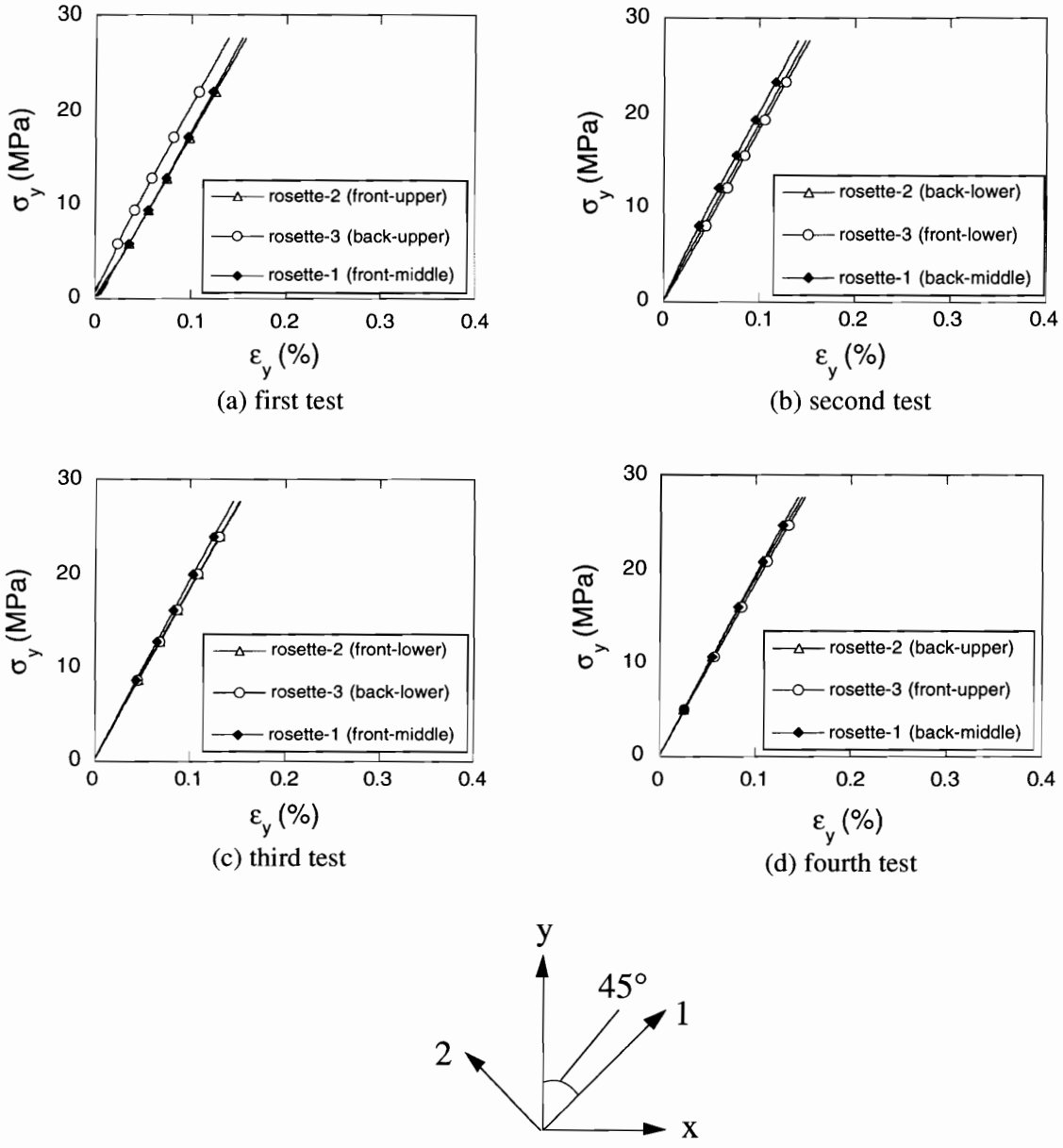

Fig. 3.42 Normal Stress-Strain Curves of ± 45° Tensile Specimen in x-y Plane
(Tested in Tinius Olsen Test Machine)

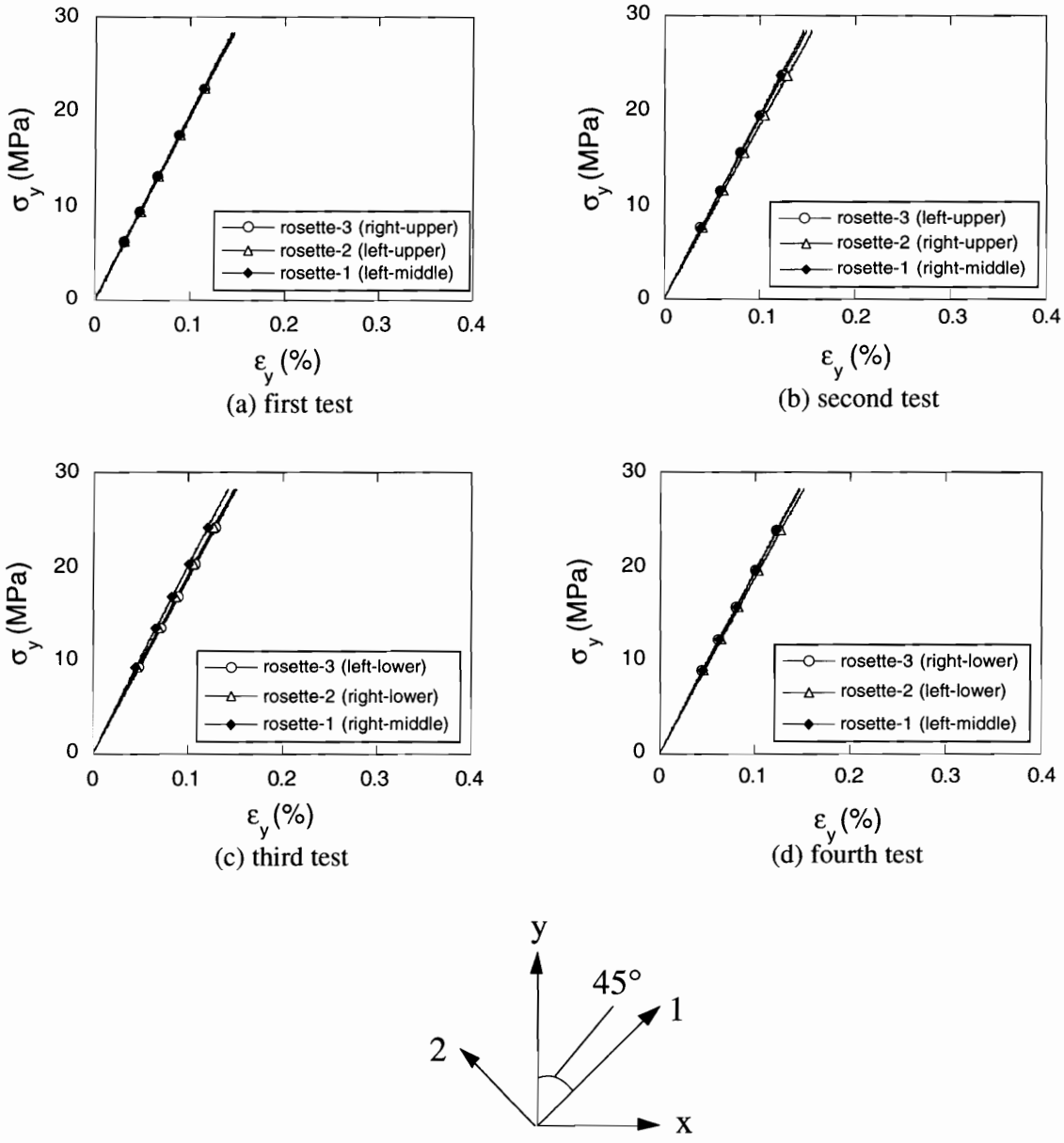

Fig. 3.43 Normal Stress-Strain Curves of ± 45° Tensile Specimen in x-y Plane
(Tested in Instron-4206 Test Machine)

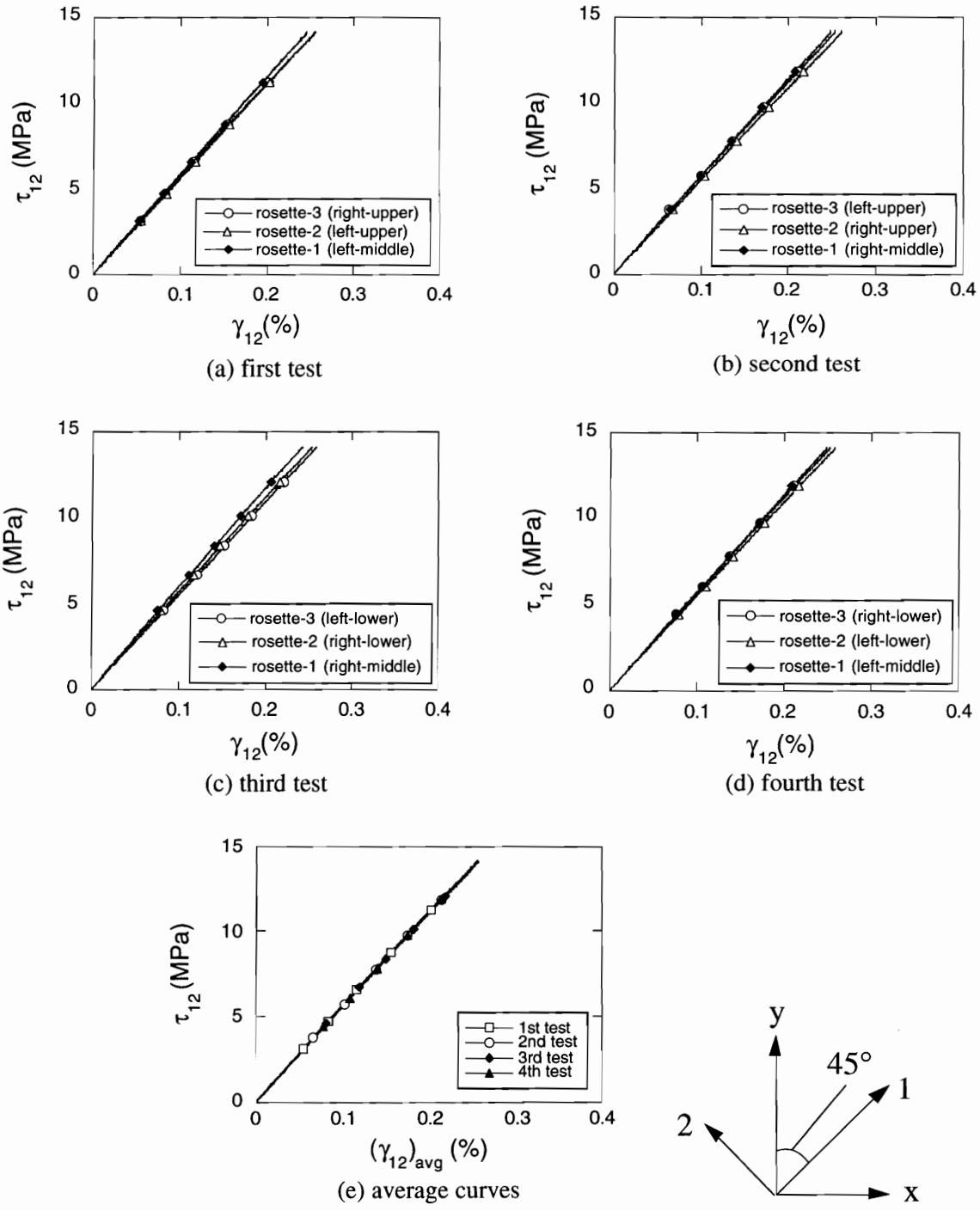

Fig. 3.44 Shear Stress-Strain Curves of ± 45° Tensile Specimen in 1-2 Plane
(Tested in Instron-4206 Test Machine)

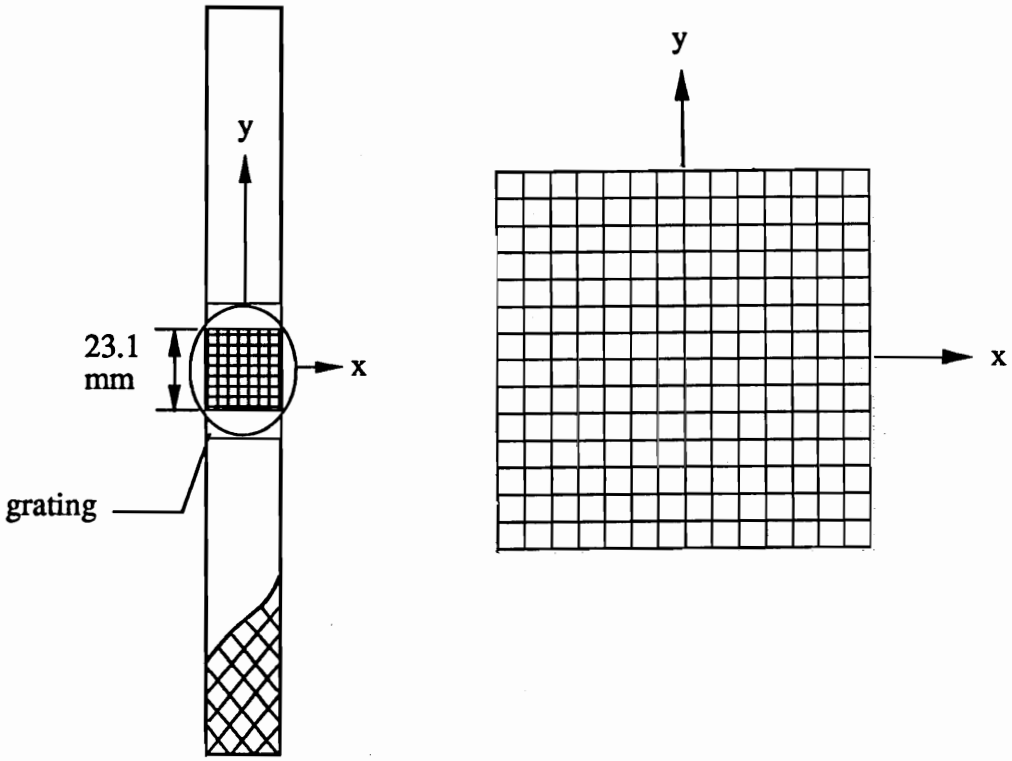

Fig. 3.45 Finite Element Mesh for Localized Hybrid Analysis of ± 45° Tensile Specimen

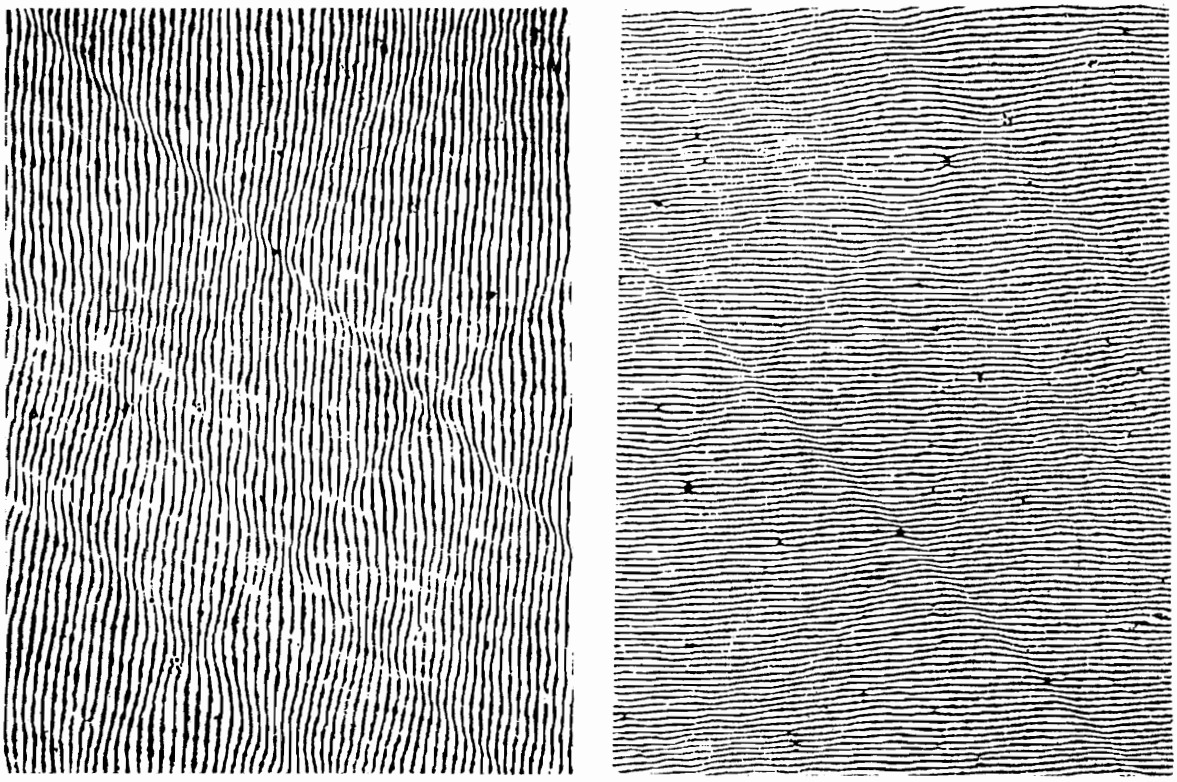

U - Field V - Field

Fig. 3.46 Moiré Fringe Patterns for ± 45° Tensile Specimen
(P = 2.67 KN)

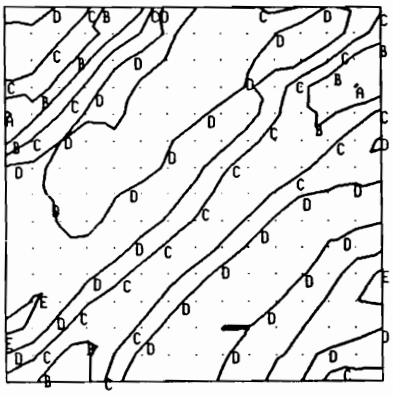

A=0.000183
B=0.000253
C=0.000323
D=0.000393
E=0.000463

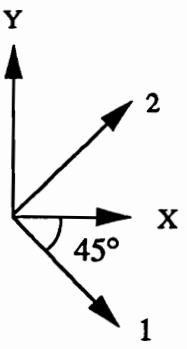

(a)

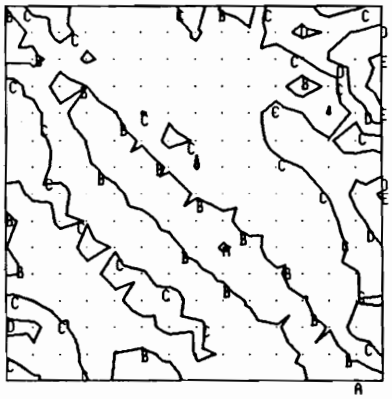

A=0.000210
B=0.000280
C=0.000350
D=0.000420
E=0.000490

Size of Strain Gage
(to the same scale)

(b)

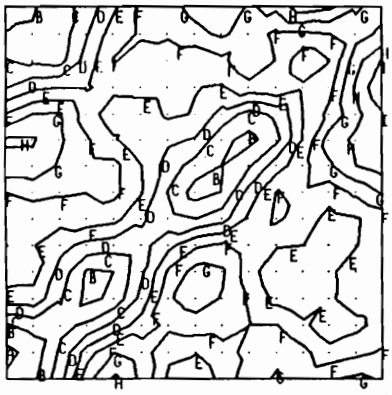

A=-0.00518
B=-0.00508
C=-0.00498
D=-0.00488
E=-0.00478
F=-0.00468
G=-0.00458
H=-0.00448
I=-0.00438

10 mm

(c)

Fig. 3.47 Strain Contours in 1-2 Plane of ± 45° Tensile Specimen
(a) ε_1, (b) ε_2, (c) γ_{12}

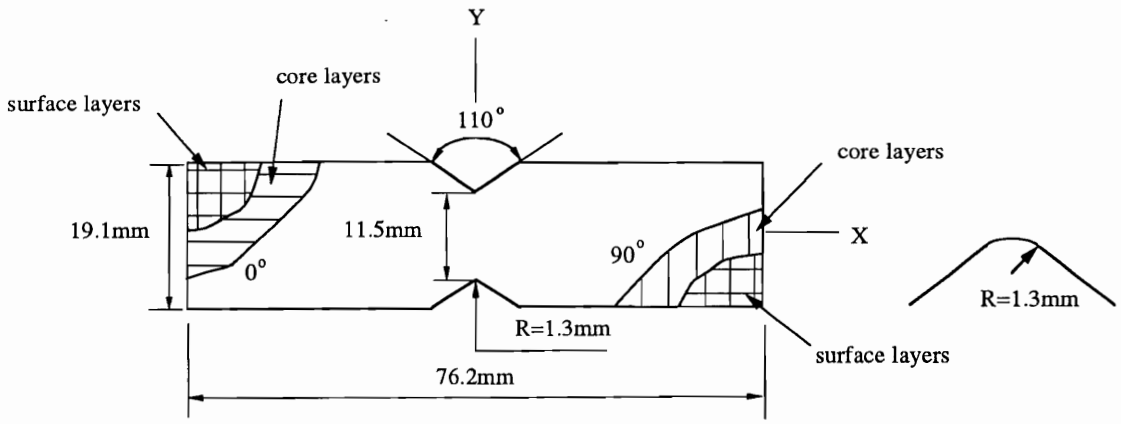

Fig. 3.48 Iosipescu Specimen of Hybrid Glass/PETP

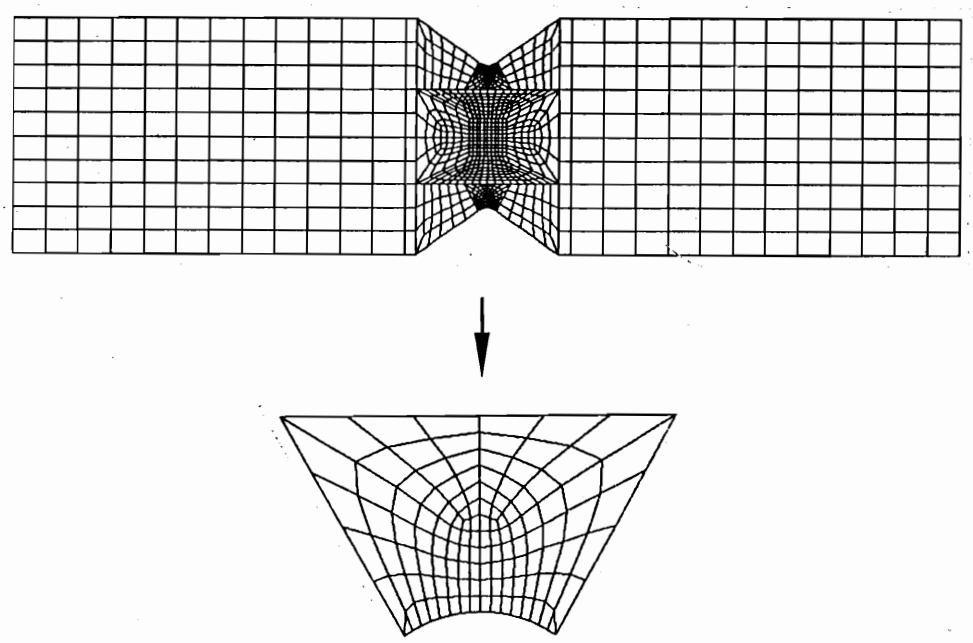

Fig. 3.49 Finite Element Mesh for Iosipescu Specimen

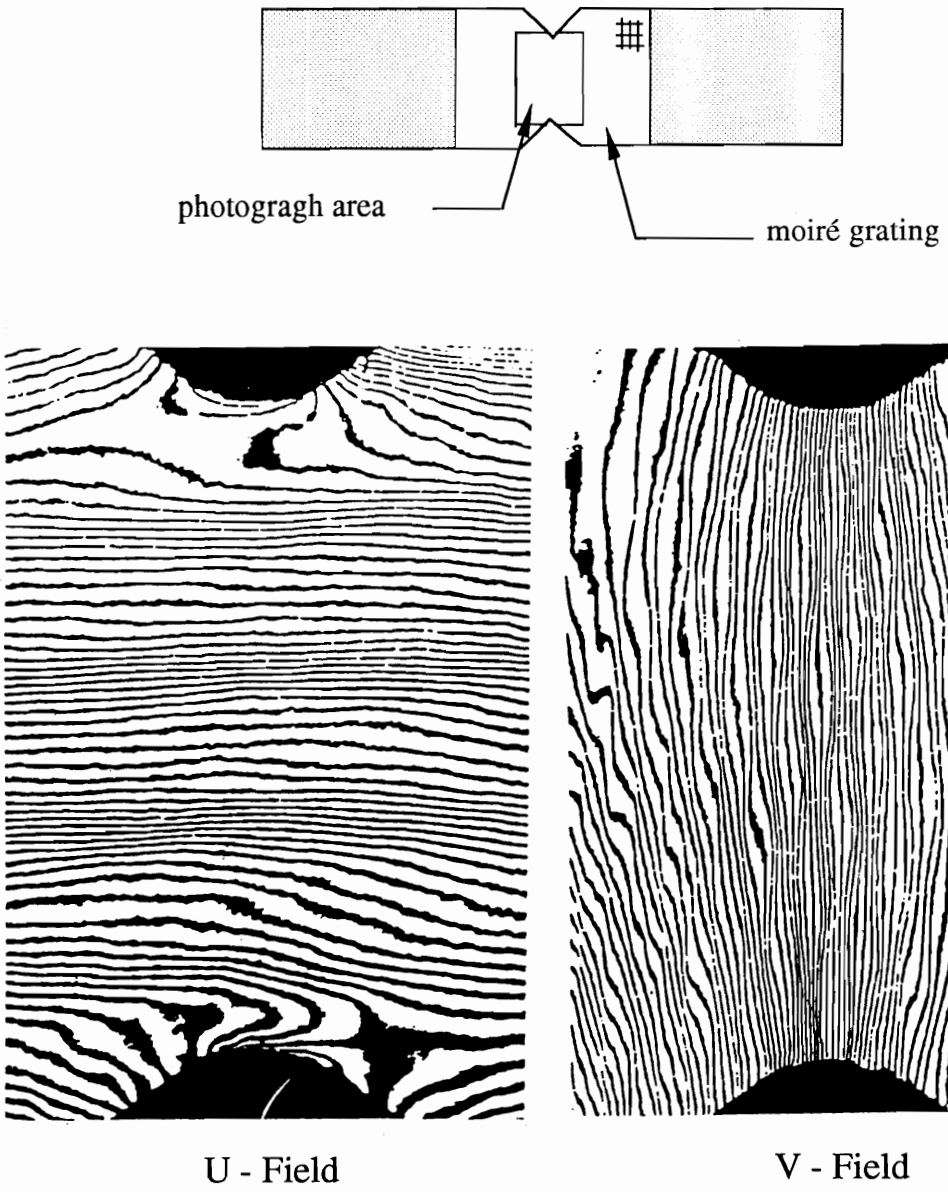

Fig. 3.50 Typical Moiré Fringe Patterns for Hybrid Glass/PETP Iosipescu Specimen - 0° Configuration

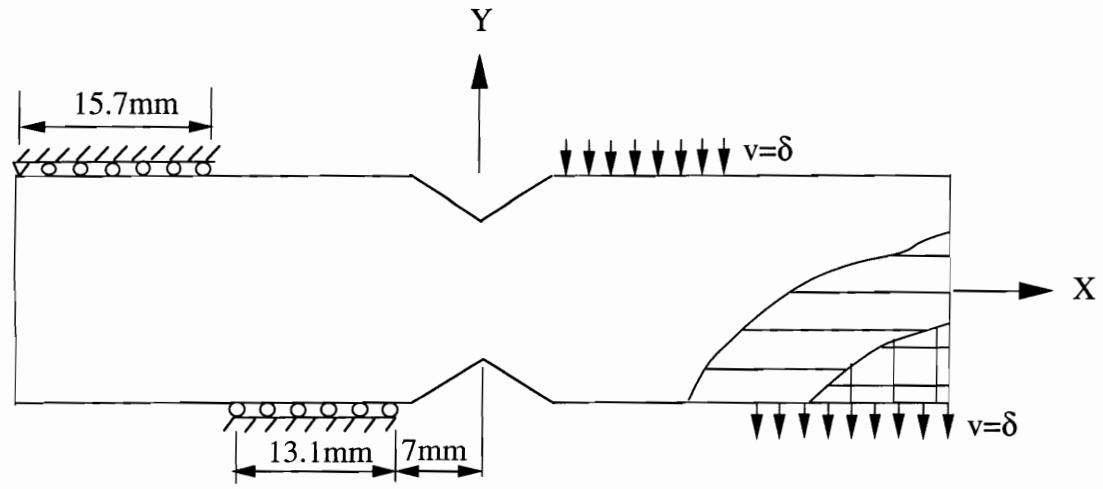

(a) 0° Specimen

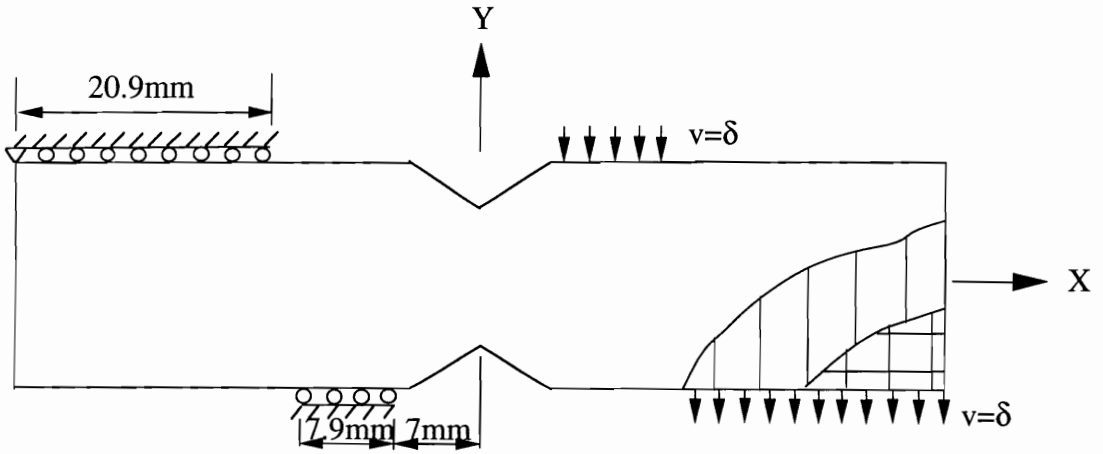

(b) 90° Specimen

Fig. 3.51 Loading Conditions for Hybrid Glass/PETP Iosipescu Specimen

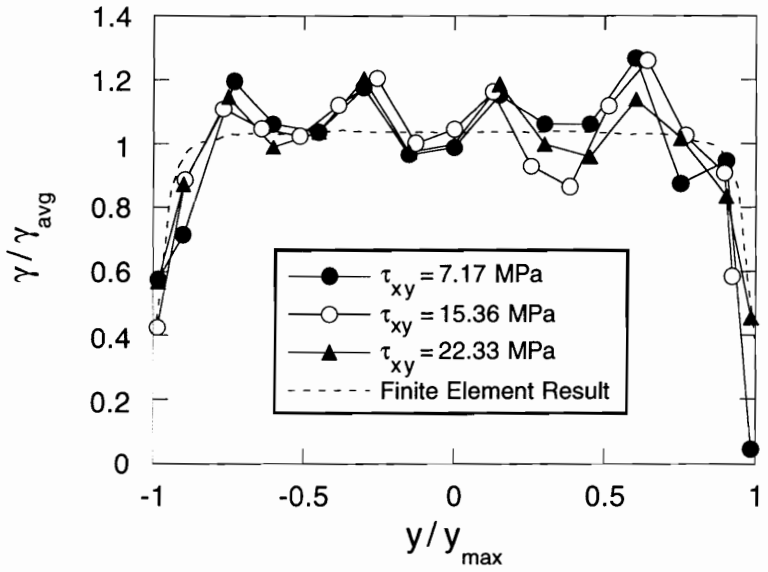

(a) 0° Specimen

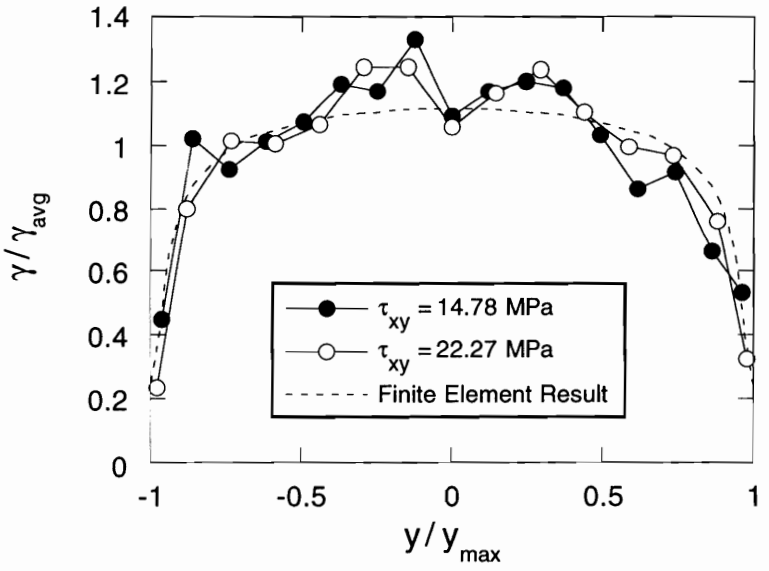

(b) 90° Specimen

Fig. 3.52 Shear Strain Distribution between Notches of Hybrid Glass/PETP Iosipescu Specimen

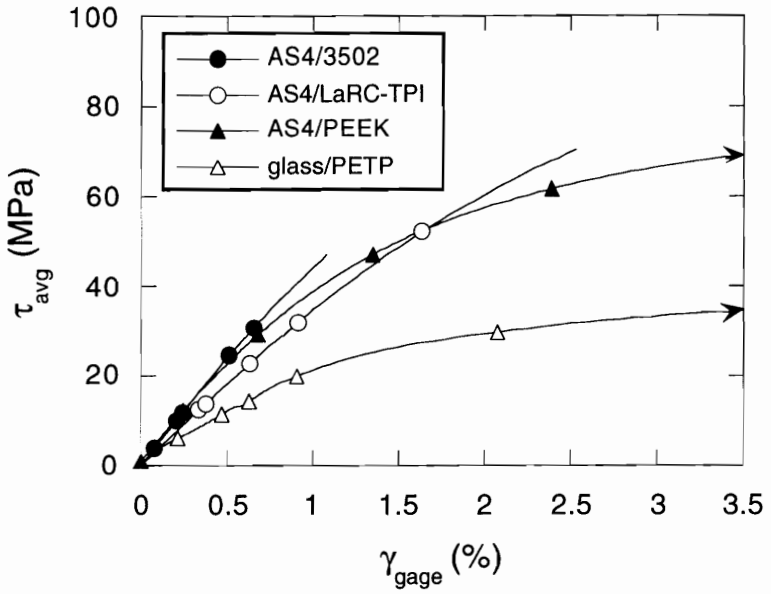

Fig. 4.1 Typical Shear Stress-Strain Curve of Various Composite Materials

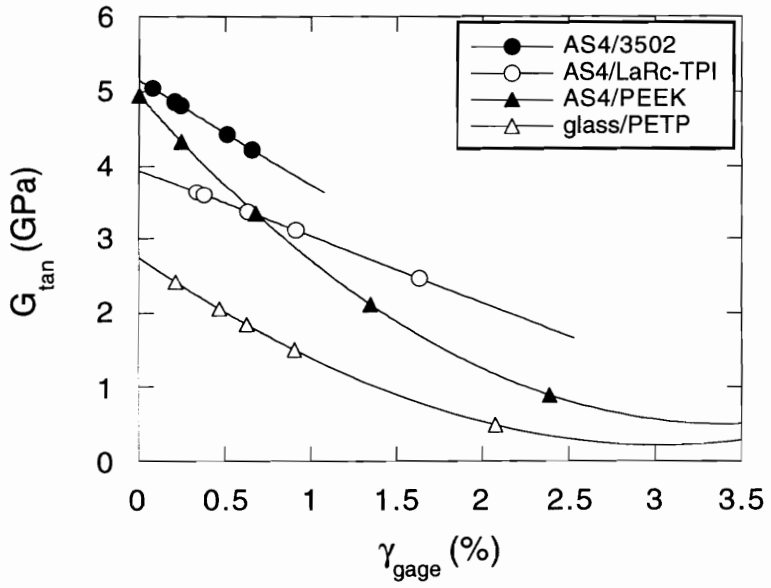

Fig. 4.2 Variation of Tangential Shear Moduli with Shear Strain

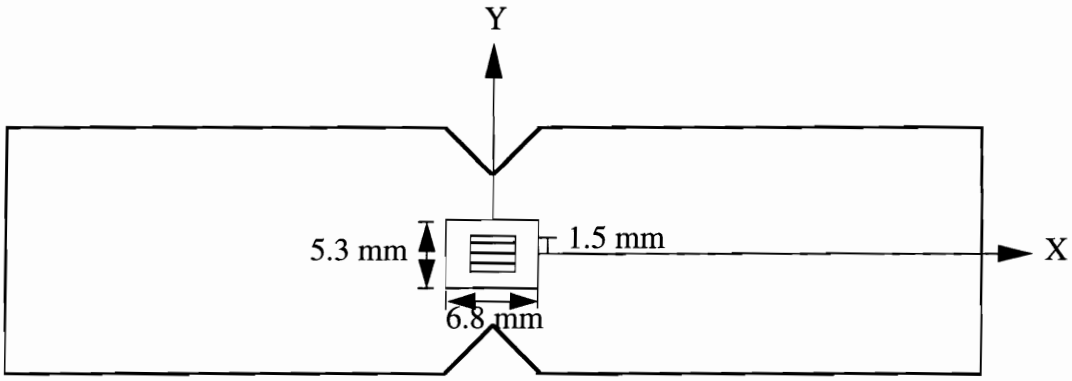

(a) front face

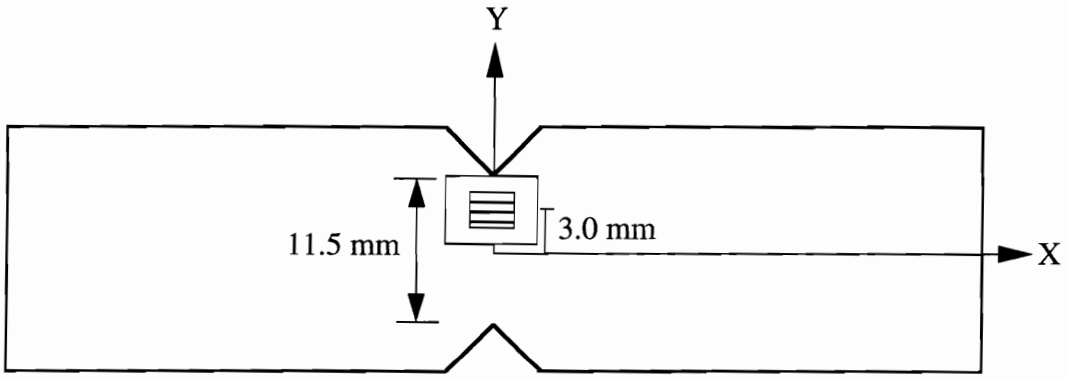

(b) back face

Fig. 4.3 Scheme of Arrangement of Strain Gage Rosettes for Iosipescu Specimen

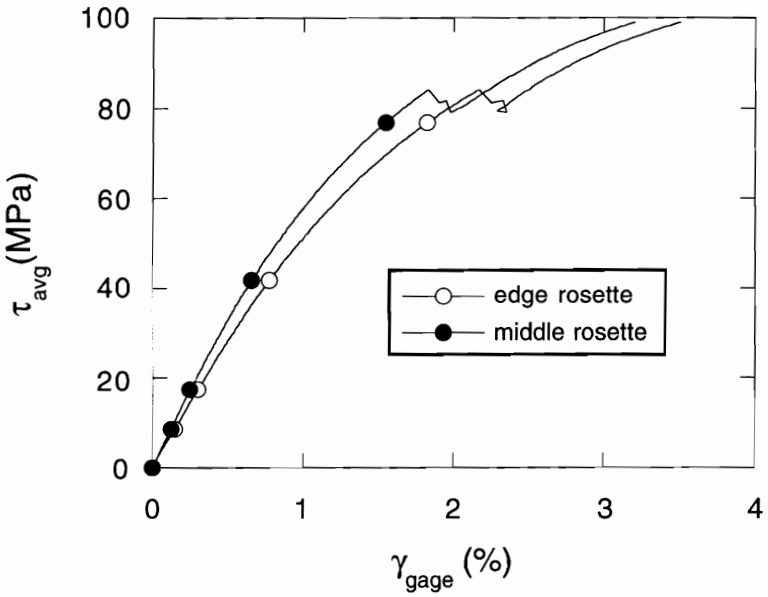

Fig. 4.4 Shear Stress-Strain Response of 0° Iosipescu Specimen

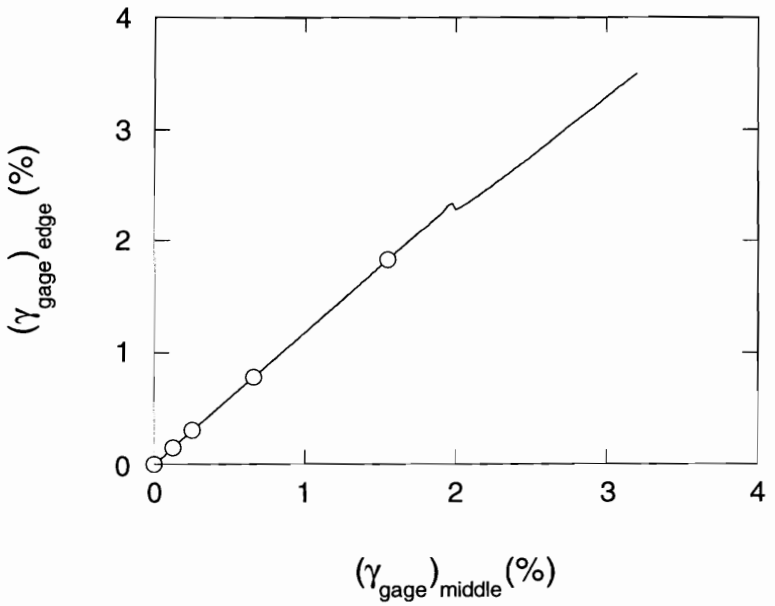

Fig. 4.5 Shear Strain Measured at Edge vs Shear Strain Measured at Middle

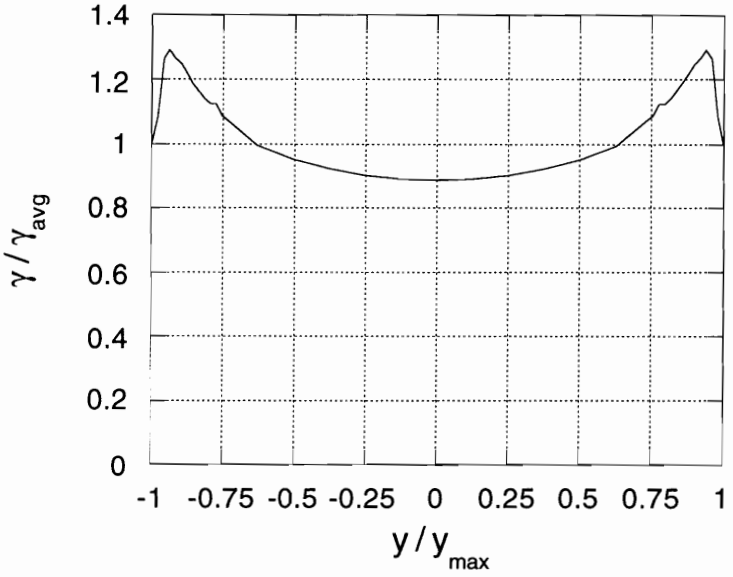

Fig. 4.6 Normalized Shear Strain Distribution of 0° Iosipescu Specimen Obtained from Linear Elastic Finite Element Analysis

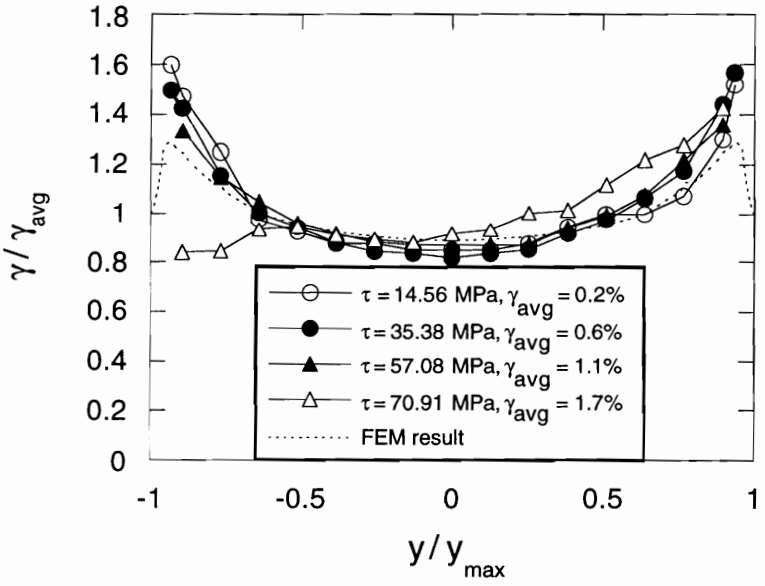

Fig. 4.7 Shear Strain Distribution of 0° Iosipescu Specimen Obtained from Moiré Data

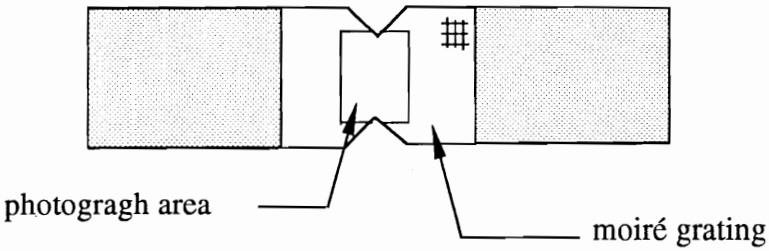

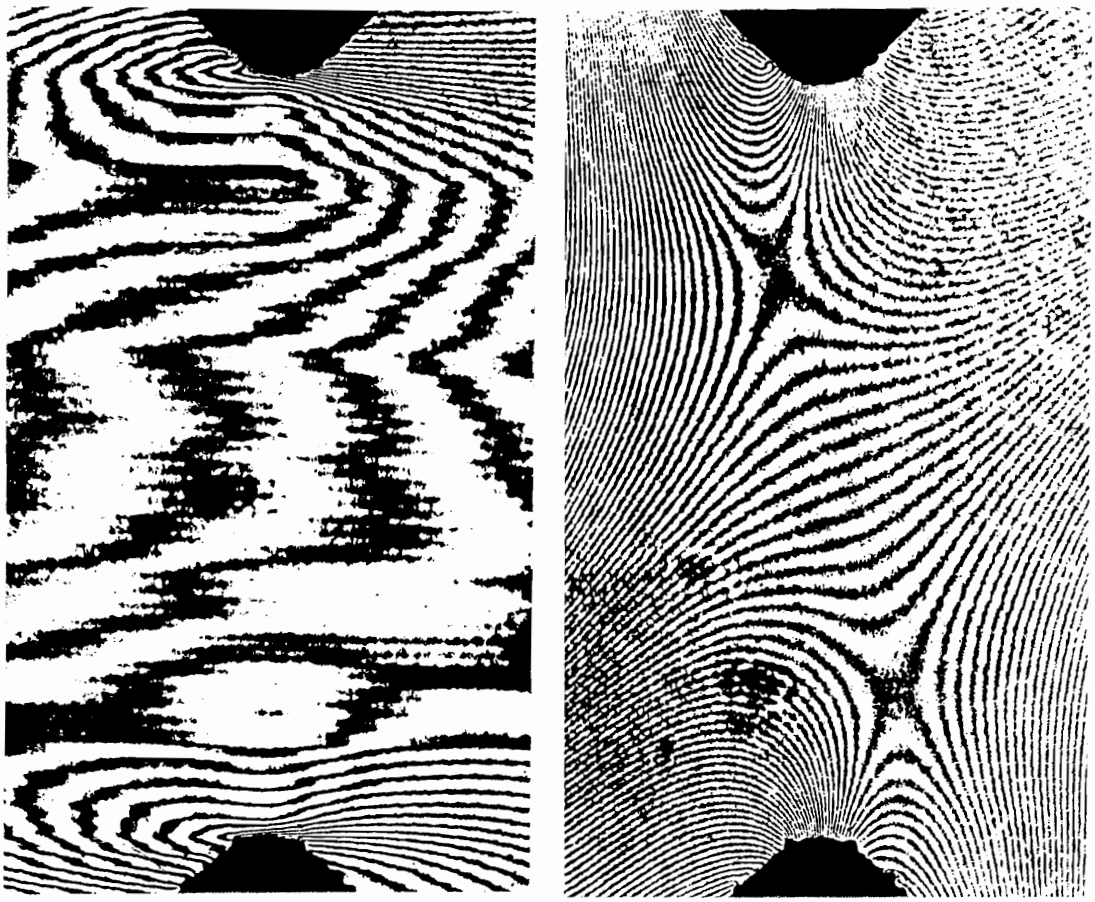

U - Field V - Field

Fig. 4.8 Moiré Fringe Patterns for AS4/3502 Iosipescu Specimen - 0° Configuration

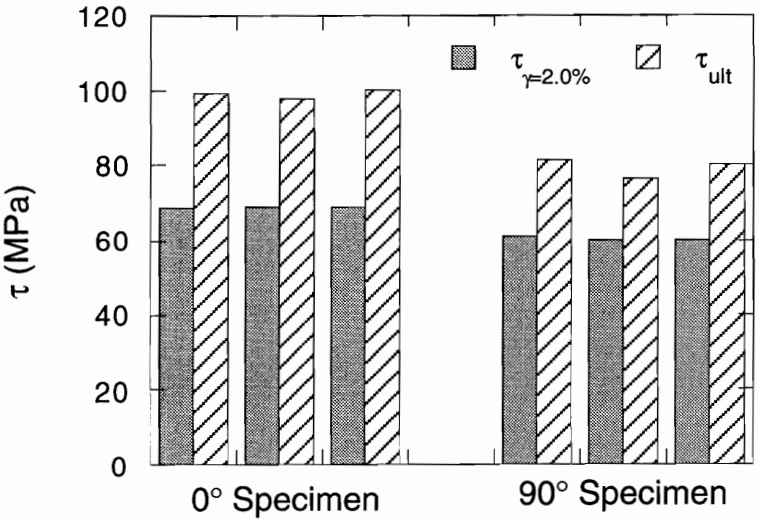

Fig. 4.9 Shear Stress at $\gamma = 2.0\%$ and Ultimate Shear Stress for Iosipescu Specimen of APC-2

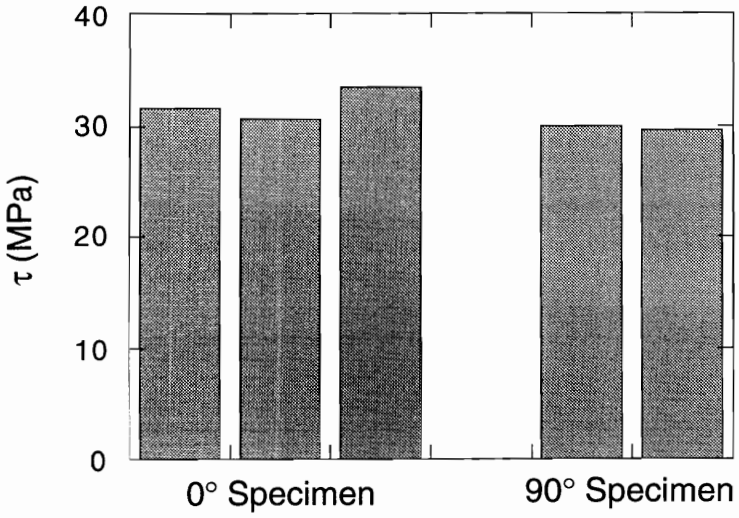

Fig. 4.10 Shear Stress at $\gamma = 2.0\%$ for Iosipescu Specimen of Hybrid Glass/PETP

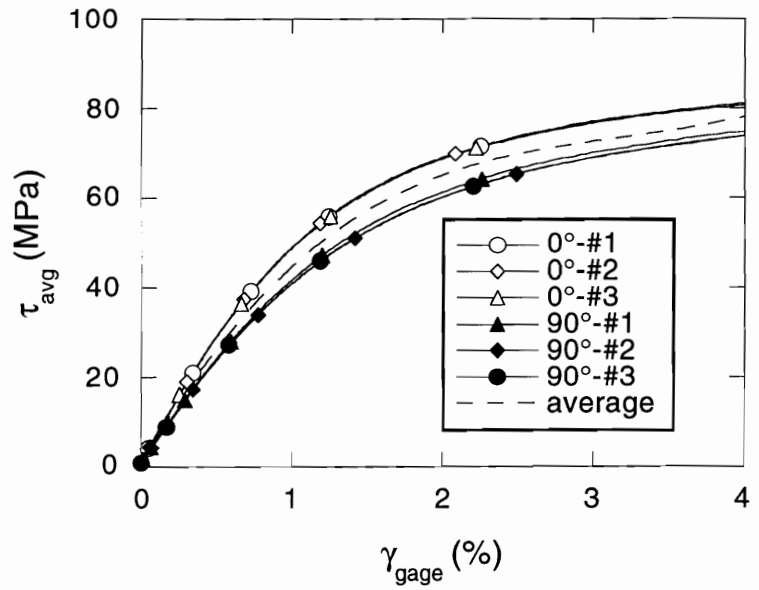

Fig. 5.1 Shear Stress-Strain Curves of APC-2

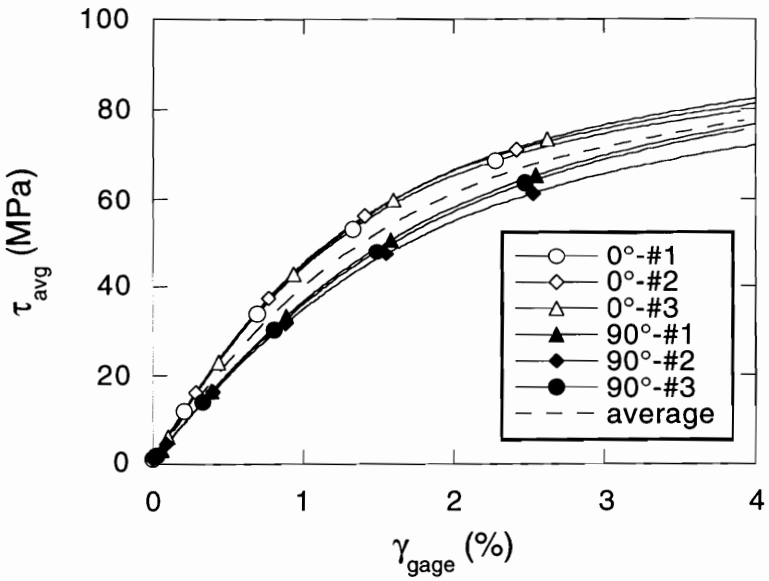

Fig. 5.2 Shear Stress-Strain Curves of AS4/PEEK+LaRC-TPI

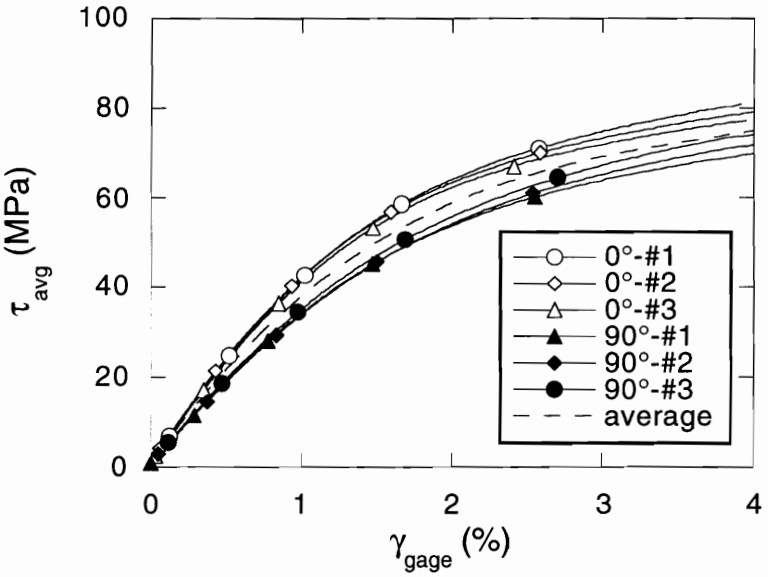

Fig. 5.3 Shear Stress-Strain Curves of AS4/PEEK+BisP-BTDA

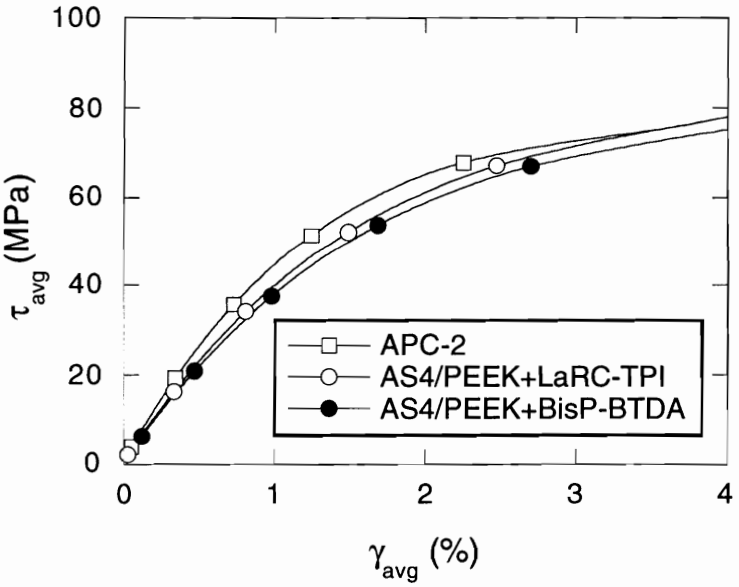

Fig. 5.4 Average Shear Stress-Strain Curves of 0° and 90° Iosipescu Specimens of AS4/PEEK System

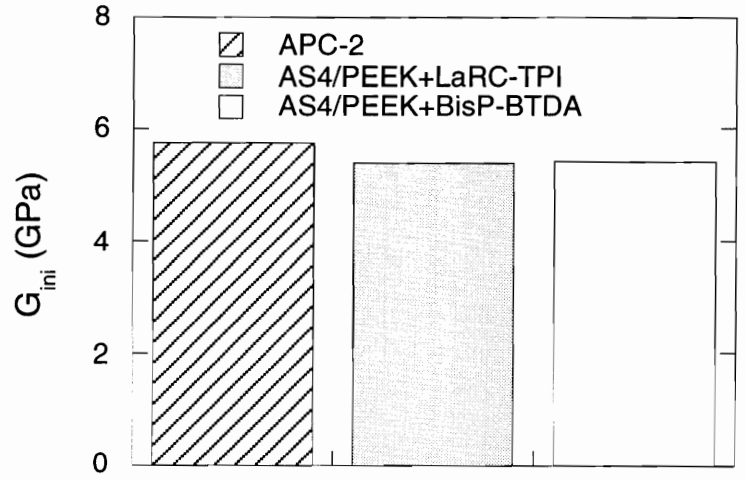

Fig. 5.5 Initial Shear Moduli of AS4/PEEK System Normalized with respect to Fiber Volume Fraction

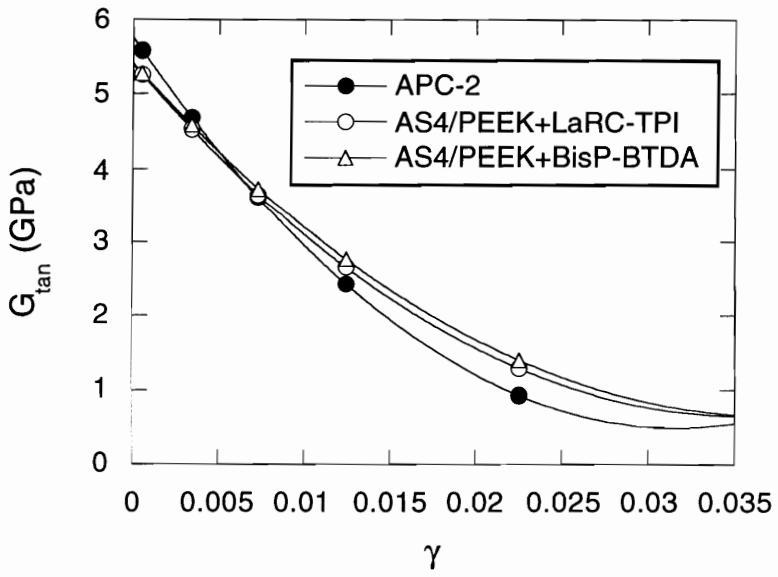

Fig. 5.6 Variation of Tangential Shear Moduli with Shear Strain for AS4/PEEK System

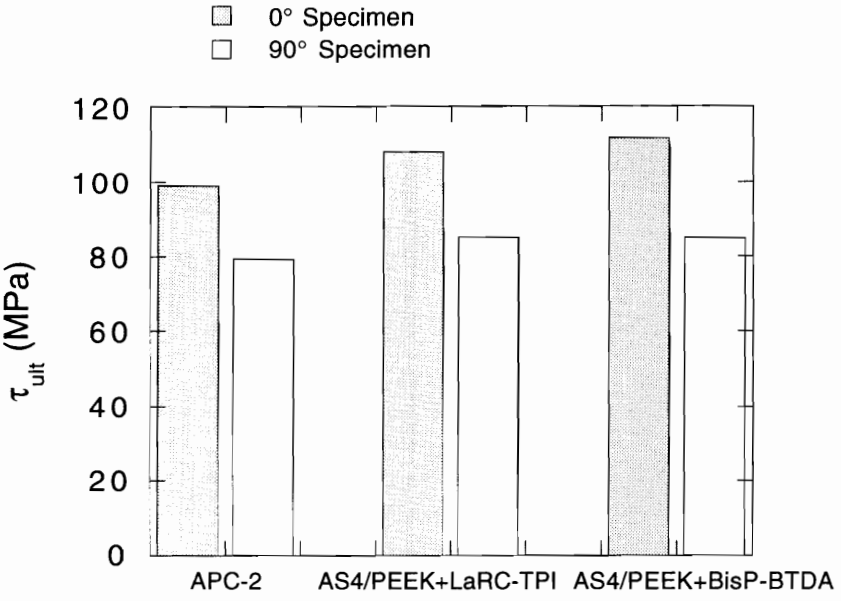

Fig. 5.7 Apparent Failure Shear Stress of AS4/PEEK System

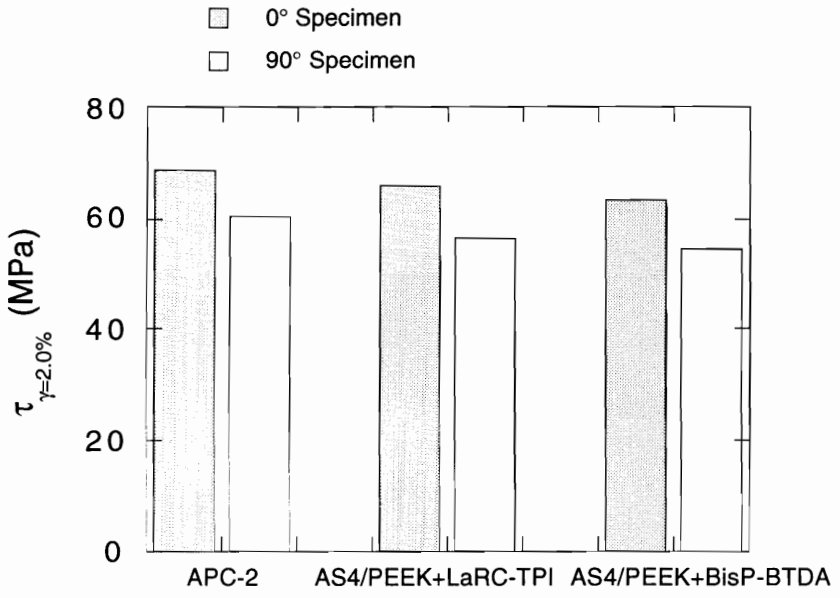

Fig. 5.8 Shear Stress at $\gamma = 2.0\%$ for AS4/PEEK System

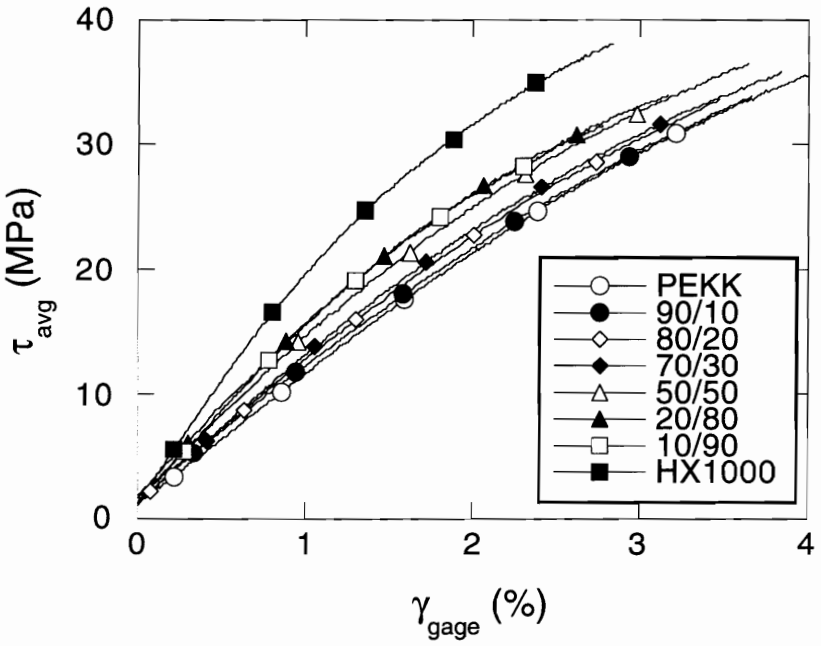

Fig. 5.9 Shear Stress-Strain Curves of PEKK/HX1000 Composite System

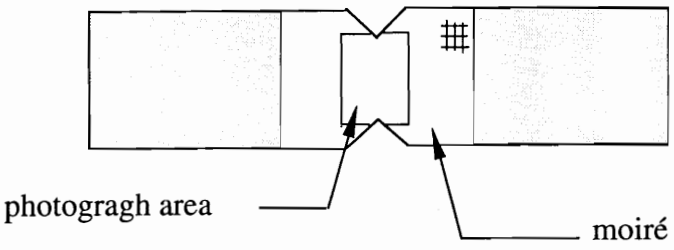

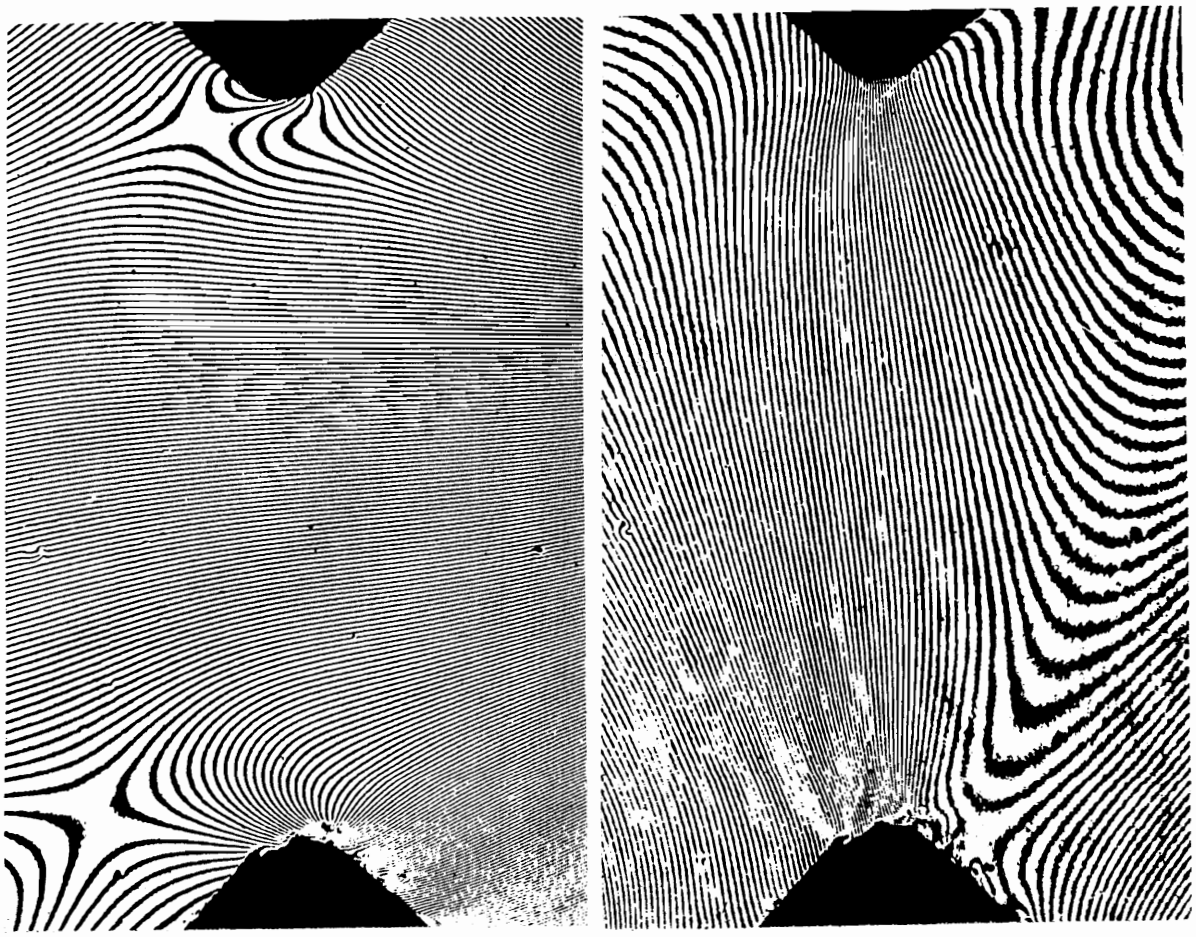

U - Field V - Field

Fig. 5.10 Typical Moiré Fringe Patterns of Neat PEKK Iosipescu Specimen

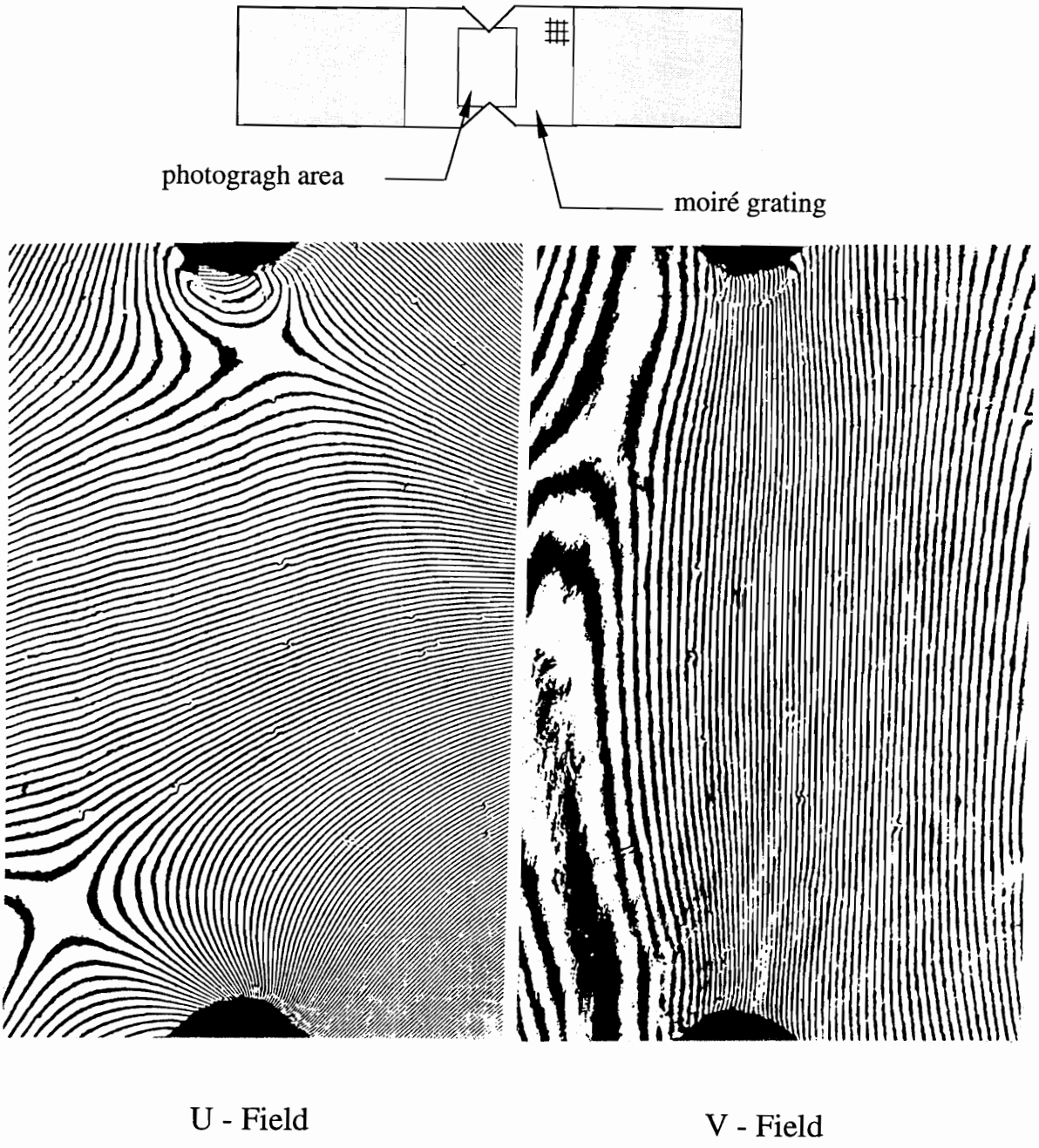

Fig. 5.11 Typical Moiré Fringe Patterns of Neat HX1000 Iosipescu Specimen

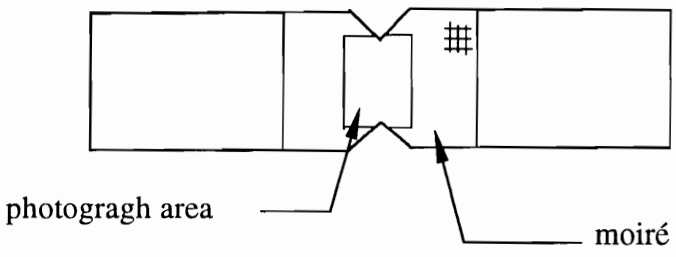

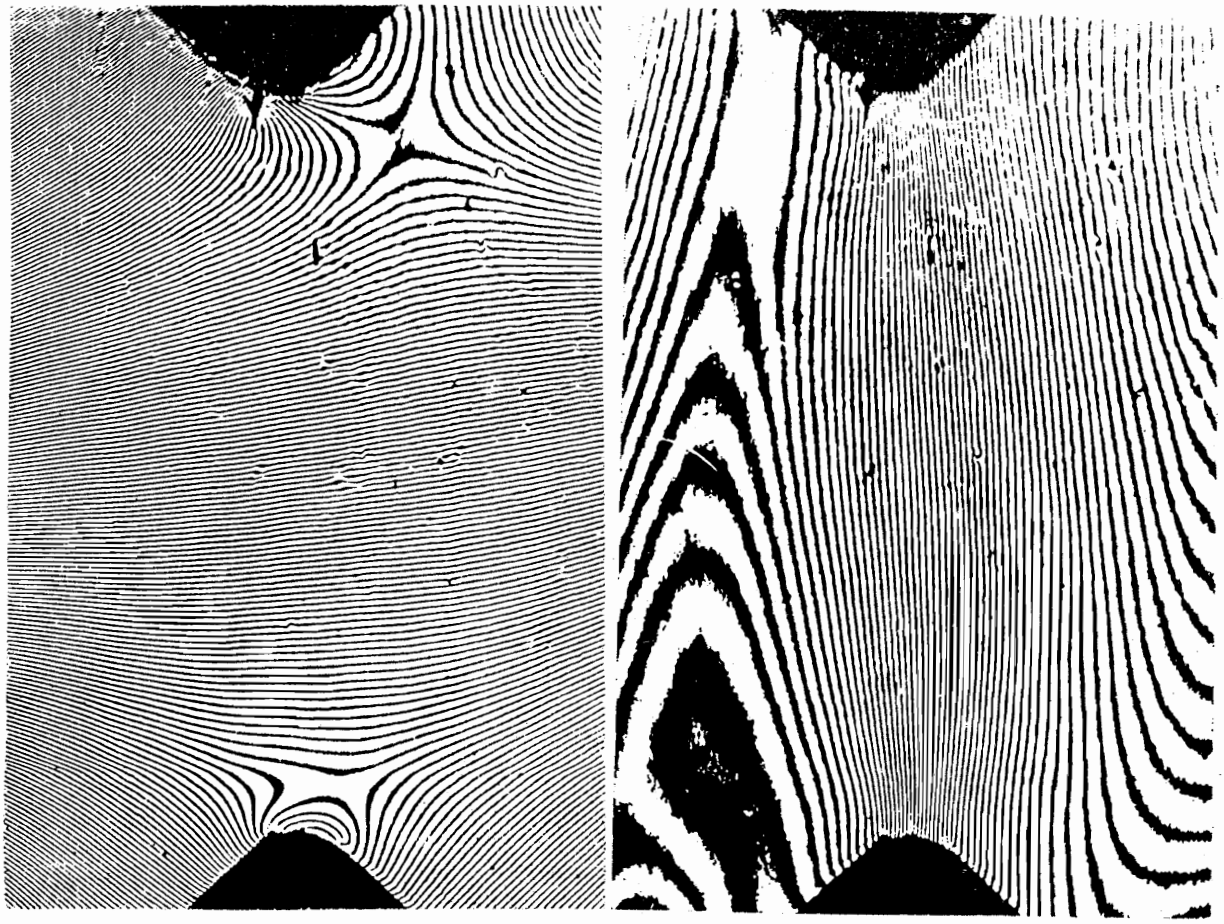

U - Field V - Field

Fig. 5.12 Typical Moiré Fringe Patterns of PEKK/HX1000 20/80 Iosipescu Specimen

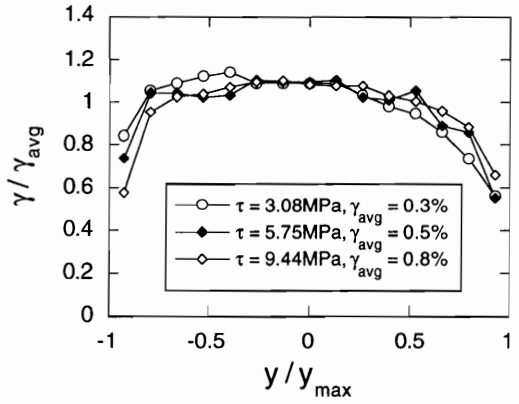

(a) PEKK Specimen

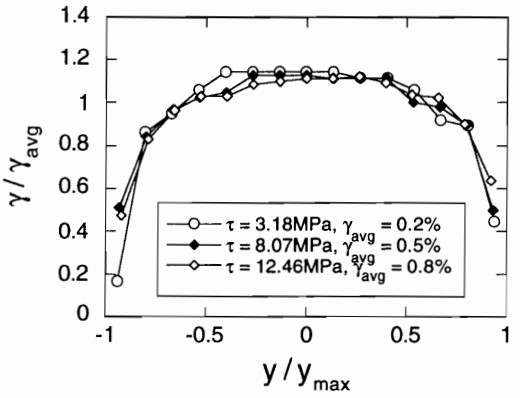

(b) 20/80 Specimen

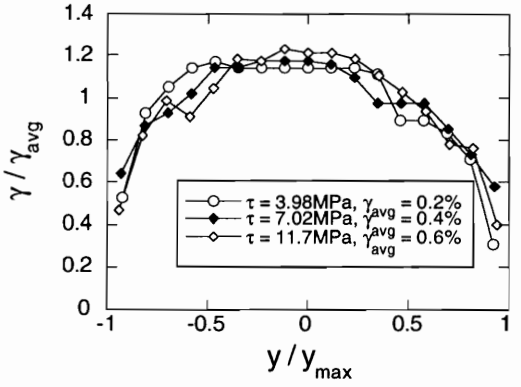

(c) HX1000 Specimen

Fig. 5.13 Shear Strain Distribution across the Notches of PEKK/HX1000 Iosipescu Specimen

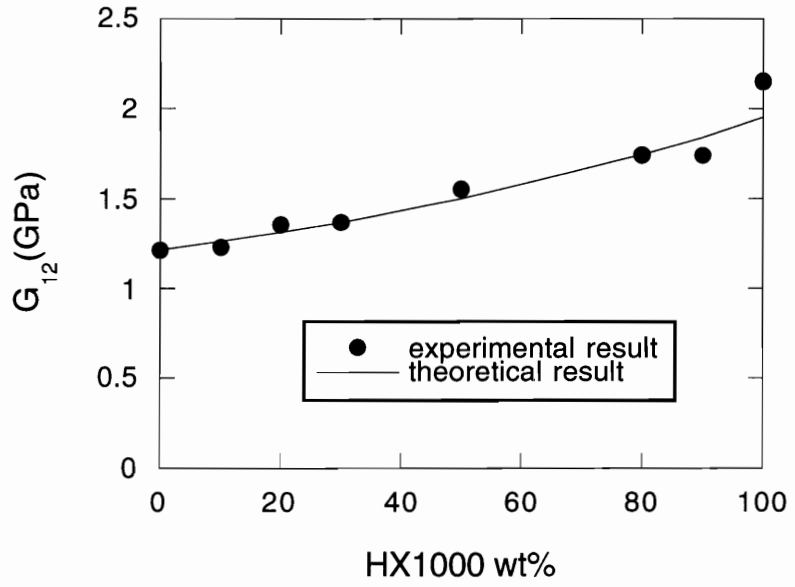

Fig. 5.14 Variation of Initial Shear Modulus with HX1000 Concentration for PEKK/HX1000

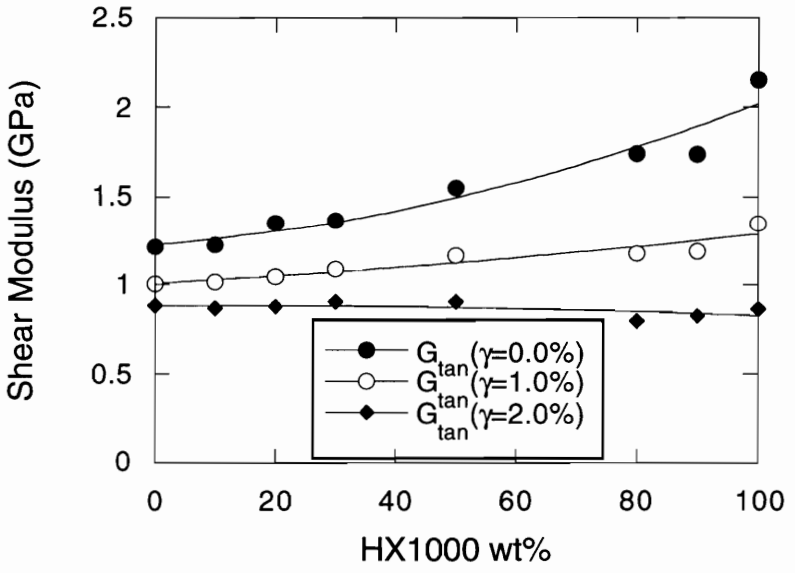

Fig. 5.15 Comparison of Shear Modulus at Different Shear Strain Levels for PEKK/HX1000 System

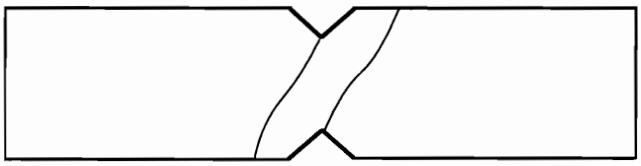

(a) 50/50 & 70/30 Specimens

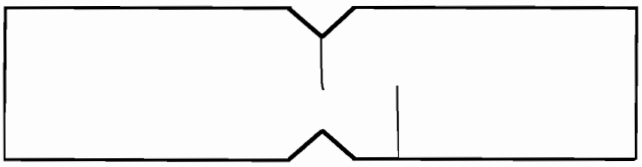

(b) HX1000, 10/90 & 20/80 Specimens

Fig. 5.16 Failure Mode of Different Specimens of PEKK/HX1000 System

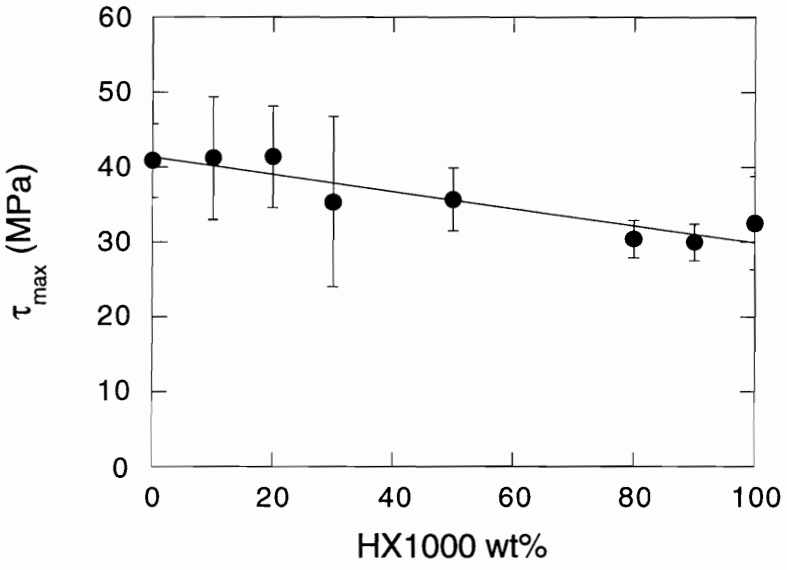

Fig. 5.17 Apparent Failure Shear Stress for PEKK/HX1000

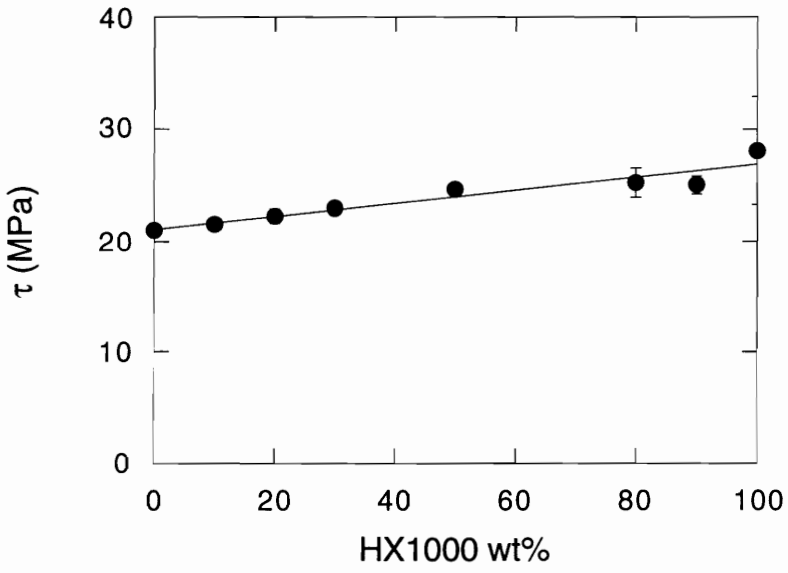

Fig. 5.18 Shear Stress at $\gamma = 2.0\%$ for PEKK/HX1000

VITA

Yanhong Zhang was born in Beijing, P. R. China where she attended Elementary and Middle school. Her middle school education was, unfortunately, interrupted by the Cultural Revolution and she was forced to work on a grain farm for six years where she completed her high school education by self-study. She then studied at a Civil Engineering Technical School for two years and was employed as an instructor there for one year. In 1978 she successfully passed a nationwide examination with high grades and was accepted by one of the top ten Engineering Colleges in China, The Beijing Institute of Aeronautics and Astronautics, where she completed her B.S. degree in Aerospace Engineering. After graduation, she passed another examination and became a Master's candidate at the Institute of Mechanics, Chinese Academy of Sciences. She received her M.S. degree in Solid Mechanics in 1984 and was employed by that institute as a research assistant in the area of fracture mechanics until 1989. In the fall of 1989, she entered the Ph.D. program at Virginia Polytechnic Institute and State University. She did her research work in composite testing and analysis under the guidance of Dr. Morton in the Department of Engineering Science and Mechanics. In May of 1994, Yanhong Zhang received her Ph.D. degree in Engineering Mechanics.